ORTA DOĞU TEKNİK ÜNİVERSİTESİ
FEN BİLİMLERİ ENSTİTÜSÜ MÜDÜRLÜĞÜ

TEZ ŞABLONU ONAY FORMU
THESIS TEMPLATE CONFIRMATION FORM

1. Şablonda verilen yerleşim ve boşluklar değiştirilmemelidir.
2. **Jüri tarihi** Başlık Sayfası, İmza Sayfası, Abstract ve Öz'de ilgili yerlere yazılmalıdır.
3. İmza sayfasında jüri üyelerinin unvanları doğru olarak yazılmalıdır. Tüm imzalar **mavi pilot kalemle** atılmalıdır.
4. **Disiplinlerarası** programlarda görevlendirilen öğretim üyeleri için jüri üyeleri kısmında tam zamanlı olarak çalıştıkları anabilim dalı başkanlığının ismi yazılmalıdır. Örneğin: bir öğretim üyesi Biyoteknoloji programında görev yapıyor ve biyoloji bölümünde tam zamanlı çalışıyorsa, İmza sayfasına biyoloji bölümü yazılmalıdır. İstisnai olarak, disiplinler arası program başkanı ve tez danışmanı için disiplinlerarası program adı yazılmalıdır.
5. Tezin **son sayfasının sayfa** numarası Abstract ve Öz'de ilgili yerlere yazılmalıdır.
6. Bütün chapterlar, referanslar, ekler ve CV sağ sayfada başlamalıdır. Bunun için **kesmeler** kullanılmıştır. **Kesmelerin kayması** fazladan boş sayfaların oluşmasına sebep olabilir. Bu gibi durumlarda paragraf (¶) işaretine tıklayarak kesmeleri görünür hale getirin ve yerlerini **kontrol edin**.
7. Figürler ve tablolar kenar boşluklarına taşmamalıdır.
8. Şablonda yorum olarak eklenen uyarılar dikkatle okunmalı ve uygulanmalıdır.
9. Tez yazdırılmadan önce PDF olarak kaydedilmelidir. Şablonda yorum olarak eklenen uyarılar PDF dokümanında yer almamalıdır.
10. Tez taslaklarının kontrol işlemleri tamamlandığında, bu durum öğrencilere METU uzantılı öğrenci e-posta adresleri aracılığıyla duyurulacaktır.
11. Tez yazım süreci ile ilgili herhangi bir sıkıntı yaşarsanız, Sıkça Sorulan Sorular (SSS) sayfamızı ziyaret ederek yaşadığınız sıkıntıyla ilgili bir çözüm bulabilirsiniz.

1. Do not change the spacing and placement in the template.
2. Write **defense date** to the related places given on Title page, Approval page, Abstract and Öz.
3. Write the titles of the examining committee members correctly on Approval Page. **Blue ink** must be used for all signatures.
4. For faculty members working in **interdisciplinary programs**, the name of the department that they work full-time should be written on the Approval page. For example, if a faculty member staffs in the biotechnology program and works full-time in the biology department, the department of biology should be written on the approval page. Exceptionally, for the interdisciplinary program chair and your thesis supervisor, the interdisciplinary program name should be written.
5. Write **the page number of the last page** in the related places given on Abstract and Öz pages.
6. All chapters, references, appendices and CV must be started on the right page. **Section Breaks** were used for this. **Change in the placement** of section breaks can result in extra blank pages. In such cases, make the section breaks visible by clicking paragraph (¶) mark and **check their position.**
7. All figures and tables must be given inside the page. Nothing must appear in the margins.
8. All the warnings given on the comments section through the thesis template must be read and applied.
9. Save your thesis as pdf and Disable all the comments before taking the printout.
10. This will be announced to the students via their METU students e-mail addresses when the control of the thesis drafts has been completed.
11. If you have any problems with the thesis writing process, you may visit our Frequently Asked Questions (FAQ) page and find a solution to your problem.

☒ **Yukarıda bulunan tüm maddeleri okudum, anladım ve kabul ediyorum. / I have read, understand and accept all of the items above.**

Name :
Surname :
E-Mail :
Date :
Signature : _____

INVESTIGATION OF THE DRUG RESISTANCE IN CAPECITABINE RESISTANT HCT-116, DABRAFENIB RESISTANT HT-29, AND SN-38 RESISTANT HT-29 CELL LINES USING CELLULAR BARCODING TECHNOLOGY

A THESIS SUBMITTED TO
THE GRADUATE SCHOOL OF NATURAL AND APPLIED SCIENCES
OF
MIDDLE EAST TECHNICAL UNIVERSITY

BY

RANA CAN BAYGIN

IN PARTIAL FULFILLMENT OF THE REQUIREMENTS
FOR
THE DEGREE OF MASTER OF SCIENCE
IN
BIOLOGY

NOVEMBER 2022

Approval of the thesis:

INVESTIGATION OF THE DRUG RESISTANCE IN CAPECITABINE RESISTANT HCT-116, DABRAFENIB RESISTANT HT-29, AND SN-38 RESISTANT HT-29 CELL LINES USING CELLULAR BARCODING TECHNOLOGY

submitted by **RANA CAN BAYGIN** in partial fulfillment of the requirements for the degree of **Master of Science** i**n Biology, Middle East Technical University** by,

Prof. Dr. Halil Kalıpçılar
Dean, Graduate School of **Natural and Applied Sciences** _____

Prof. Dr. Ayşe Gül Gözen
Head of the Department, **Biology** _____

Assist. Prof. Dr. Ahmet Acar
Supervisor, **Biology, METU** _____

Examining Committee Members:

Assoc. Prof. Dr. Can Özen
Biotechnology, METU _____

Assist. Prof. Dr. Ahmet Acar
Biology, METU _____

Assoc. Prof. Dr. Bala Gür Dedeoğlu
Biotechnology, Ankara University _____

Date: 03.11.2022

I hereby declare that all information in this document has been obtained and presented in accordance with academic rules and ethical conduct. I also declare that, as required by these rules and conduct, I have fully cited and referenced all material and results that are not original to this work.

Name Last name: Baygın, Rana Can

Signature :

ABSTRACT

INVESTIGATION OF THE DRUG RESISTANCE IN CAPECITABINE-RESISTANT HCT-116, DABRAFENIB-RESISTANT HT-29, AND SN-38-RESISTANT HT-29 CELL LINES USING CELLULAR BARCODING TECHNOLOGY

Baygın, Rana Can
Master of Science, Biology
Supervisor: Dr. Ahmet Acar

November 2022, 111 pages

Cancer is a complex disease, and understanding its biology holds great importance. Tumor cells exhibit hallmarks of cancer, including aberrantly activated signaling pathways and gain or loss genomic alterations that result in alterations in their differentiation programs, survival, proliferation, and programmed cell death. Developing resistance to therapeutic agents is one of the major problems in cancer therapies. Exploiting drug resistance using the principles of clonal evolution can pave the way to overcoming or controlling drug resistance in cancers. Collateral sensitivity as a second-line therapy strategy positively impacts the treatment of cancer, and it could offer novel therapeutic strategies to overcome or control drug resistance. In this study, it was aimed to monitor the development of drug resistance using cellular barcoding technology to identify second-line therapeutic agents that sensitize initially drug-resistant cell populations. To develop the evolutionary-informed strategy for drug resistance and to study the effect of second-line therapy in colorectal cancer cell lines, barcoded HCT-116 and HT-29 cell lines were used. The barcode analysis showed that the capecitabine resistance in HCT-116 cells was

caused by de novo, dabrafenib resistance in HT-29 cells was caused by de novo, and the SN-38 resistance in HT-29 cells was caused by pre-existing alterations in the population. The cell viability assays of drug-resistant cells indicated that collateral sensitivity exists for other drugs. Thus, the development of drug resistance in colorectal cancer cells was associated with pre-existed or de novo mutations depending on a cell line or a drug in the preferred experimental model system and potentially had a great impact on mediating collateral sensitivity as a second-line therapy option.

Keywords: Colorectal cancer, drug resistance, collateral sensitivity, second-line therapies

ÖZ

İLAÇ DİRENCİNİN KAPESITABİN DİRENÇLİ HCT-116, DABRAFENİB DİRENÇLİ HT-29 VE SN-38 DİRENÇLİ HT-29 HÜCRE HATLARINDA HÜCRE BARKODLANMASI TEKNOLOJİSİYLE İNCELENMESİ

Baygın, Rana Can
Yüksek Lisans, Biyoloji
Tez Yöneticisi: Dr. Ahmet Acar

Kasım 2022, 111 sayfa

Kanser karmaşık bir hastalıktır ve onu biyolojisini anlamak büyük bir önem arz eder. Tümör hücreleri düzensiz bir şekilde sinyal yolaklarını aktif hale getirir ve bu hücrelerde farklı genetik değişiklikler meydana gelir. Bu genetik değişikliklerden dolayı kanser hücreleri, ortamda bulunan hücresel farklılaşma, hayatta kalma, proliferasyon ve ölüm sinyallerine sağlıklı bir hücre gibi cevap veremezler. Kanser tedavisinde kullanılan ilaca karşı direnç oluşması büyük bir problemdir. Klonal evrim ilaç direnci mekanizmasını araştırmak ve önleyebilmek için önemli bir mihenk taşıdır. Kollateral hassasiyet ikinci basamak terapide ilaç dirençli kolon kanseri hastaları için sonraki tedaviyi belirlemede önemli bir yere sahiptir. Barkodlanmış kolon kanseri hücre hatları HCT-116 ve HT-29 ilaç direnci evriminin ve ikinci basamak tedavinin etkilerini anlamak için kullanılmıştır. Barkod analizleri ilaç direncinin kapesitabin dirençli HCT-116 hücre hattında daha önce görülmeyen, dabrafenib dirençli HT-29 hücre hattında popülasyonda önceden bulunan ve SN-38 dirençli HT-29 hücre hattında daha önce görülmeyen faktörlerden kaynaklandığını göstermiştir. Hücre canlılığı deneyleri ilaç direncinin diğer ilaçlara kollateral hassasiyet yarattığını göstermiştir. Böylece, ilaç direnci oluşumunun sadece

popülasyonda önceden var olan faktörlerden değil aynı zamanda daha önce görülmeyen faktörlerden kaynaklandığı ve kollateral hassasiyetin ikinci basamak tedavi etkisini arttırdığı gözlemlenmiştir.

Anahtar Kelimeler: kolon kanseri, ilaç direnci, kollateral hassasiyet, ikinci basamak tedavi

“It was the best of times; it was the worst of times….”

To all women who burden challenges

ACKNOWLEDGMENTS

First and foremost, I would like to thank my supervisor, Dr. Ahmet Acar, for the guidance, comments, and support. I am very grateful for his time devoted to this study, the opportunity he presented, and his scientific lead. He has launched me on the path of becoming an independent researcher.

I would like to thank my thesis committee members Assoc. Prof. Can Özen and Assoc. Dr. Bala Gür Dedeoğlu for their time, kind interest, and contributions.

I would like to thank my laboratory mates for their support, friendship, and help. I thank Arda Temena for not only performing the bioinformatic part but also for academic advising and Nurseda Danışık for sharing the barcoding journey. I would like to express my thanks to Gizem Damla Yalçın for her support and help; to Can Ildız and Tuğçe Dilber for their valuable friendship. Lastly, I would like to thank Özlem Neyişçi, İrem Yücel, and İdil Gül Karakaya for their friendship.

I would like to thank Dr. Altuğ Özçelikkale for his generous help. I also want to acknowledge Barış Dedekargınoğlu for his support, patience, and fun friendship.

I am genuinely grateful to all my dearest friends at METU. I am thankful to Rüya Tombuloğlu for her support and proofreading of this thesis. I thank Elif Nisa Güler for her help and morale in every academic struggle. I am grateful to Gizem Turan for her guidance and precious friendship. I thank Zeyneb Vildan Çakıl for her support and for always sharing my excitement.

I also wish to express my thanks to Nergis İlayda Baygın for her exciting and funny stories throughout the times when the research was immeasurable and for drawing the figures in photoshop.

I am grateful to Ömer S. Fesli for his constant support, encouragement, sacrifices, and eternal patience.

Finally, I am very grateful to my parents. I would like to thank my father, Mustafa Baygın, for his tenacity and for sharing my dreams. He always gave me encouragement, love, and guidance through my education. I learned dedication and perseverance from him, and I always admire his foresight. I wish to express my deep appreciation to my mother, Emine Baygın, for her emotional support, for sharing my enthusiasm, and for being at my side during all my hard times. I thank my lovely brother Güneş for his quick travels and for sharing my Ankara journey. They had been there for me my entire life, and I would not be the person I am today without their love.

This work is funded by the Scientific and Technological Research Council of Turkey under grant number TUBİTAK 118C197.

TABLE OF CONTENTS

ABSTRACT v

ÖZ vii

ACKNOWLEDGMENTS x

TABLE OF CONTENTS xii

LIST OF TABLES xvi

LIST OF FIGURES xvii

1 INTRODUCTION 1

1.1 Colorectal Cancer 1

1.2 Evolutionary Tracking of Drug Resistance by Barcoding 6

1.3 The Barcode library 9

1.4 Kras signaling 10

1.5 Braf signaling 13

1.6 Development of Drug Resistance 15

1.7 Chemotherapeutics 17

1.8 Targeted Drugs 19

1.9 Collateral Sensitivity 20

1.10 Drug combinations 23

1.11 The aim of the study 24

2 MATERIALS AND METHODS 25

2.0 Cell Line Characteristics 25

2.1 Cell Lines and Growth Conditions 25

2.2 Transformation 26
2.3 Determining of Minimum Lethal Dose of Puromycin 26
2.4 Generation of Lentiviruses 26
2.5 Transduction 27
2.6 Generation of Barcoded Cells 27
2.7 Proliferation Assay 28
2.8 MTT Assay 29
2.9 Determining Chemotherapeutic Dosages 29
2.10 Developing Stable Drug-Resistant Cell Lines 29
2.11 Determining Drug Sensitivity on Resistant Cell Lines 31
2.12 Determining Synergistic Effect 31
2.13 Colony Formation Assay 31
2.14 Total Protein Isolation 32
2.15 Western Blot 32
2.16 Statistical Analysis 33
2.17 Analysis of Barcodes 34
2.18 Wound healing assay 35
3 RESULTS AND DISCUSSION 37
3.0 Generation of Barcoded Cells 37
3.1 Effects of barcode vector on cellular proliferation 40
3.2 Determining chemotherapeutic dosages 41
3.3 Developing capecitabine resistance in HCT-116 cells 44
3.4 The Barcode Analysis of Capecitabine Resistant Barcoded HCT-116 cells 46

3.5 Developing dabrafenib resistance in barcoded HT-29 cells 51

3.6 Barcode analysis of Dabrafenib resistant HT-29 cells..... 54

3.7 Developing SN-38 resistance in barcoded HT-29 cells..... 59

3.8 Barcode analysis of SN-38 resistant HT-29 cells 61

3.9 Tracking the SN-38 resistance dynamics in barcoded HT-29 cells..... 66

3.10 Investigation of capecitabine resistance effect on the proliferation 69

3.11 Investigation of dabrafenib and SN-38 resistance effect on the proliferation 71

3.12 Effect of capecitabine resistance on drug sensitivity..... 73

3.13 Effect of dabrafenib resistance in HT-29 cells on drug sensitivity..... 76

3.14 Effect of SN-38 resistance in HT-29 cells on drug sensitivity 79

3.15 The investigation of changes in the MAPK pathway in relation to capecitabine resistance in HCT-116 cells..... 83

3.16 The investigation of changes in MAPK pathway in relation to dabrafenib and SN-38 resistance in HT-29 cells 85

3.17 Inhibition strategies for activation of p-ERK on dabrafenib-resistant HT-29 cell line 87

3.18 Investigation of the synergistic effect of chemotherapeutics on dabrafenib-resistant HT-29 cells..... 89

3.19 Inhibition strategies for activation of p-ERK on SN-38-resistant HT-29 cell line 92

94

3.20 Effect of dabrafenib and SN-38 resistance on clonogenic capacity 95

3.21 The investigation of motility capacities on Dabrafenib and SN-38 resistant HT-29 cells 97

4 CONCLUSION AND FUTURE DIRECTIONS.....101

REFERENCES 105

LIST OF TABLES

TABLES

Table 2. 1 List of antibodies used in this study. 33

Table 3. 1 The table of comparison for IC50 and drug resistance fold of capecitabine. 46

Table 3. 2 The table of comparison for IC50 and drug resistance fold of dabrafenib. 53

Table 3. 3 The table of comparison for IC50 and drug resistance fold of SN-38... 61

LIST OF FIGURES

FIGURES

Figure 1. 1 Drug resistance mechanism 4
Figure 1. 2 Tumor heterogeneity..... 5
Figure 1. 3 Barcoding of cells 7
Figure 1. 4 The barcode vector 9
Figure 1. 5 Kras signaling pathway 12
Figure 1. 6 Braf family and activation of Braf signaling pathway..... 13
Figure 1. 7 Biological determinants of drug resistance..... 17
Figure 1. 8 The list and target of chemotherapeutics for CRC 20
Figure 1. 9 Collateral sensitivity shown..... 22
Figure 2. 1 Representation of cellular barcoding. 28
Figure 2. 2 The experimental design of development of drug resistance. 30
Figure 2. 3 Schematic representation of the reads……..34
Figure 3. 1 Puromycin kill curves of A in HCT-116 and B in HT-29…….. 38
Figure 3. 2 The determination of virus amount..... 39
Figure 3. 3 The images of barcoded HCT-116 and barcoded HT-29 40
Figure 3. 4 The effects of barcode vector on cellular proliferation of HCT-116 and HT-29 cells..... 41
Figure 3. 5 The dose-response curves of chemotherapeutics..... 43
Figure 3. 6 Dose-response curve and comparison of IC values of capecitabine in barcoded HCT-116 cell lines 45
Figure 3. 7 Barcoding sequence results of capecitabine-resistant barcoded HCT-116 cells 51
Figure 3. 8 Dose-response curve and comparison of IC values of dabrafenib in barcoded HT-29 cells..... 53
Figure 3. 9 Barcoding sequence results of dabrafenib-resistant barcoded HT-29 cells. 58

Figure 3. 10 Dose-response curve and comparison of IC values of SN-38 in barcoded HT-29 cells 60
Figure 3. 11 Barcoding sequence results of SN-38-resistant barcoded HT-29 cells 65
Figure 3. 12 Temporal frequencies for the floating barcodes in replicate A of SN-38 treated barcoded HT-29 68
Figure 3. 13 The effects of capecitabine resistance in proliferation 70
Figure 3. 14 The effects of dabrafenib and SN-38 resistance in proliferation 72
Figure 3. 15 The effect of capecitabine resistance in HCT-116 cells in the exposure of irinotecan, oxaliplatin, and SN-38 drugs 74
Figure 3. 16 The effect of dabrafenib resistance in HT-29 cells in the exposure of SN-38, oxaliplatin, capecitabine, and irinotecan drugs 78
Figure 3. 17 The effect of dabrafenib resistance in HT-29 cells in treating irinotecan, capecitabine, oxaliplatin, and dabrafenib drugs 81
Figure 3. 18 Expression of p-ERK, p-MEK, and p-EGFR in barcoded HCT-116, barcoded HCT-116 DMSO, and capecitabine-resistant barcoded HCT-116 cell lines with western blot 84
Figure 3. 19 The protein levels of p-ERK, p-MEK, and p-EGFR in barcoded HT-29, barcoded HT-29 DMSO, dabrafenib-resistant barcoded HT-29, and SN-38-resistant barcoded HT-29 86
Figure 3. 20 The synergistic effect of SCH77982 and dabrafenib in barcoded HT-29, barcoded HT-29 DMSO, and dabrafenib-resistant barcoded HT-29 cells. 88
Figure 3. 21 The cell viability results from a combination of capecitabine and oxaliplatin 90
Figure 3. 22 The cell viability results from the combination of dabrafenib and oxaliplatin 91
Figure 3. 23 The synergistic effect of SCH77982 and SN-38 in barcoded HT-29, barcoded HT-29 DMSO, and SN-38-resistant barcoded HT-29 cells 94
Figure 3. 24 The effects of dabrafenib and SN-38 resistance on clonogenic capacity in HT-29 cells 97

Figure 3. 25 Effect of dabrafenib and SN-38 resistance on the motility of HT-29 cells 99

CHAPTER 1

INTRODUCTION

Cancer is a complex disease defined as the rapid formation of abnormal cells that can grow, invade, and spread (Hanahan & Weinberg, 2000). Carcinogenesis's evolution occurs with genetic and epigenetic alterations (Fouad & Aanei, 2017). Accumulating these alterations is the main reason for transforming malignant cells from normal cells (Hanahan & Weinberg, 2000). Self-sufficiency in growth signals, evading apoptosis, insensitivity to anti-growth signals, sustained angiogenesis, tissue invasion and metastasis, limitless replicative potential, reprogramming energy metabolism, and evasion of immune destruction is crucial alterations found for malignant growth (Hanahan & Weinberg, 2011), (Hanahan & Weinberg, 2000).

1.1 Colorectal Cancer

Colorectal cancer (CRC) accounts for second with 9.4% in terms of mortality and third with 10% out of all cancers (Sawicki et al., 2021). Lifestyle, body fatness, and dietary patterns such as consumption of alcohol, cigarettes, red and processed meat can cause an increase in morbidity. The survival of colorectal cancer depends on the diagnosed stage, with earlier stage diagnosis having a 90% survival rate (Q. Wang et al., 2022).

1.1.1 Risk Factors

There are three main risk factors associated with colorectal cancer. Firstly, family and personal medical history related to inherited genetic factors. Having

inflammatory bowel disease (IBD), colon polyps, diabetes mellitus, and cholecystectomy increase the risk of CRC. Secondly, lifestyle has an essential role in developing carcinogenesis. It impacts anti-inflammatory properties, oxidative and retinoic acid metabolism, antioxidants, and releasing factors, including hormones and cytokine secretions (Sawicki et al., 2021). Dietary patterns like a diet high in red and processed meat, a diet low in fiber, fruits, and vegetables, and a diet low in calcium, vitamin D, and dairy products are associated with the risk of developing colorectal cancer. Finally, gut microbiota, age, gender, and race influence the risk of developing CRC (Sawicki et al., 2021).

1.1.2 Signaling Pathways

Different signaling pathways play a crucial role in CRC pathogenesis, and it is a heterogeneous disease that depends on clinical and histopathological information. According to The Cancer Genome Atlas project (TCGA), three groups were identified in CRC based on genomic and transcriptomic characterization: ultramutated cancers, chromosomal instability, and hypermutated cancers (Caputo et al., 2019).

Ultramutated cancers in 3% of CRC patients are related to incorrect nucleotides at DNA replication by DNA polymerase (Hino et al., 2019). The change in the chromosomal instability pathway (CIN pathway) gene is responsible for 70-85% of all CRC cases (Velho et al., 2008) K-ras is one of the genes that are essential for the serrated pathway (Domenica et al., 2019). Change in the KRAS gene cause inactivation of tumor suppressors and the activation of oncogenes. Microsatellite instability (MSI) is related to hypermutated cancers. Microsatellite unstable (MSI) colorectal tumors are sporadic and inherited forms and are associated with repetitive and non-repetitive sequence mutations (Caputo et al., 2019). The repetitive sequences are targets of defective mismatch repair systems. KRAS and BRAF gene mutations are non-repetitive sequence mutations of sporadic colorectal cancer (CRC)

(Domenica et al., 2019). In 45% of CRC patients, KRAS mutations are observed, while BRAF mutations are observed in 10% of CRC patients (Hino et al., 2019).

1.1.3 The cancer therapies

One major problem in cancer therapies is the development of resistance to chemotherapeutic agents and targeted drugs (Q. Wang et al., 2022). Genetic mutations, epigenetic changes, and cellular and molecular mechanisms during drug efflux lead to pharmaceutical treatment tolerance in various types of cancer (X. Wang et al., 2019). The chemotherapeutic agents cause DNA damage to block cancer growth and proliferation; however, it has relatively high toxicity since the non-specificity of cancer cells (Caputo et al., 2019). Targeted drugs were developed to overcome this problem and to block cancer growth and proliferation precisely where these drugs showed a significant effect during the initial treatment (Q. Wang et al., 2022). Although chemotherapeutics and targeted drugs are good options for cancer treatment, most patients develop resistance.

Drug resistance can be categorized depending on the time it is developed: acquired or intrinsic resistance (Zugazagoitia et al., 2016). Acquired resistance gradually diminishes the anticancer effect of a drug during drug treatment (Chan et al., 2017). Changes in the tumor microenvironment can cause the activation of the second proto-oncogene, mutations, or altered expression levels of drug targets (X. Wang et al., 2017). Intrinsic resistance exists before the drug treatment, and it can reduce the therapy efficiency (Pluchino et al., 2012). Pre-existing genetic mutations, tumor heterogeneity, and intrinsic pathways activation can lead to intrinsic resistance (Pluchino et al., 2012). Both acquired and intrinsic resistance mechanisms can exist in tumor progression and, notably in cancer treatment (Saus et al., 2019).

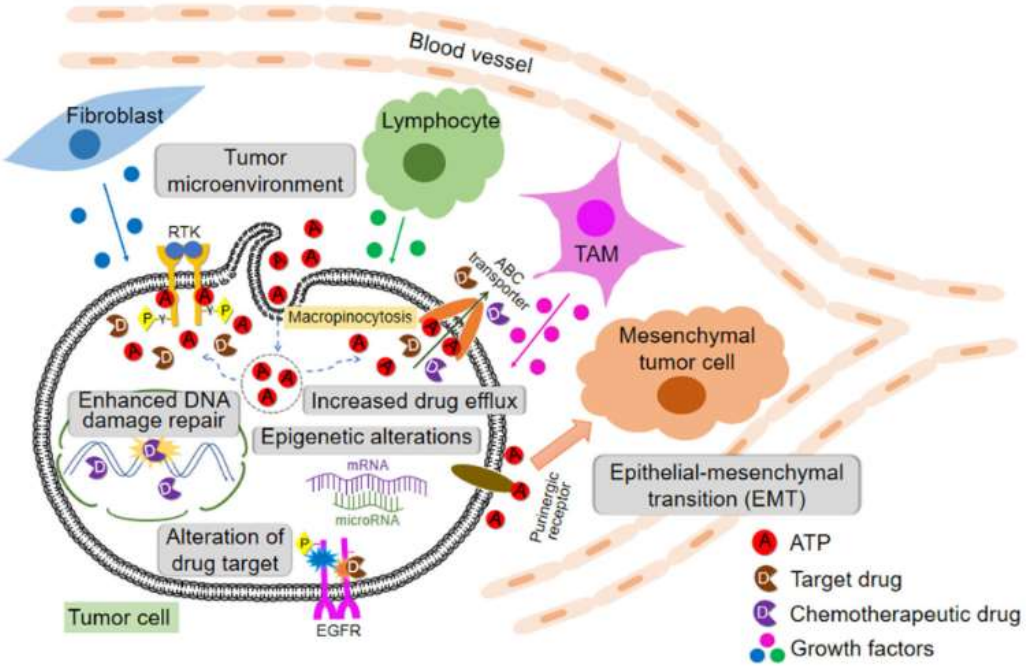

Figure 1. 1 Drug resistance mechanism (X. Wang et al., 2019)

Tumors are heterogeneous and can be situated in various effects, including the basement membrane, vasculature, immune cells, and tumor microenvironment, among other components. Changes in the tumor's physical parameters, genome, and surrounding environment drive drug resistance

1.1.4 Tumor Heterogeneity

Tumor heterogeneity contributes to drug resistance and therapeutic failure (M Greaves, 2015). Genetic heterogeneity, metabolic heterogeneity, phenotypic heterogeneity, and temporal heterogeneity are the levels of heterogeneity (X. Wang et al., 2019). Both genetic alterations and epigenetic mechanisms, including chromatin remodeling, DNA methylation, and post-translational modifications of histones, lead to intra-tumor heterogeneity (M Greaves, 2015). Selection and Darwinian evolution have an essential impact on intratumor heterogeneity (ITH) (M

Gerlinger, 2010). The composition of genomic heterogeneity consisted of tumor subclones populations under the drug treatment changes at different stages based on the Darwinian selection manner pressure (Mel Greaves & Maley, 2012).

Tumor tissues s consist of cancer cells, various types of cells such as fibroblasts, immune cells, and extracellular matrix (ECM) (D'Angelo et al., 2020). Tumor growth and survival depend on ECM, blood vessels, fibroblast, immune and inflammatory cells, and signaling molecules (Sugimoto et al., 2006). Studying the tumor microenvironment is essential to understand why the tumor niche develops resistance to therapy, especially intrinsic resistance (Pluchino et al., 2012). It can mediate resistance through stimulating paracrine growth factors, immune clearance of tumor cells, and hindering drug absorption (Sharma et al., 2017).

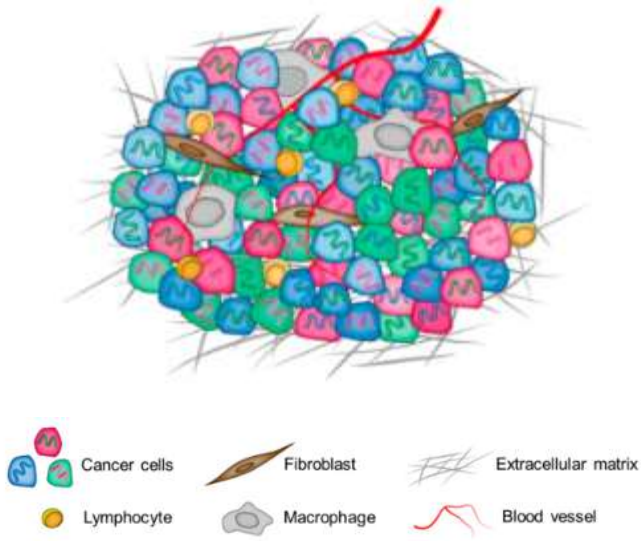

Figure 1. 2 Tumor heterogeneity (Lin & Lin, 2019)

Genomic and epigenomic heterogeneity by phenotypically distinct cells and microenvironmental components were shown.

The composition of the tumor microenvironment can change after treatment which causes reducing drug efficacy (Costa et al., 2018). Tumor cells can shape the microenvironment according to their favorable growth environment in terms of

hypoxia, acidosis, immune predation, and resource limitations (McGranahan & Swanton, 2017).

Epigenetic changes and genetic heterogeneity cause phenotypic variation between cancer cells (Östman & Augsten, 2009). Clonal evolution is a necessary process not only for intra-tumor heterogeneity but also for driving tumor initiation, progression, and treatment resistance (McGranahan & Swanton, 2017). In tumor evolution, mutations, genetic drift, and selection are crucial, and chromosomal instability is central to it (McGranahan & Swanton, 2017).

1.2 Evolutionary Tracking of Drug Resistance by Barcoding

The evolution of large cell populations depends on mutational, circulating nucleic acids (CNA), and single nucleotide variants (SNV) (Hino et al., 2019). These determinants facilitate cancer progression and drug resistance (Hino et al., 2019). A quantitive method is needed to understand which mutations, CAN, and SNV are the underlying components of this evolution. A quantitative understanding of the evolutionary dynamics can determine which mutations, CNA, and SNV, are higher in population fitness and contribute to resistance development.

The net outcome of beneficial mutation rates is a critical concept both in large and small populations, many beneficial mutations occur in the population, and one can compete with one another (Blundell & Levy, 2014). Clonal interference, which diminishes the effect of one mutation on the population, is crucial for small populations (Mel Greaves & Maley, 2012). Thus, even in low frequencies, adaptive mutations impact the evolutionary dynamics (Blundell & Levy, 2014).

Barcoding of the genome provides lineage tracking of evolution and drug resistance (Blundell & Levy, 2014). The specific identity of mutations and their fitness effect and times of occurrence can be measured by barcoding the genome with unique random DNA sequences (Kebschull & Zador, 2016).

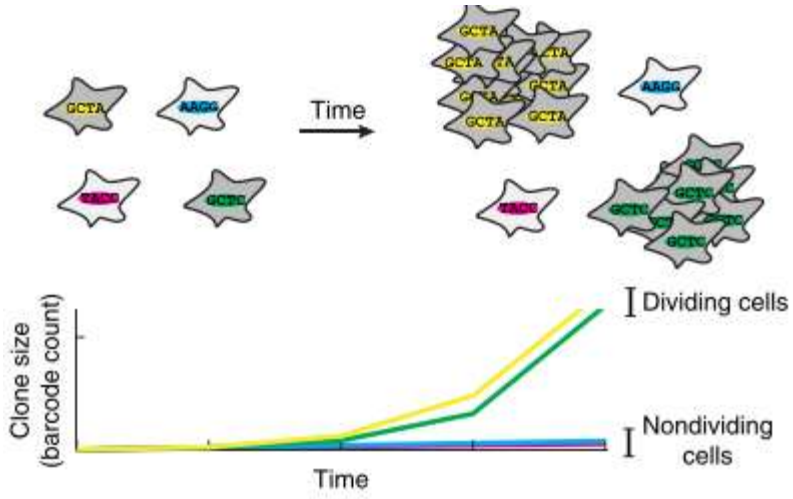

Figure 1. 3 Barcoding of cells (Kebschull & Zador, 2018)

The cells contain different barcodes to allow tracking during evolution.

Population size and mutation rate are crucial to determine the mutation's fitness which shows the expanding time of a mutation in a population since the impact of beneficial mutations could be different on evolutionary dynamics (Blundell & Levy, 2014). Indeed, in small and large populations, the accumulation of beneficial mutation is different (Blundell & Levy, 2014). In large populations, the effect of a mutation occurs relatively quickly (Levy et al., 2015). Therefore, the fitness effects on the population size and the mutation rates impact evolutionary dynamics (Levy et al., 2015).

The beneficial mutations are rare, and when a small lineage is found in the population, the frequency of mutation can be increased by genetic drift (Blundell & Levy, 2014). The lineage trajectory can be used to find the properties of the mutation (Levy et al., 2015).

There are limitations to the sequencing of the population. The frequency of mutations can give a clue about dynamics. In large populations, low-frequency mutations, which were observed at less than 1%, play a crucial role in driving the evolutionary dynamics, and they could be abundant (Blundell & Levy, 2014). Because linkage information does not exist for population sequencing, there is no information about

specific genotypes found in the population (Blundell & Levy, 2014). The relative frequencies can detect small indels and single nucleotide polymorphisms in the population (Levy et al., 2015). Replicate sequencing will be a powerful way to study the evolutionary process; however, there is still a challenge in observing alleles that exist at low frequencies (Blundell & Levy, 2014).

Genetically incorporated stable, heritable and sequence-able barcodes can be used to determine lineage tracking (Kebschull & Zador, 2016). Some critical points for creating a barcode library include no misidentification of one barcode with another, no generation of erroneous restriction sites, and having constant and low complexity surrounding regions for being easily sequence-able by next-generation sequence (NGS). Also, there should be spacers between random regions to differentiate barcode DNA from the host DNA.

Understanding the dynamics of tumor growth, metastasis, and drug resistance in cancer and determining the cellular evolutionary process is a great hallmark; however, the major challenge is determining which mutations represent beneficial mutations and which represent pre-existing, neutral, and deleterious mutations (Acar et al., 2020). These classifications are essential for determining the drivers of drug resistance in cancer. The sequencing of the initial and drug-resistant population with NGS can show why the resistance to chemotherapeutics exists. These can be caused by mutations found as pre-existing resistant, sensitive, and de novo mutations (Acar et al., 2020). These types are determined accordingly to the computational analysis of barcode sequences and comparing replicates.

1.3 The Barcode library

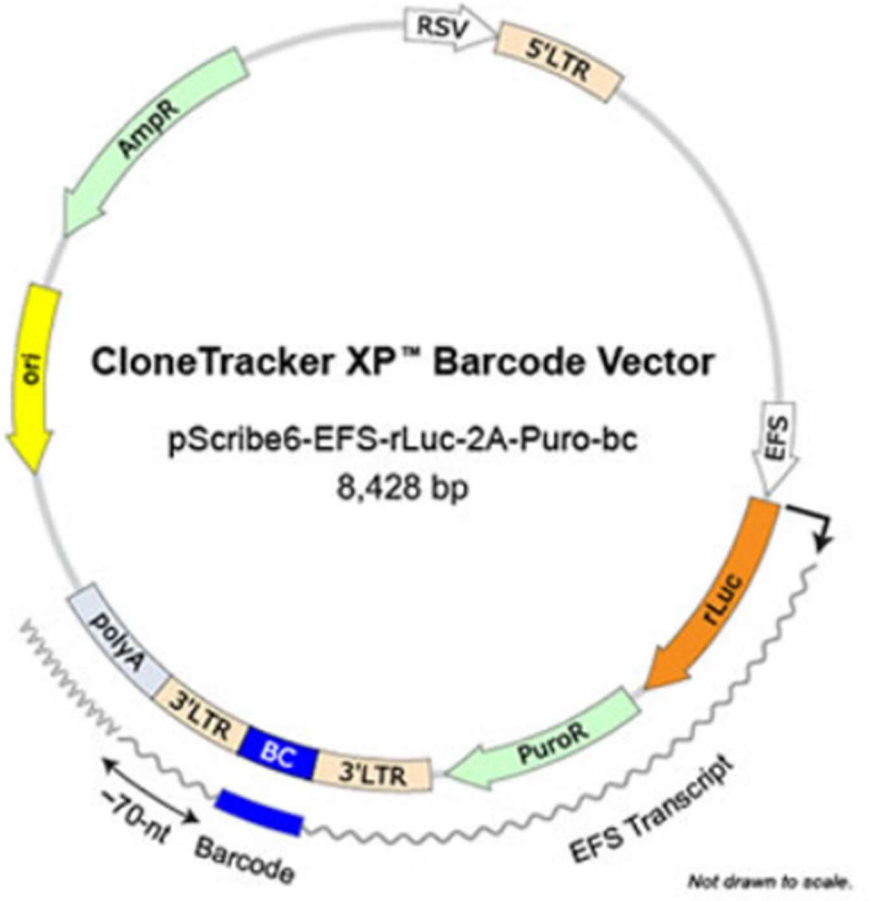

Figure 1. 4 The barcode vector

CloneTracker XP™ 1M Barcode-3' Library Pool 1 with RFP-Puro.

The vector provides tracking of individual clones with using Next-Gen Sequencing (NGS) via genomic DNA or RNA-seq. The library contains one million unique lentiviral constructs that express unique barcode sequences. The barcodes integrate into the genomic DNA of host cells through transducing of barcode library and it provides cells to have different DNA-sequenceable barcodes in nearly every cell in the population. The barcode is stably integrated, and it is passed onto any cell progeny during DNA replication which provides tracking of all the progeny derived from each individual cells.

The barcode library can be used to identify expression profiles with single-cell RNA-Seq. The barcode vector contains promoter region and poly A tail for barcode transcription. Promoter region is crucial for transcription initiation and poly A tail makes the RNA molecule more stable and prevents its degradation and plays significant role in mRNA molecule exportation from the nucleus and translated into a protein by ribosomes in the cytoplasm. Different cells can activate different signaling pathways and clonal populations of cells from a single progenitor can be identified by cellular barcoding.

The barcode library is in a lentiviral vector that express TagRFP and Puro resistance genes under an EFS promoter. The barcode vector contains 48 bp including the barcode region consisting of 14 bp region, four by linker region, and 30 bp Celesta barcode region. Through this technology barcode identification using NGS analysis can be performed from genomic DNA can be achieved.

The barcode library can be used for identification of genetic heterogeneity of cell populations since it facilitates heritable, stable, and sequenceable barcodes in every individual cell of population. The barcoded cells treated, grown for several passages, frozen and thawed and the lentiviral vector that contains barcode sequence remain in the host cell. Thus, it can be used in identifying and quantifying barcodes present in the selected cell population after drug treatment.

1.4 Kras Signaling

KRAS is a proto-oncogene, and it encodes a small GTPase transductor protein KRAS (Liu et al., 2019). RAS superfamily is a group of guanosine triphosphate (GTP) binding proteins. The three RAS genes encoding the RAS proteins, HRAS, NRAS, and KRAS, are the most frequently mutated in cancer (Waters & Der, 2018). It ranges from 50% to 60% (L. Liang et al., 2018).

There is an on-off molecular switch for KRAS protein via binding to GTP and guanosine diphosphate (GDP) (L. Liang et al., 2018). The activation mechanism is regulated by guanosine nucleotide exchange factors (GEFs) and GTPase-activating proteins (GAPs) (Waters & Der, 2018). KRAS, predominantly GDP-bound and RAS-GEFs nucleotide binding, releases the nucleotide in the presence of stimulation (Waters & Der, 2018). GTP binding to KRAS causes a conformational change, which activates KRAS interactions with GAPs and affects the GEFs interactions, lead GTP release (Liu et al., 2019). The mitogenic processes can be controlled by receptor tyrosine kinases (RTKs) and other cell-surface receptors activation by RAS-GTP formation that regulates intracellular signaling via effector proteins (Waters & Der, 2018)

There are three mutational hotspots found in the RAS genes. Glycine-12 (G12), glycine-13 (g13), and glutamine-61 (Q61) are the most frequently observed missense mutations that encode single amino acid substitutions (Velho et al., 2008). G12 mutation cause activation of RAS, G13 mutation cause decreased GAP binding and hydrolysis, and mutation at Q61 reduce the hydrolysis rate (Liu et al., 2019).

The crucial cellular processes, especially cell differentiation, growth, chemotaxis, and apoptosis, depend on signaling molecules' activation (Mo & Moschos, 2005). KRAS signaling allows the transmission of the transducing signals from the cell surface to the nucleus (Liu et al., 2019). Three essential processes are found in the activation of KRAS signaling: proper post-translational modifications, plasma-membrane-localization, and interaction with effector proteins (Waters & Der, 2018).

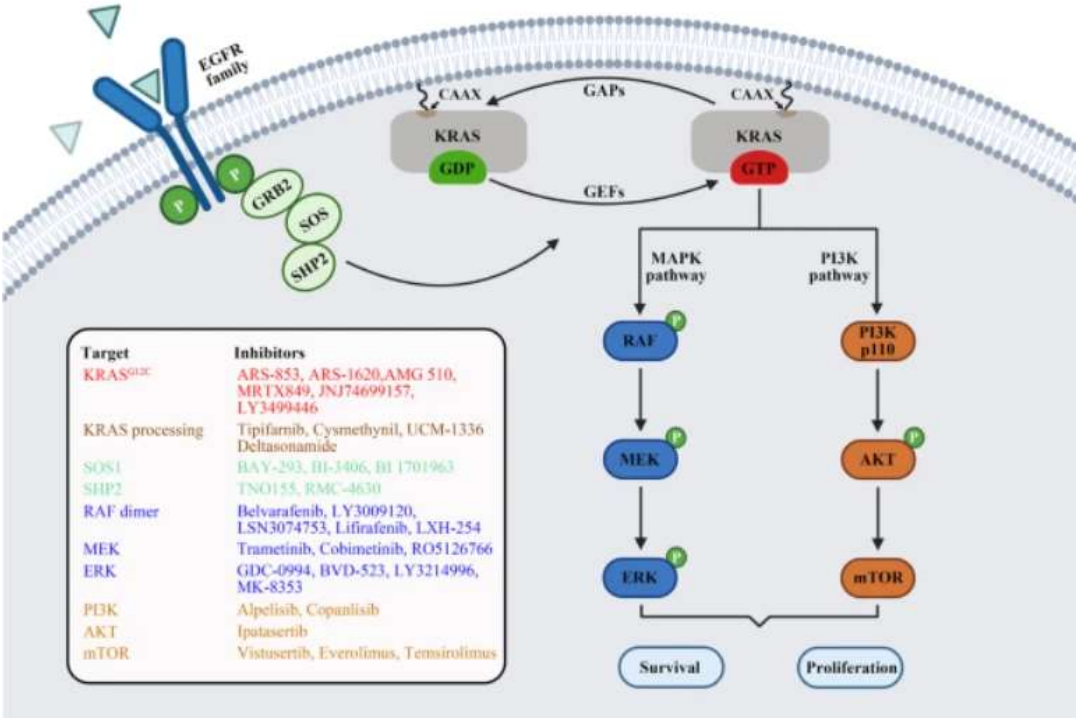

Figure 1. 5 Kras signaling pathway (Zhu et al., 2021)

Receptor tyrosine kinase activation causes GRB2 combination with the guanine nucleotide exchange factor SOS and interaction with KRAS protein. Activation of KRAS regulated by GEFs and GAPs with GTP-GDP cycling. KRAS mutation cause disruption of this cycle and accumulation of active state KRAS. Thus, the downstream MAPK and PI3K signaling cascade cell proliferation and survival.

Activation of KRAS with the conversion from RAS-GDP to RAS-GTP triggers multiple downstream pathways that promote cell growth and survival, such as rapidly accelerated fibrosarcoma (RAF), mitogen-activated protein kinase (MEK), extracellular signal-related kinase (ERK) and phosphatidylinositol 3-kinase (PI3K)-protein kinase B (AKT)- the mechanistic target of rapamycin (mTOR) pathways (Zhu et al., 2021). RAS-GTP can directly bind to RAF protein and activate it, which causes chain phosphorylation/activation reactions to downstream substrates (Zhu et al., 2021).

1.5 Braf signaling

Braf is a signal transduction protein that serine/threonine protein kinase and has a crucial role downstream of the KRAS mitogen-activated protein kinase (MAPK) pathway (Caputo et al., n.d.). Braf gene drives cell proliferation, differentiation, migration, survival, and angiogenesis (Yaeger & Saltz, 2012).

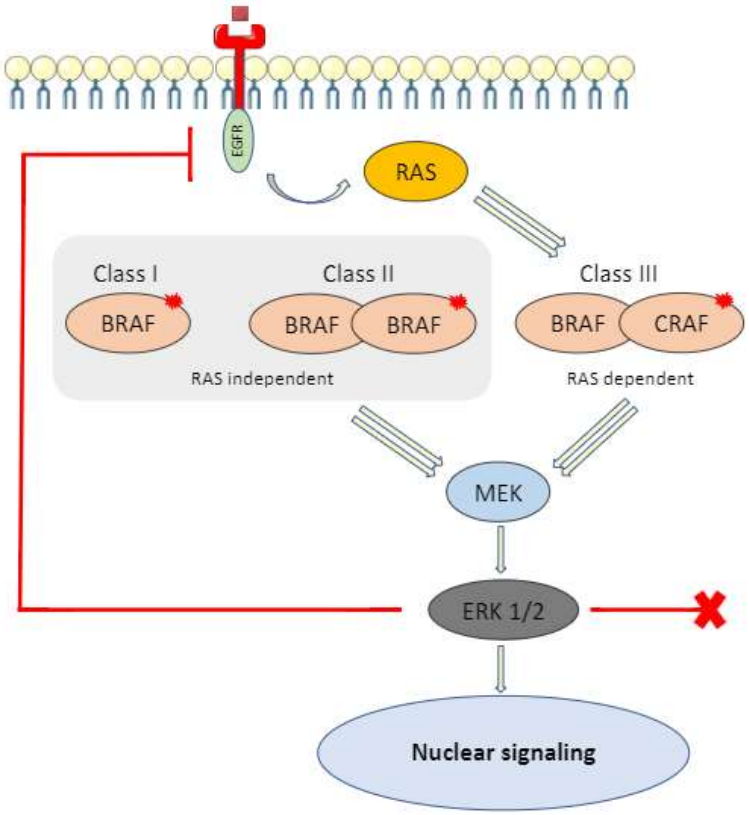

Figure 1. 6 Braf family and activation of Braf signaling pathway (Bellio et al., 2021)

Class, I BRAF mutants capable of signaling via monomers, and Class II BRAF mutants are capable of signaling via dimers. Both of them are RAS independent and enable the activation of MEK and ERK. ERK has a negative feedback response on RAS inactivation by phosphorylation. Class III BRAF mutant is a heterodimer, RAS dependent, and enables MEK and ERK activation. There is no feedback response for RAS inactivation.

RAS small guanidine triphosphatase (GTPase) activates the RAF family proteins, including BRAF (De Falco et al., 2020). Activated BRAF can cause phosphorylation and activation of MEK proteins that lead to phosphorylation and activation of ERKs. Phosphorylated ERK can phosphorylate multiple transcription factors (Caputo et al., 2019). Dysregulation of the MAPK pathway can cause tumorigenesis.

There are three classes of BRAF mutations based on kinase activity and acting as monomers or dimers. Class I mutations, including BRAF ^{V600E} signaling as monomers and Class II mutations as dimers, are RAS independent and cause a gain of function in the MAPK pathway by BRAF kinase activation (Bellio et al., 2021). Class III mutations are RAS-dependent and amplify ERK signaling by impaired BRAF kinase activity (Schaufler et al., 2021). Both Class I and Class II mutations depend on RAS activation for overcoming negative feedback from ERK; however, Class III mutations activate RAS by the high activity of receptor tyrosine kinases (RTKs) (Bellio et al., 2021). Although Class I and II are intrinsically resistant to EGFR inhibitors, Class III mutants can have a higher sensitivity to EGFR inhibitors (Yaeger & Corcoran, 2019). Oncogenic mutations cause both three classes (Bellio et al., 2021).

BRAF ^{V600E} mutation is the most frequent mutation, caused by a valine amino acid substitution with glutamic acid at codon 600 (Chan et al., 2017). It leads to an increase in BRAF activity of about 10-folds compared to wild-type, which increases the stimulation of downstream effector proteins MEK and ERK via phosphorylation (Caputo et al., 2019), (Chan et al., 2017). Thus, BRAF mutations cause melanoma cell survival, proliferation, tumor angiogenesis, and metastasis by ERK signaling pathway (Pratilas et al., 2015).

A patient who has BRAF ^{V600E} mutation can be categorized into two groups according to gene expression profile (Caputo et al., 2019). The first group (BM1) has poorer survival since the high activation of KRAS/mTOR/AKT/4EBP1 signaling and epithelial-mesenchymal transition (EMT) and macrophage infiltration genes

(Caputo et al., 2019). The second group (BM2) is involved with activated cell-cycle checkpoint-associated genes (Caputo et al., 2019).

1.6 Development of Drug Resistance

Chemotherapy, molecular targeted therapy, and immunotherapy are the treatment options for CRC patients. Anticancer drugs have to be metabolized into their active forms and transported to the target location to cause the death of tumor cells (Q. Wang et al., 2022). Highly proliferating intrinsic or extrinsic aggressors lead to drug resistance development (Heydt et al., 2021). Tumor growth, tumor burden, physical barriers, tumor heterogeneity, immune system and tumor microenvironment, therapeutic pressure, and undruggable genome are biological determinants of resistance (Vasan et al., 2019).

Tumor burden and growth kinetics are essential for developing cancer and metastasis since advanced tumors present enhanced metastatic risk (Vasan et al., 2019). Although, according to the Golie-Coldman hypothesis, mutation rate and tumor size significantly impact drug-resistant clones, therapy and resistance cause changes in tumor growth and kinetics (Goldie, 1989).

Tumor heterogeneity results in genetic diversity, and the different genomic alterations cause it through mutation (Chung et al., 2017). Genomic and chromosomal instability have different evolutionary speeds; large chromosomal alterations can cause macro-evolutionary events (McGranahan & Swanton, 2017). Therapeutic pressure has an essential effect on change in tumor phenotype by the disappearance of targeted cellular clones and acquisition of new mutations (Vasan et al., 2019). Thus, in the presence of selection pressure, these mutational processes lead to tumor heterogeneity (N McGranahan, 2017).

Effective exposure to a drug from a tumor is affected the physical barriers of a tumor (Vasan et al., 2019). The tumor cells create a hypoxic environment and prevent

adequate blood flow. These situations diminish the efficiency of drug exposure and therapy resistance (Jain, 2005).

Immune cells, stroma, fibroblast cells, and vascularity are the composition of the tumor microenvironment (Hanahan & Weinberg, 2011). The tumor microenvironment can cause drug resistance by hindering drug absorption, and immune clearance, and stimulating growth factors, especially paracrine growth factors. Immune evasion and immunosuppressive cancer microenvironments can lead to the failure of immunotherapy (Sharma et al., 2017).

Selective therapeutic pressure and undruggable genomic drivers can cause the failure of treatment (Mel Greaves & Maley, 2012). Although some target oncogenic driver mutations exist, undruggable tumor suppressor genes remain (Vasan et al., 2019). The pressure of chemotherapy and radiotherapy induces immune responses and increases genomic instability (Q. Wang et al., 2022). This situation contributes to the acquired resistance. Negative feedback mechanisms and epigenetic modulations are found in the early adaptive stage of these changes (Sun & Bernards, 2014).

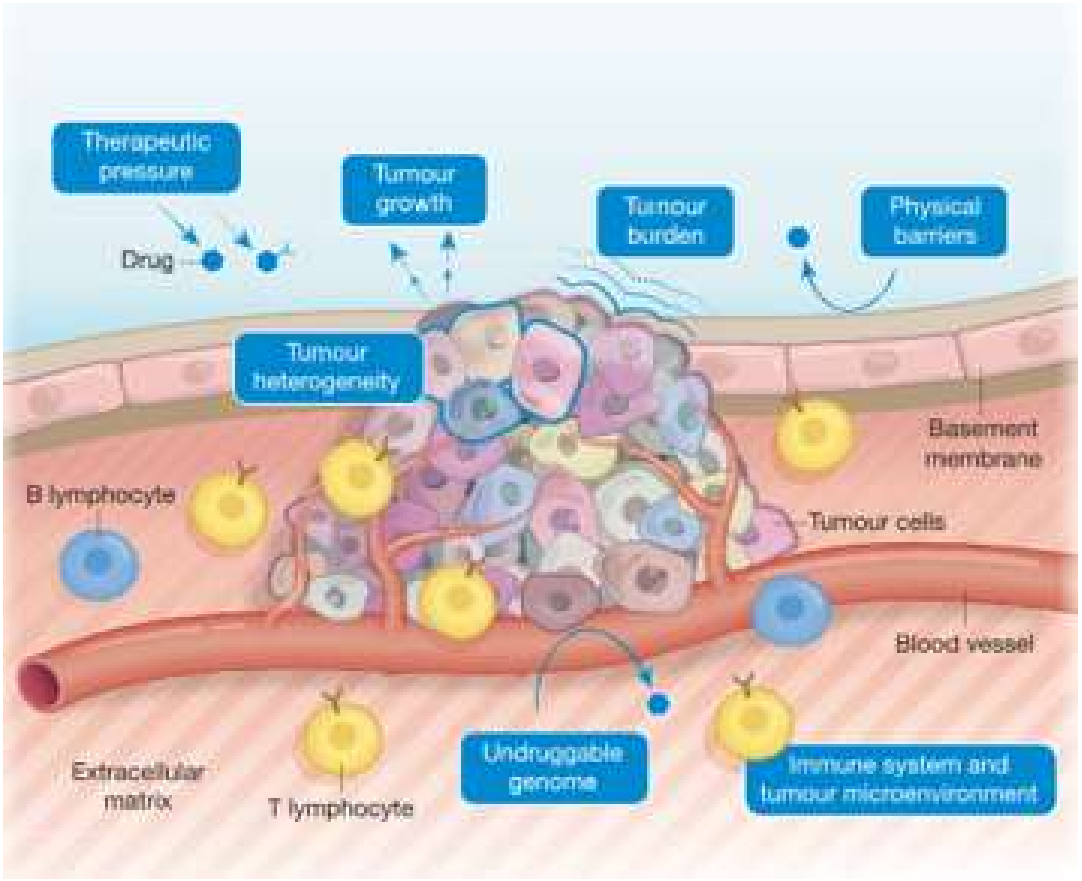

Figure 1. 7 Biological determinants of drug resistance (Vasan et al., 2019)

Developing drug resistance depends on some biological parameters, especially changes in genome and environment, tumor heterogeneity, tumor growth, tumor microenvironment, and physical pressure.

1.7 Chemotherapeutics

Chemotherapy or surgery supplemented with chemotherapy is used in treating CRC patients (Q. Wang et al., 2022). 5-fluorouracil, capecitabine, irinotecan, and oxaliplatin are chemotherapeutic agents used in treating CRC patients (Shao et al., 2022). These drugs are metabolized into their active form and transported to the target location to eradicate tumor cells (Shao et al., 2022).

1.7.1.1 Capecitabine

Capecitabine is cytotoxic via inhibition of DNA synthesis (Mcgavin et al., 2001). It is activated in cells by transforming its active form of 5-fluorouracil (5-FU) to maximize the anti-tumor effect (Shao et al., 2022). This process is mediated by thymine phosphorylase (TP), a tumor-associated angiogenesis factor, and its expression promotes tumor growth (Q. Wang et al., 2022). 5-FU inhibits the thymidylate synthase (TS) and binds DNA and RNA (Q. Wang et al., 2022). Fluorudeoxyuridine monophosphate (FdUMP) and fluorouridine triphosphate (FUTP) are the catabolized molecules of fluorouracil, which are cytotoxic as they inhibit thymidylate synthase and get incorporated into RNA as false nucleotides (Mcgavin et al., 2001). Thus, the anti-DNA mechanism and anti-RNA effects are the anti-tumor mechanisms of fluorouracil. The capecitabine sensitivity in tumors is related to TP's activity and expression (Van Cutsem et al., 2005). Capecitabine or 5-FU resistance in CRC is associated with the lower expression of metabolic enzymes that has a crucial role in the transformation of active anticancer metabolites (Van Cutsem et al., 2005). There is a three-step enzymatic reaction found in cells. Orotate phosphoribosyl-transferase (OPRT), uridine monophosphate (UMP) synthetase (UMPS), and UMP kinase (UMPK) are essential enzymes for this transformation (Q. Wang et al., 2022).

1.7.1.2 Irinotecan

Irinotecan inhibits DNA replication and transcription via topoisomerase 1 (TOP-1), an essential nuclear enzyme during DNA replication and transcription. Irinotecan is a pro-drug and its active metabolite is SN-38 (Jensen et al., 2016). Carboxylesterase 2 (CES2) is crucial for this conversion, and its expression is related to irinotecan sensitivity in CRC (Q. Wang et al., 2022). Some metabolites such as uridine diphosphate glucuronosyltransferase 1A1 (UGT1A1), β-glucuronidase, and cytochrome P450-3A4 (CYP3A4) can cause resistance to Irinotecan or its activated

form SN-38 (Q. Wang et al., 2022). Low Top1 expression can also be a mediator of drug resistance since it has a vital role in genetic mutations, gene copy number alterations, mRNA and protein expression levels, and enzyme activity levels which significantly impact the sensitivity to treatment (Jensen et al., 2016). Therefore, resistance to SN-38 is directly correlated with Top1 activity via mutations or DNA methylation (Jensen et al., 2016).

1.8 Targeted Drugs

Rather than chemotherapies that disrupt rapid cell proliferation and kill cells, targeted therapies inhibit the specific target protein and prevent the growth of cancer cells (C. Wang et al., 2019). However, the alteration of drug targets with a secondary mutation in the target protein or epigenetic alterations in its expression can cause the development of resistance (X. Wang et al., 2019).

1.8.1.1 Dabrafenib

Dabrafenib is a BRAF V600E-specific inhibitor that disrupts the RAF/MEK pathway (Kirouac et al., 2017). Dabrafenib has a five-membered heterocyclic group with a central ring locking and an affinity to binding BRAF; therefore, there is reversible competitive inhibition of potent adenosine triphosphate, which selectively inhibits the BRAF (V600E) kinase domain (H. Wang et al., 2017). Although BRAF inhibitors inhibit the target in all cells, V600E BRAF inhibitors inhibit only mutated BRAF protein -which is monomer-not the wild-type BRAF – dimer- (Chan et al., 2017). Thus, this can be the main reason for developing drug resistance since negative feedback on MAPK pathway inhibition causes the formation of Raf dimers and resistance to RAF inhibitors (Heidorn et al., 2010).

Activation of MEK/ERK (which is found downstream of RAS/RAF) causes survival and cell proliferation in RAF mutated cells (Kirouac et al., 2017). ERK inhibition can inhibit the proliferation of CRC cells (Kirouac et al., 2017). Targeting multiple

agents of the MAPK pathway in CRC can enhance the anti-tumor effect of the treatment (H. Wang et al., 2017). In the presence of an ERK inhibitor, targeting BRAF has a synergetic effect (Q. Wang et al., 2022). Thus, RAF inhibitors, in combination with ERK inhibitors, can play a crucial role in BRAF V600E mutated tumors. An ERK inhibitor, SCH772984, can inhibit MAPK signaling and enhance treatment sensitivity in CRC patients (Q. Wang et al., 2022).

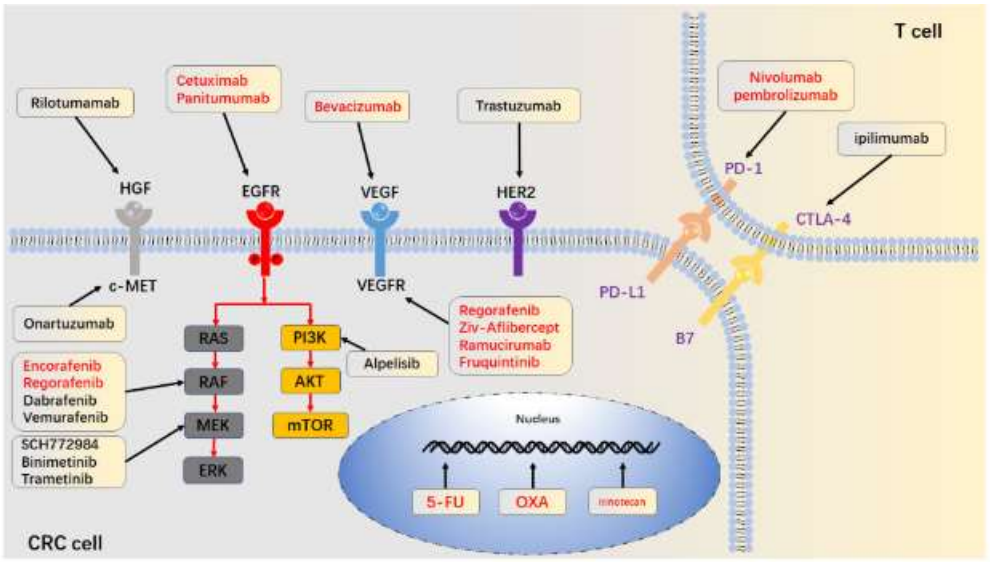

Figure 1. 8 The list and target of chemotherapeutics for CRC (Q. Wang et al., 2022)

The targets 5-FU, irinotecan and dabrafenib in cell.

1.9 Collateral Sensitivity

Collateral sensitivity is sensitivity to a drug in therapeutic resistance evolution (Scarborough et al., 2020). Although chemotherapy is a standard treatment for metastatic and hematological malignancies, the development of resistance to chemotherapy is often (Pluchino et al., 2012). The resistant cancer cells can have resistance to other drugs that differ structurally and mechanistically, called multidrug resistance (MDR). In the presence of MDR, cancer cells have less chemotherapy response. Collateral sensitivity can be essential in MDR cell growth and tumor

resensitization (Pluchino et al., 2012). Thus, collateral sensitivity can create an excellent opportunity to improve the ability to target cancer cells.

Cellular alterations include changes in gene and protein expression, reduction in drug accumulation, mutations that decrease the binding of the drug to its target, changes in drug metabolism, and apoptotic signaling diminishing can cause MDR (Gottesman et al., 2002). These cellular alterations can resist a drug and sensitize cells to other drugs. Thus, there can be a positive correlation or negative correlation in the presence of drug resistance. If resistance to a drug cause MDR, it will be a positive correlation; however, if resistance to a drug cause collateral sensitivity, it will be a negative correlation in terms of the fitness landscapes (Scarborough et al., 2020). Therefore, the evolution of one drug resistance can lead to variable changes in the second drug response in cancer cells.

There are four possible putative mechanisms of collateral sensitivity. The first one is the modulation of collateral sensitivity by reactive oxygen species that cause an increased amount of cellular ATP hydrolysis (Hall et al., 2009). In the presence of an increase in the hydrolysis of ATP, cells suffer from oxidative stress because of an increase in ROS production or an indirect result of a decrease in antioxidant defenses (Pluchino et al., 2012). Collateral sensitivity can cause futile hydrolysis of ATP. The second one has increased sensitivity to changes in energy levels by cellular metabolic pathways such as glycolysis or oxidative phosphorylation (Hall et al., 2009). Thus, the agents that affect cellular ATP stores can be used in MDR cells. The third one is extruding endogenous substrates that are needed for cell survival. The collateral sensitivity agents can indirectly facilitate or stimulate the endogenous essential molecules extrusion (Pluchino et al., 2012). The final one is membrane perturbation since some collateral sensitivity agents, such as Triton X detergents, impact the alteration of membrane biophysical properties (Pluchino et al., 2012).

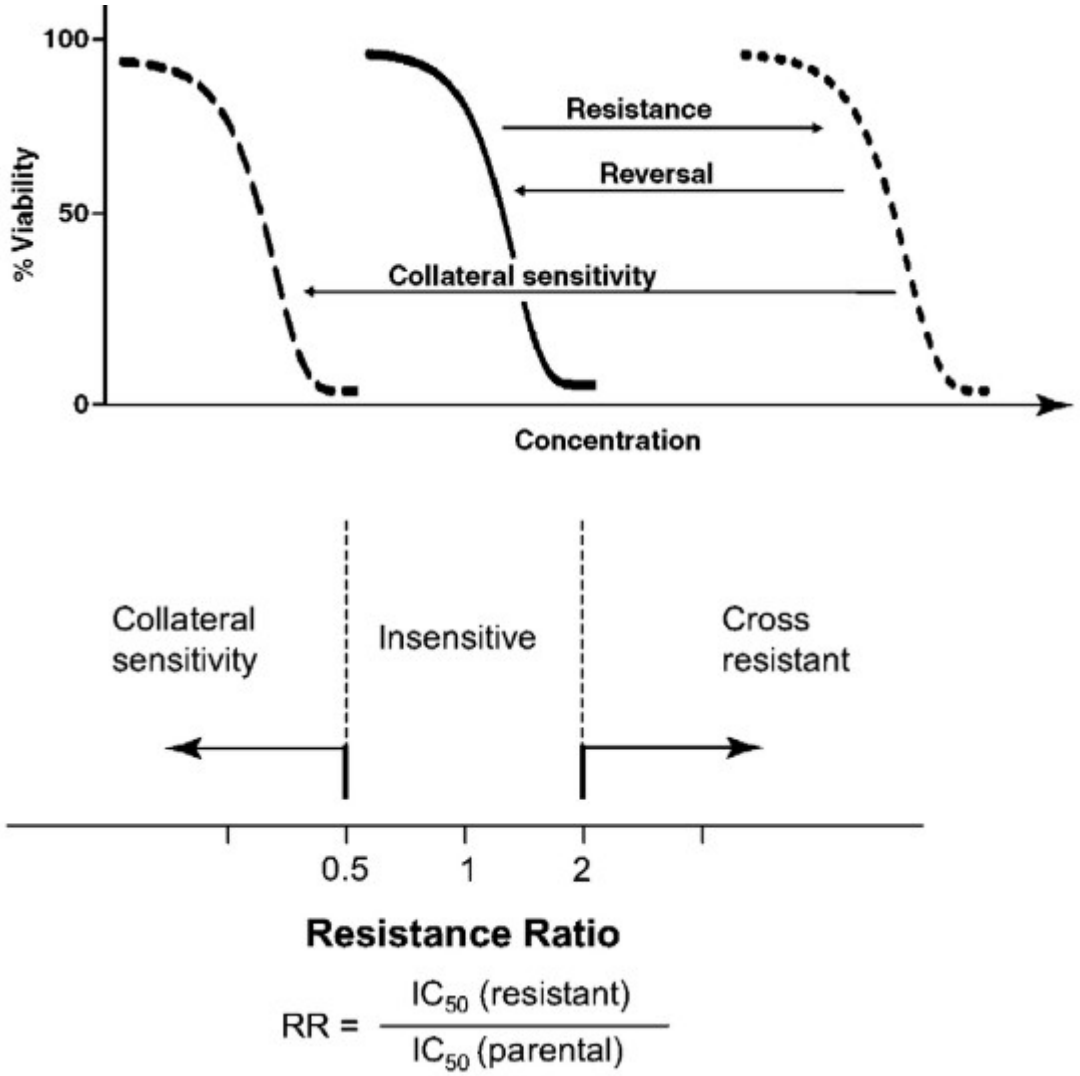

Figure 1. 9 Collateral sensitivity shown (Hall et al., 2009)

Dose-response curve of the representative cell line (solid line belongs to parental cells, and the dotted line belongs to drug-exposed cells (A). Determination of collateral sensitivity and multidrug resistance (B).

Collateral sensitivity can be determined by calculating a drug's cytotoxicity (IC50) and comparing parental and resistant cells (Gottesman et al., 2002). In MDR, the second drug will have lower efficiency in cytotoxic effect against drug-resistant than parental cell lines, that is, cross-resistance (Scarborough et al., 2020). In collateral

sensitivity, the second drug has high cytotoxicity against drug-resistant than parental cell lines (Gottesman et al., 2002).

1.10 Drug combinations

Overcoming drug resistance is challenging since the high heterogeneity during tumor growth and the complexity of tumor progression. Combinational and personalized therapies are required to treat drug resistance since the individual differences in mutations during drug exposure (Yalcin et al., 2020) (C. Wang et al., 2019). The single drug used in therapeutic strategies can cause the death of sensitive cells, but resistant cells survive and proliferate (Mel Greaves & Maley, 2012). On the other hand, combinational therapies use two or more drugs that allow targeting of multiple driver genes at the same time (Bellio et al., 2021). Hence, it creates a more complex environment for cancer cells for selection and growth.

To enhance the chemotherapeutic effect of drugs on colorectal cancer patients, chemotherapy with oxaliplatin combinations can be used (Hattori et al., 2019). The combination treatment can be used in the second-line therapy in advanced colorectal cancer cells after a treatment failure. In second-line therapies, oxaliplatin-based doublets could be utilized (Guglielmi et al., 2007). Oxaliplatin combinations with capecitabine, irinotecan, or dabrafenib are highly used in CRC (Lurie et al., 2021).

According to NCCN colon cancer guidelines, 2021, capecitabine and oxaliplatin combination (CAPEOX) can be used in CRC as first and second-line therapy, and it could be beneficial in the presence of metastasis. The response rate of cells increases compared to single-agent therapies under CAPEOX treatment (Guglielmi et al., 2007).

Oxaliplatin, combination with dabrafenib, can be used in BRAF V600E mutated cells. This combination can increase the survival rate of patients with minimal toxicities (D'Angelo et al., 2020). Inhibition of BRAF with MAPK signaling can also

overcome the monotherapy resistance. Thus, a combination of dabrafenib and MEK or ERK inhibitors can increase the survival rate of patients (Williams et al.,2015).

Oxaliplatin, combination with irinotecan (IRINOX,) can be used as second-line therapy in CRC (Lurie et al., 2021). IRINOX treatment can increase the response rate of cancer cells compared to a single chemotherapeutic treatment (Guglielmi et al., 2007). IRINOX treatment could benefit patients with FU or FU prodrug (capecitabine) contraindicated (Guglielmi et al., 2007).

1.11 The aim of the study

This study aimed to investigate the development of drug resistance using the cellular barcoding technology and the reasons behind it such as pre-existing cellular alterations or de novo mutations. This study also aimed at the second-line therapy effect on colorectal cancer cells. HCT-116 and HT-29 cell lines were used for this purpose. To pursue this;

1.) Barcoded the colorectal cancer cells (HCT116 and HT-29) by lentiviral barcodes,
2.) Generated Capecitabine-resistance in HCT-116 cells, Dabrafenib-resistance in HT-29 cells and SN-38-resistance in HT-29 cells,
3.) Assessed secondary drug sensitivity in capecitabine-resistant HCT-116 cells, dabrafenib-resistant and SN-38-resistant HT-29 cells,
4.) Assessed combine therapy effect on dabrafenib resistant and SN-38 resistant HT-29 cells,
5.) Investigated dabrafenib and SN-38 resistance effect on clonogenic capacity in HT-29 cell line,
6.) Assessed the dabrafenib resistance and SN-38 resistance effect on cellular mobility in HT-29 cells.

CHAPTER 2

MATERIALS AND METHODS

2.0 Cell Line Characteristics

According to ATCC, HCT-116 is a colon carcinoma cell isolated from a male. HCT-116 cells carry a mutation in codon 13 of the KRAS proto-oncogene. KRAS has a critical role in colon carcinogenesis and the HCT-116 cell line harboring G13D mutation (DOI: 10.18632/oncotarget.5021). According to ATCC, HT-29 is a primary tumor cell isolated from a female patient with colorectal adenocarcinoma. HT-29 cell line carries BRAF V600E mutation. BRAF is one of three RAF genes that has an effect on KRAS signaling (Roma et al., 2016). Both cell lines carry highly observed mutations in CRC patients. Therefore, we selected these cell lines to track the evolutionary dynamics of drug resistance.

2.1 Cell Lines and Growth Conditions

HCT-116 (Human colorectal carcinoma cell line) described previously (Liu et al., 2022) were maintained in Roswell Park Memorial Institute 1640 Medium (RPMI, BI, 01-100-1A) supplemented with 10% fetal bovine serum (Biological Industries, USA, 04-007- 1A), %1 L-glutamine (BI, 03-020-1B) and 1% Penicillin/Streptomycin (BI, 03-031- 1B).

HT-29 (Human colorectal adenocarcinoma cell line) described previously (Grohmann et al., 2012) were maintained in high glucose (4.5 g/L) Dulbecco's Modified Eagle Medium (DMEM, BI, 01-052-1A) supplemented with 10% fetal bovine serum (Biological Industries, USA, 04-007- 1A), %1 L-glutamine (BI, 03-020-1B) and 1% Penicillin/Streptomycin (BI, 03-031- 1B).

293T (Human embryonic kidney cells) described previously (Yang et al., 2021) were maintained in high glucose (4.5 g/L) Dulbecco's Modified Eagle Medium (DMEM, BI, 01-052-1A) supplemented with 10% fetal bovine serum (Biological Industries, USA, 04-007- 1A), %1 L-glutamine (BI, 03-020-1B) and 1% Penicillin/Streptomycin (BI, 03-031- 1B).

2.2 Transformation

For transfection, envelop vector; pCMV-VSV-G (Plasmid #8454), packaging vector; pCMV-dR8.2 (Plasmid #8455), which were purchased from Addgene, were used. These vectors transformed into chemically induced competent cells. 16h after the transformation, single colonies grown on LB agar ampicillin plates were picked, put into a 5 ml LB-Ampicillin medium, and incubated on an orbital shaker overnight. Plasmids were isolated from these overnight grown cultures using the ZymoPURE Plasmid Miniprep Kit (Zymo Research, USA, D4211).

2.3 Determining of Minimum Lethal Dose of Puromycin

HCT-116 (150,000/well) and HT-29 (150,000/well) cells seeded in 6-well plate. After 48 hours of seeding, puromycin dilutions were prepared, and the cells were treated for 72 hours. MTT (Serva, SE2039502) assay was used to determine cell viability.

2.4 Generation of Lentiviruses

To generate the lentiviruses, 2 X 106 293T cells were seeded into Poly-L-Lysine (Serva, SE3322501) coated cell culture dishes with a complete growth medium. After the allowing of attachment, the cells were co-transfected with the envelope vector pCMV-VSV-G (Addgene, Plasmid #8454), packaging vector pCMV-dR8.2 (Addgene, Plasmid #8455), and pRS19 Barcode-CloneTracer (Cellecta, USA) in the

presence of lipofectamine 2000 transfection reagent (ThermoFisher Scientific, USA). After 24h, the medium was changed, and the viruses were harvested 72 hours post-transfection and stored at -80ºC.

2.5 Transduction

For transduction experiments, 150,000 cells/well of HCT-116 and HT-29 were seeded in two separate 6-well plates. After the cells allow attachment for 24 hours, different virus amounts are transduced in the presence of polybrene (Santa Cruz, sc-134220) to enhance transduction efficiency. Puromycin selection was used to determine the 10% transduced population over the whole population, which is MOI 0.1 ratio.

2.6 Generation of Barcoded Cells

For barcoding of HCT-116 cells, $15x10^6$ cells were seeded in 3 different 15 cm tissue culture dishes ($5x10^6$ cell/dish) and allowed attachment for 24 hours. Pre-determined virus amount (3.266 ul) transduced in two different 15 cm tissue dishes in the presence of polybrene (Santa Cruz, sc-134220) (8ug/ml), and there was no virus induction on the third dish, which is negative control. After 24 hours from transduction, the cells were treated with a pre-determined puromycin dosage (1ug/ml) for 72 hours. Barcoded cells were selected with puromycin until there was no living cell in the negative control dish containing wild-type cells. Selected cells grew on a complete medium. When the barcoded cells reached confluency, they were taken to the pellet for further analysis, frozen, and stored at -80ºC.

For barcoding of HT-29 cells, $5x10^6$ cells per 15cm tissue culture dish were seeded into three different dishes and allowed attachment for 24 hours. For transduction, a pre-determined virus amount (6.666ul) was transduced into two different dishes with 8ul/ml polybrene (Santa Cruz, sc-134220), and the cells allowed transduction for 24 hours. One of the seeded dishes was negative/puromycin control; thus, there was no

transduction. The cells were treated with a pre-determined puromycin dosage (1.5ug/ml) for 72 hours. After puromycin selection, there was no living cell in the dish containing wild-type cells. The selected cells grow on a complete medium, and when the cells reach confluency, taken cell pellet for further analysis and frozen and stored at -80ºC.

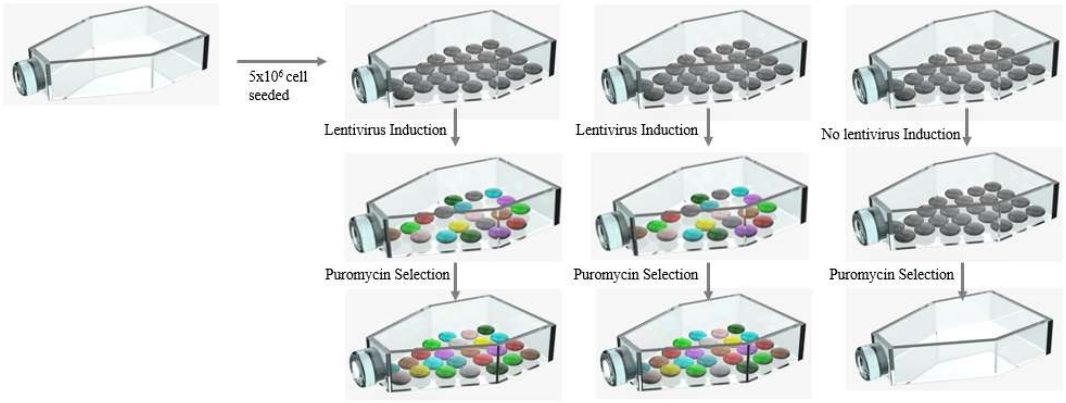

Figure 2. 1 Representation of cellular barcoding.

2.7 Proliferation Assay

The pre-barcoded and barcoded cells were seeded into 96-well plates as 10.000 cells per well to observe barcode vectors' effect on cells in terms of proliferation. After three days of seeding, the cells were fixed with a solution of 2% formaldehyde (Serva SE3162802) diluted in phosphate-buffered saline (PBS) (BI 02-023-1A). After two hours, the cells were stained with 0.1% crystal violet (Amresco 0528) diluted in water. Eight minutes later staining solution was removed by washing with dH_2O and left to dry overnight. 10% acetic acid (Merck 1.00056.2500) solution in water used to dissolve crystal violet and microplates were read using a microplate spectrophotometer (Multiskan GO; Thermo Fisher Scientific, USA) at 570 nm.

2.8 MTT Assay

3-(4,5-dimethylthiazol-2-yl)-2,5 diphenyltetrazolium bromide (MTT) assay was used to observe the cytotoxic effect of chemotherapeutics. For the MTT assay, the cell lines were seeded in 96-well plates as $10x10^3$ cells per well and incubated for 24 hours to allow attachment. Different concentrations of capecitabine, dabrafenib, and SN-38 were treated for 72 hours. 10 ul of MTT solution (5 mg/ml in PBS) (Serva, SE2039502) was added to cells and incubated for the synthesis of formazan crystals for four hours. SDS-HCl solution (0.01M HCl in 10%SDS in dH_2O) was applied to dissolve formazan crystals and incubated overnight. The 96-well plate was read using a microplate spectrophotometer (Multiskan GO; Thermo Fisher Scientific, USA) at 570 nm. The relative cell viability was found by accepting the untreated groups' viability was 100%, and treated cells' viability was determined accordingly.

2.9 Determining Chemotherapeutic Dosages

The IC50 dosage of chemotherapeutics was determined and used to develop drug resistance on colorectal cancer cell lines. For the HCT-116 cell line, capecitabine was used in a dilution of 1:2 ratio from 10mm. For the HT-29 cell line, dabrafenib 1:2 ratio from 700 nm and SN-38 1:2 ratio from 10 um were used. Cells treated were described in section 2.9. The IC50 dosage was calculated with log(inhibitor) vs. normalized response curves at Graphpad Prism 8.1 (GraphPad Software Inc., USA).

2.10 Developing Stable Drug-Resistant Cell Lines

For the HCT-116 cell line, barcoded cells were thawed and seeded in a 15 cm dish. When the cells reached confluency, they were divided into four 15 cm dishes by seeding $2x\ 10^6$ cells per dish, and cell pellets were taken for further analysis. After four days, cells reached the confluency and started the capecitabine treatment with IC50 dosage in three dishes for seven months. In the fourth dish, when the cells were

~70% confluency, growth for three passages in the presence of solvent (DMSO), then cell pellets were taken for further analysis, and cells were frozen and stored at the -80ºC. After the treatment of capecitabine, developing resistance was controlled with an MTT cell viability assay, and the cells were frozen and stored at -80ºC, and cell pellets were taken for further analysis.

For the HT-29 cell line, two cryovials of barcoded cells were thawed and seeded 15 cm dish. After the cells reached confluency, they were divided into four 15 cm dishes by seeding 2x 10^6 cells per dish, and the cell pellets were taken for further analysis. After five days, when the cells reached confluency, treatment of dabrafenib at 2xIC50 dosage started for three dishes and one dish used for DMSO control, and treatment of SN-38 at IC50 dosage started for three dishes and the fourth dish was solvent (DMSO) control. Dabrafenib treatment continued for three months, and the cells were passaged every month with a ratio of 1/10. SN-38 treatment continued for four months; there was a drug holiday every 20 days for ten days. This group passaged the 1:10 ratio three times. When cells reached confluency, the cell viability assay was performed to control the development of drug resistance. Solvent control dish passaged three times with a 1/10 ratio. Resistant cells and solvent control cells were frozen, and the cell pellet was taken for further analysis.

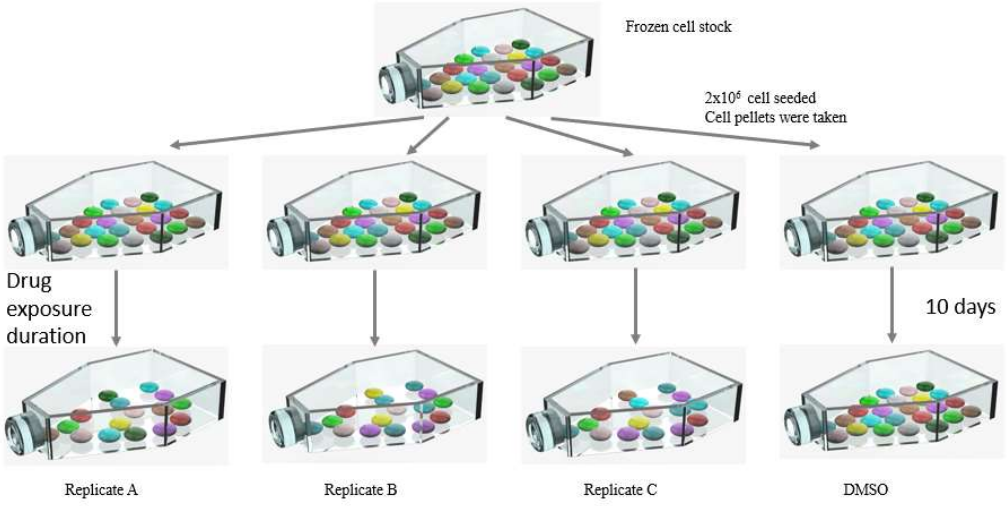

Figure 2. 2 The experimental design of development of drug resistance.

2.11 Determining Drug Sensitivity on Resistant Cell Lines

To determine the resistance to one chemotherapeutics creates drug sensitivity on another chemotherapeutic, drug-resistant cells were seeded into a 96-well plate as 10.000 cells per well. Cells were treated with drugs 1:2 ratio and performed cell viability assay as described in section 2.9.

2.12 Determining Synergistic Effect

Synergy assays were carried out to determine the effect of the ERK inhibitor (SCH77298) and chemotherapeutics. For the SN-38 resistant HT-29 cell line, SN-38 dosage was 4x IC50, 2xIC50, IC50 (0.5µM), and SCH77298 dosage was applied from 250 nm to 7 nm with a 1:2 ratio. For dabrafenib resistant HT-29 cell line, Dabrafenib dosage was 8xIC50, 4xIC50, and 2xIC50 (200nM), and SCH77298 was applied from 250 nM to 7 nM with a 1:2 ratio.

To determine the synergistic effect of dabrafenib plus oxaliplatin combination and capecitabine plus oxaliplatin in dabrafenib resistant HT-29 cell line were used. For the combination of dabrafenib and capecitabine, the dabrafenib dosage was 8xIC50, 4xIC50, and 2xIC50 (200nM), and the oxaliplatin dosage was 60 µM to 0.9 µM with a 1:2 ratio. For the combination of capecitabine and oxaliplatin, the capecitabine dosage was 3 mM to 0,75 mM with a 1:2 ratio and the oxaliplatin ratio was 60 µM to 0.9 µM with a 1:2 ratio.

The synergistic effect and the synergy doses were determined from SynergyFinder (Ianevski et al., 2020a).

2.13 Colony Formation Assay

To observe the effect of resistance in single cell growth into a colony, 20.000 cells per well were seeded into 6-well plates and allowed attachment for 24 hours. The treatments started with IC50 dosages of chemotherapeutics, and the medium changed

twice a week. Thirty days later, the cells were fixed with a solution of 2% formaldehyde (Serva SE3162802) diluted in phosphate-buffered saline (PBS) (BI 02-023-1A). After two hours, the cells were stained with 0.1% crystal violet (Amresco 0528) diluted in water. Eight minutes later staining solution was removed by washing with dH_2O and left to dry overnight.

2.14 Total Protein Isolation

$5x10^6$ cells were collected and washed with cold PBS. Cells were lysed in 50 µl RIPA buffer (Serva, 39244), including 1x protease inhibitor (Serva, 39102) and phosphatase inhibitor (Serva SE3905501). After collecting cell extracts in RIPA buffer, extracts were kept on ice for 5-minutes. Extracts were then centrifugated at 7500rpm for 15 minutes at 4°C. Supernatants were collected, and protein concentration was measured by using the Quick Start Bradford Protein assay (Bio-Rad, USA, 5000205).

2.15 Western Blot

50 µg of total protein was denatured in 10x Laemni buffer (Eco-tech, Turkey), which contains 30% B-mercaptoethanol at 95º C for 5 minutes and loaded into 10% SDS-PAGE gel. Proteins were then transferred onto a nitrocellulose membrane through a wet transfer system for 75 minutes at 120 V. After the membrane was blocked with 5% Skim milk in 0.05 Tris Buffered Saline-Tween (TBS-T) for 1 hour, the membrane was then incubated with the primary antibody for overnight at +4ºC. After primary antibody incubation, the membrane was washed with 0.05 TBS-T three times 5 minutes each. The secondary antibody was added to the membrane and incubated for 2 hours at room temperature.

For imaging, the membrane was incubated with Clarity Max Western ECL substrate (BR, 1705062) in a 1:1 luminol-enhancer reagent: peroxide reagent ratio in the dark for 2 minutes. ChemiDocTM MP system (Bio-Rad, USA) was used for imaging the

membrane, and Image Lab 5.1 (BioRad, USA) program was used for analyzing the image results. For molecular weight marker in the 10-250 kDa range, PageRuler Plus Prestained Protein Ladder (Thermo Fisher Scientific, USA) was used.

The membranes were stripped with mild stripping buffer when required. The mild strip buffer was applied to the membrane for 15 minutes when it was heated. Then the membrane was washed with TBS-T three times for 5 minutes each.

Table 2. 1 List of antibodies used in this study.

Name of antibody	Company (Catalog #)	Host	Molecular Weight (kDa)	Dilution	Blocking Agent
p-EGFR Antibody	Santa Cruz sc-377547	Mouse	170 kDa	1:200	BSA
p-ERK-1/2 antibody	Santa Cruz sc-7383	Mouse	44/42 kDa	1:500	Skim milk
p-MEK-1/2 antibody	Santa Cruz sc-81503	Mouse	47/45 kDa	1:500	Skim milk
GAPDH antibody	Santa Cruz Sc-32233	Mouse	36 kDa	1:1000	Skim milk
IgG-HRP	Santa Cruz sc2005	Goat	-	1:10000	Skim milk

2.16 Statistical Analysis

All experiments were carried out with at least two or three different biological replicates, and each had at least three technical replicates. GraphPad Prism 8.1 (GraphPad Software Inc., USA) was used for data analysis of cell viability assays. Student's t-test, One-way ANOVA, was carried out to determine significance where a *p-value* < 0.05 was considered statistically significant.

2.17 Analysis of Barcodes

Barcode analysis was carried out by Arda Temena. For quality statistics of barcode reads, both raw and trimmed reads were computed using FastQC. After filtering Fastq files with a quality score >20 in all nucleotide positions, FASTQ reads were trimmed to correspond to the variable barcode region (48bp). This barcode region consists of a 14 bp region, four bp linker region, and 30 bp Celesta barcode region from the library excel file (Cellecta-NGS-QC-CloneTracker-XP10x1M-Barcode3-Lib-RFP.xls).

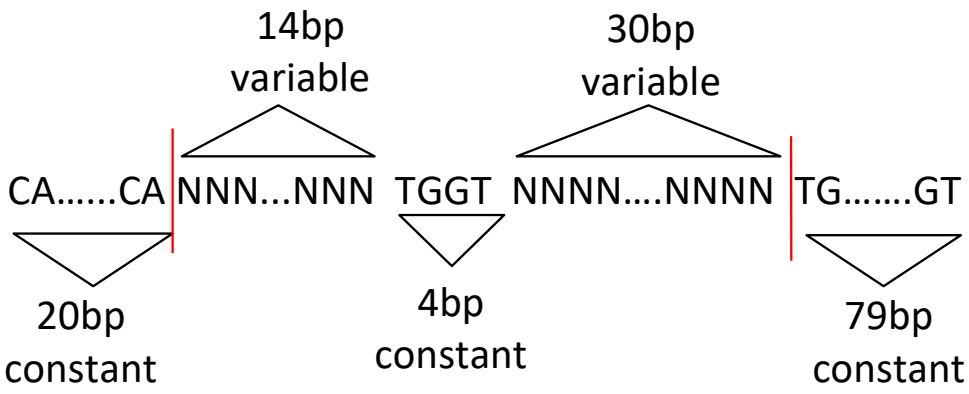

Figure 2. 3 Schematic representation of the reads.

Each variable barcode(represented as the sequence between the red lines) is flanked by constant sequences (20bp to the left) and (79bp to the right).

Indexing of barcodes was used to count the barcodes with Salmon Salmon (Patro et al., 2017). The -k 47 parameter was used for the index function in Salmon.

The number of barcodes in forward and reverse reads were quantified and written an SF fine using the quant in Salmon function and converted to a JSON file that was used to read and write the counts of barcodes.

The growth rate is crucial for annotating each barcode with a phenotype. For determining the growth rate under each condition, barcode frequencies were used as described previously (Acar et al., 2020). The representative frequency of barcodes

was calculated as the frequency of each barcode in the corresponding DMSO replicates in each replicate. The formula for growth rate is found below:

$$\text{Growth Rate} = \log(f_R/f_0)\ 1/T$$

Here, f_R represents the frequency of barcode, f_0 represents the maximum frequency of DMSO replicates, and T is the duration of the drug exposure in terms of the week. Barcodes have a positive growth rate (>0) and were observed for two or more replicates called resistant, which have positive growth rates but were observed in one replicate called de novo, and have negative growth rates (<0) called sensitive. The barcodes were observed only in replicates, not in the initial or DMSO population called not determined.

Four different mediums were collected at equal intervals for tracking barcodes, and barcode frequencies were used to trace the resistant barcodes. The barcodes detected in the initial or DMSO population were not counted if it was not observed in the medium. Resistant barcodes which have a positive growth rate, and sensitive barcodes were plotted for comparison.

2.18 Wound healing assay

A wound healing assay was carried out to determine the resistance effect on the motility of the HT-29 cell line. The initial and DMSO population of HT-29 cells were seeded 200,000 cells/well, and the dabrafenib-resistant and SN-38-resistant cells were seeded 250,000 cells/well into a 24-well plate. The cells reach 80%c confluency 24 after the seeding. Cells were incubated with 5 µg/ml mitomycin C to prevent cell division for two hours. The scratch wounds were made with a sterile 200 µl pipette tip. Cell washed three times with PBS to remove cell debris. Every four-hour scratch wound imaging was carried out with a Nikon Eclipse ti2e Fluorescence Microscope in the laboratory of Dr. Altuğ Özçelikkale (METU, Mechanical Engineering). The area of the scratch was calculated with ImageJ.

CHAPTER 3

RESULTS AND DISCUSSION

3.0 Generation of Barcoded Cells

Lentiviruses carried the barcode sequence generated in the HEK293T cell line described in 2.5. The optimization of infection is crucial for barcoding experiments. The barcode vector has a puromycin resistance gene for selection. Before the lentivirus transduction, the puromycin dosages and the virus amounts were determined. Determining the minimum lethal dosage of puromycin in both HCT-116 and HT-29 cells is vital for selection after the lentivirus transductions (Figure 3.1A). For tracking the barcoded cell, the cells should carry one unique barcode since if the cell integrates more than one barcode, there will be multiple integration events, and the diversity of the population will be directly affected (Serrano et al., 2022). The multiplicity of infection (MOI) refers to the virion amount added per cell, and the optimal MOI is crucial for the cells containing one barcode. In that case, the highest MOI should be 0.1 to avoid multiple integrations (Serrano et al., 2022). For that, the cells were transduced with different amounts of virus, and a cell viability assay was performed to determine which dosage caused the maximum of 10% cell viability (Figure 3.1B). The number of starting cells is essential for the diversity of barcodes. The barcode library has 1,000,000 unique barcodes; for getting the highest barcode diversity transducion of 10,000,000 cells. To optimize the required virus amount, the barcoding experiments were performed. The assamptions of this experiment was that the barcoded populations carried one million unique barcode sequences and every barcode sequence was found once after the puromycin selection in barcoded population.

The determined minimum lethal puromycin dosages were; 1 µl/ml in HCT-116 cells and 1.5 µl/ml in HT-29 cells (Figure 1A). MOI 0.1, 1 million virions transduced into

10 million cells, represents one cell transduced with one virion; thus, the cells carried only one barcode. The HCT-116 cells have an MOI 0.1 (40 µl lentivirus/150,000 cells) and the HT-29 cells have an MOI 0.05 (100 µl lentivirus/ 150,000 cells) (Figure 1B). Therefore, 2 ml 667 µl lentivirus was used in HCT-116 cells, and 6 ml 667 µl lentivirus was used in HT-29 cells. The puromycin selection was continued until the wild-type non-transduced control cells were dead in both cell types. The cells were expanded and stored, and the expression of the barcode plasmid that carried the RFP sequence was confirmed by controlling of expression of RFP with microscopy (Figure 3.2).

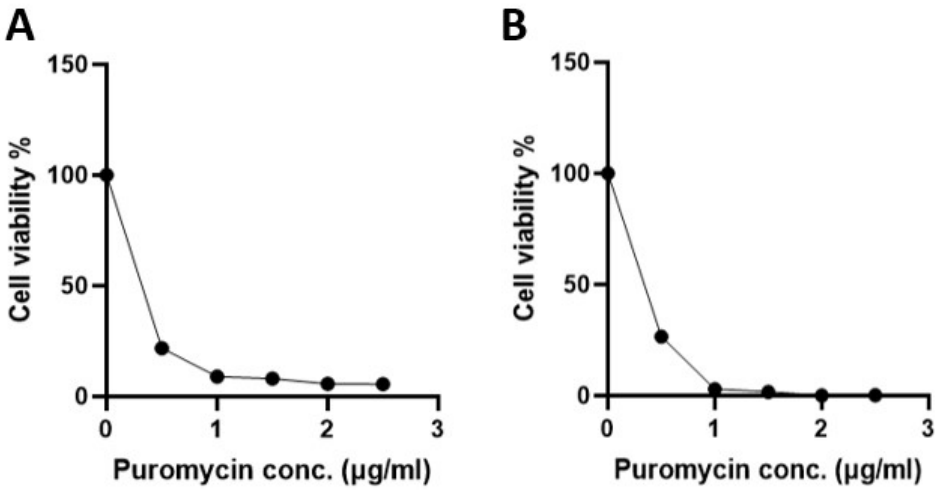

Figure 3. 1 Puromycin kill curves of A in HCT-116 and B in HT-29

The minimum lethal dose of puromycin was determined in both HCT-116 and HT-29 cell lines. Both cells were seeded into 6-well plates, and different puromycin doses were applied to the cells and treated for 72 hours. Cell viability assay processed according to standard techniques. (A) Puromycin kill curve of HCT-116 cell line. (B) puromycin kill curve of HT-29 cell line.

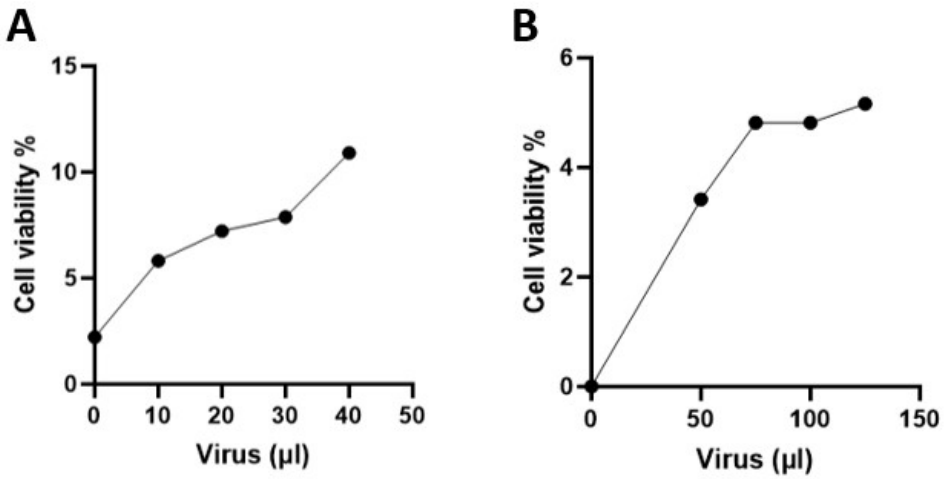

Figure 3. 2 The determination of virus amount

The multiplicity of infection (MOI) represents the number of virions added per cell during transduction. The cells were seeded and transduced with different amounts of viruses in the presence of polybrene and selected with puromycin. Cell viability assay was processed according to standard techniques. (A) Cell viability assay of HCT-116 cells with different amounts of lentivirus transduction under the puromycin selection. (B) Cell viability assay of HT-29 cells with different amounts of lentivirus transduction under the puromycin selection.

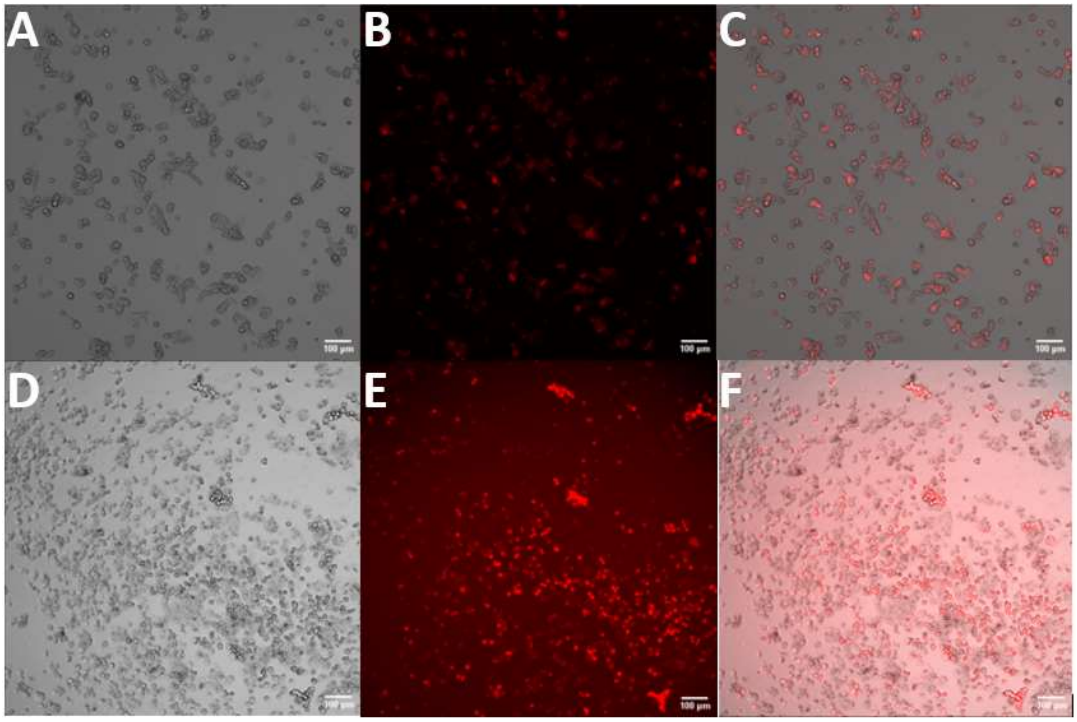

Figure 3. 3 The images of barcoded HCT-116 and barcoded HT-29

The brightfield and red fluorescence microscopy images of barcoded HCT-116 and barcoded HT-29 cells. The brightfield image of barcoded HCT-116 (A), RFP image of barcoded HCT-116 (B), and composite images (C). the brightfield image of barcoded HT-29 (D), RFP image of barcoded HT-29 (D), and composite image (E).

3.0 Effects of barcode vector on cellular proliferation

A proliferation assay with crystal violet was conducted to determine whether the presence of a barcode vector affected cellular proliferation in HCT-116 or HT-29 cells. Wild-type (WT) cells were used as controls to differentiate the effect of lentiviral transduction in terms of proliferation. There were no significant changes between WT HCT-116 and Barcoded HCT-116 and WT HT-29 and Barcoded HT-29 cells, which shows there is no effect of barcode vector in the proliferation of the cells (Figure 3.4)

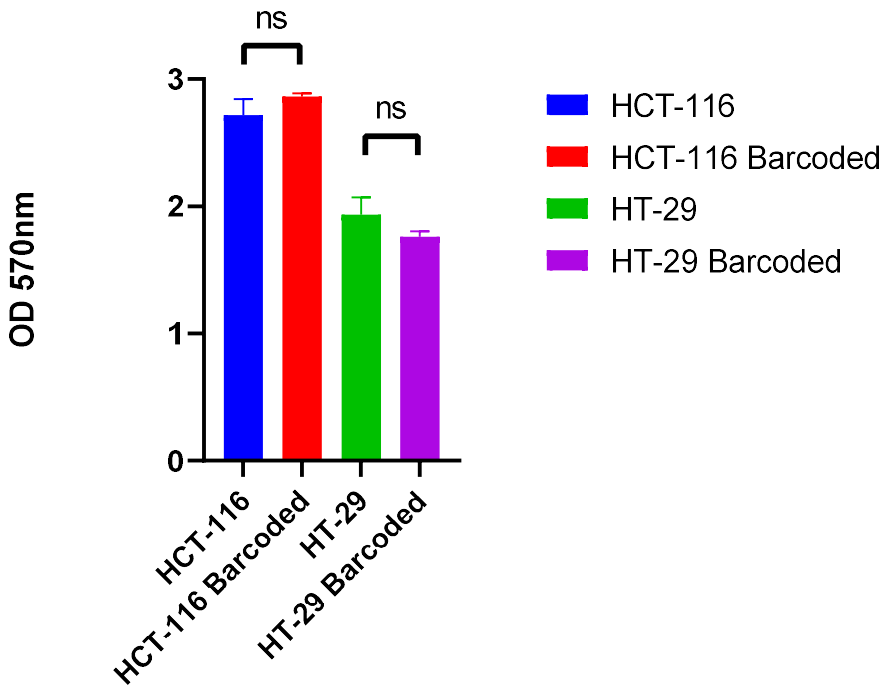

Figure 3. 4 The effects of barcode vector on cellular proliferation of HCT-116 and HT-29 cells

HCT-116 wild type and barcoded cells and HT-29 wild type and barcoded cells were seeded. Seventy-two hours after the seeding, cells were fixed with 2% formaldehyde and stained with 0.1% crystal violet. 10% acetic acid solution was used to dissolve crystal violet, and the absorbance at 570 nm was measured using a microplate reader. Two independent biological replicates were carried out. No significant changes in cellular proliferation were observed.(p-value > 0.05, ANOVA).

3.1 Determining chemotherapeutic dosages

The cell viability assay was performed to determine chemotherapeutic dosages in both HCT-116 and HT-29 cells (Figure 3.5). Capecitabine, dabrafenib, and SN-38 are the chemotherapeutics that mostly develop resistance in CRC patients (De Falco et al., 2020). HCT-116 cell line carries a mutation on the KRAS gene, and the

patients have mutation status on KRAS treated with capecitabine in the clinic (Domenica et al., 2019). HT-29 cell line carries V600E mutation on BRAF gene; dabrafenib is a targeted drug for this mutation (Roma et al., 2016). SN-38 is one of the highly used chemotherapeutics in the clinic; it is used in HT-29 cells (Paillas et al., 2011). Therefore, capecitabine treatment was applied in HCT-116 cells, and dabrafenib and SN-38 treatment were used in HT-29 cells.

For the treatment, IC50 dosage (1.7 mM) of capecitabine was carried in HCT-116 cells (Figure 3.5A). For the HT-29 cell line 2xIC50 (200 nM) of dabrafenib was carried (Figure 3.5B). For SN-38 IC50 (0,54 μM) determined for drug treatment in HT-29 cells (Figure 3.5C).

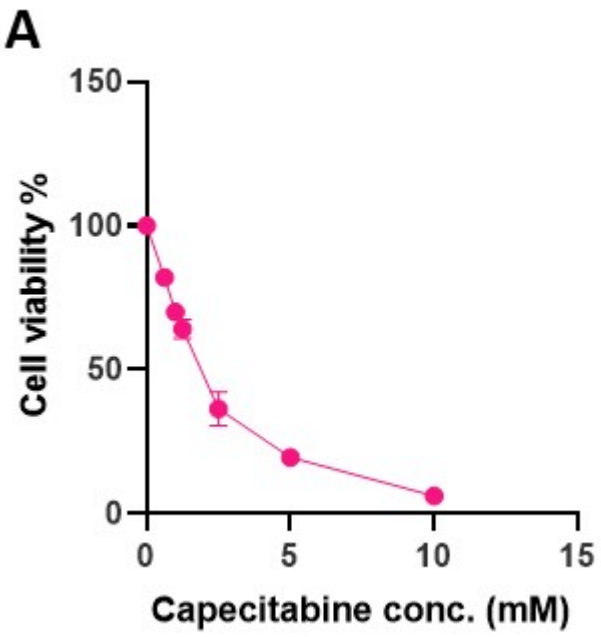

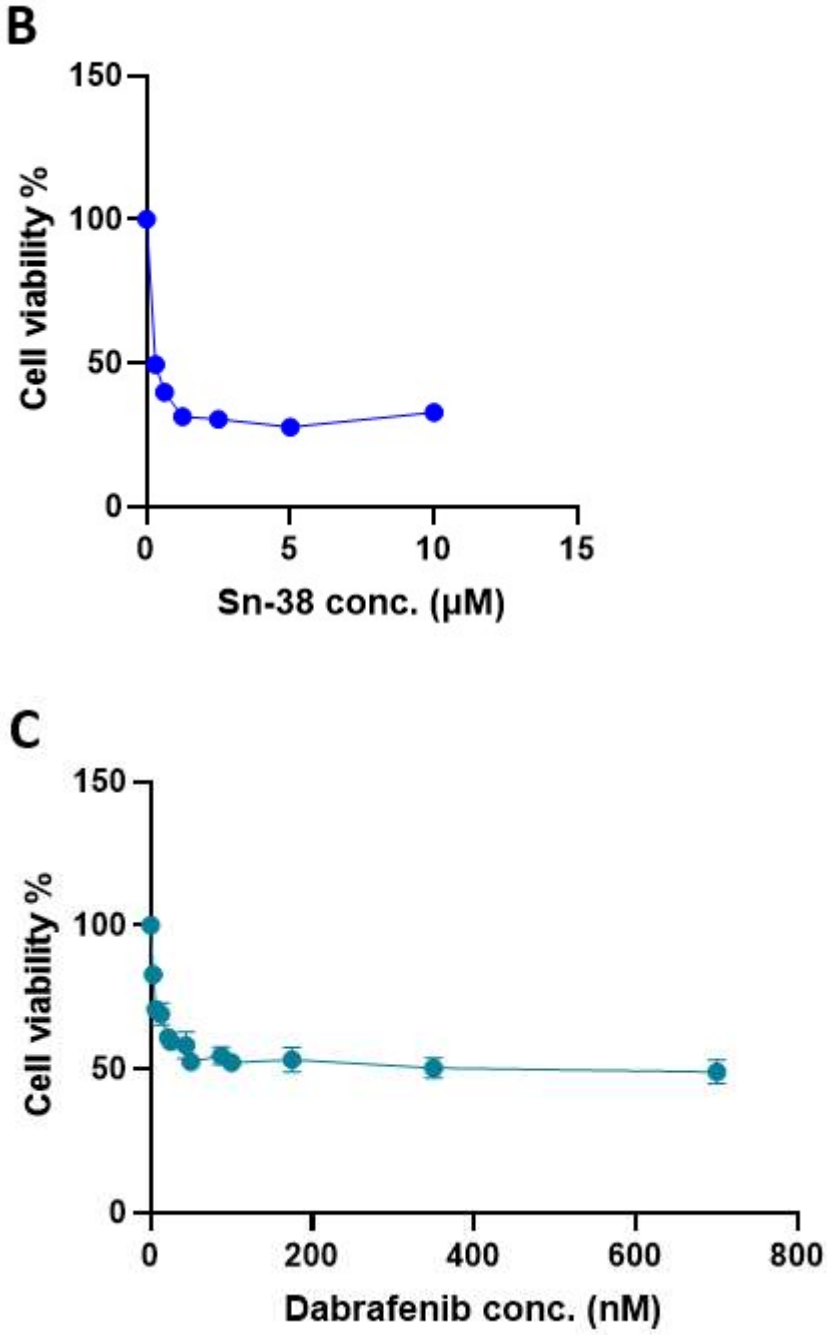

Figure 3. 5 The dose-response curves of chemotherapeutics

The HCT-116 and HT-29 cells were plated and allowed to attach for 24 hours. The cell was treated for 72 hours with serially diluted chemotherapeutics. The MTT cell

viability assay was done according to standard techniques. Three independent technical replicates for each group were carried out. (A) Dose-response curve of capecitabine in HCT-116 cell line. IC50 of capecitabine is 1.786 mM. (B) Dose-response curve of dabrafenib in HT-29 cell line. IC50 of dabrafenib is 99,8nM. (C) Dose-response curve of SN-38 in HT-29 cell line. IC50 of SN-38 is 0.54 µM.

3.3 Developing capecitabine resistance in HCT-116 cells

To develop capecitabine resistance in HCT-116 cells, barcoded cells thawed and seeded when they reached confluency cells divided into four flasks. (described in 2.11) The capecitabine treatment started after the seeded cells reached confluency in three flakes, and the other flask was solvent (DMSO) control. When the solvent control plate reached the confluency, the cells were frozen, and cell pellets were taken. The cells found in drug-treated replicates were treated with an IC50 dosage (1.7 mM) of capecitabine until cells reached confluency under the capecitabine treatment (seven months). The treated cells were frozen, cell pellets were taken when they reached confluency, and the cells were seeded into 96-well plates to perform an MTT cell viability assay for whether cells developed drug resistance (Figure 3.5.A) The cell viability assay result shows the change in viability in the presence of drug treatment. The resistance fold change was calculated according to the proportion of IC50 values of the drug-treated and control groups. The control group was the DMSO group of barcoded HCT-116 cells. There was a significant change in terms of the IC50 value of capecitabine between drug-treated, initial, and DMSO control cells (Figure 3.5.B). The resistance fold changes were determined with the ratio of IC50 of the drug-treated group to the DMSO group. The resistance fold changes in each drug-treated group versus DMSO were shown (Table 3.1).

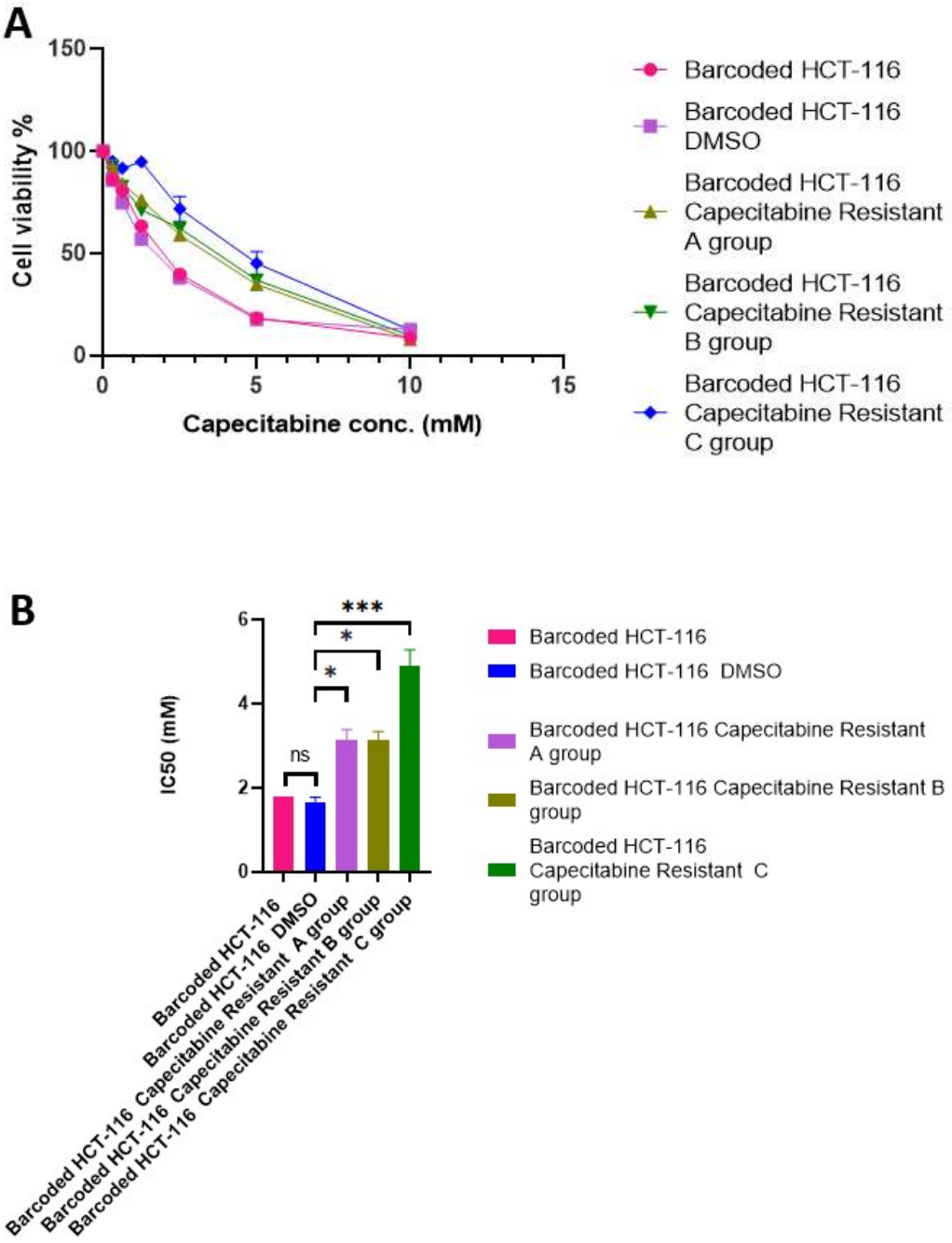

Figure 3. 6 Dose-response curve and comparison of IC values of capecitabine in barcoded HCT-116 cell lines

Barcoded HCT-116, barcoded HCT-116 DMSO, and three independent replicates of drug-treated barcoded HCT-116 cells were seeded at a density of 10,000 cells per well in a 96-well. After 24 hours of seeding, cells were incubated with the serial

diluted capecitabine treatment for 72 hours. MTT cell viability assay was performed according to standard procedure. Two independent biological replicated and three technical replicated for each group are shown. (A) dose-response curve of capecitabine. (B) bar graph of the IC50 values of barcoded HCT-116, barcoded HCT-116 DMSO, and capecitabine treated barcoded HCT-116 cells. The significant change in IC50 values of capecitabine was found. ($p<0.05$, one-way ANOVA test).

Table 3. 1 The table of comparison for IC50 and drug resistance fold of capecitabine

Cell line	IC_{50} Control group	IC_{50} Drug resistant	Resistance fold
Hct-116 Cape A	1,764 ± 0,206 mM	2,853 ± 0,429 mM	1,617
Hct-116 Cape B	1,764 ± 0,206 mM	2,929 ± 0,452 mM	1,66
Hct-116 Cape C	1,764 ± 0,206 mM	4,488 ± 1,11 mM	2,544

Capecitabine treated HCT-116 cells versus DMSO. Data are presented as means SD (n=2).

Three capecitabine-treated groups showed significant resistance fold change (figure 3.5B). The most significant change in resistance fold was observed in group C capecitabine-resistant barcoded HCT-116 (Table 3.1); thus, this group was chosen for further investigations.

3.4 he Barcode Analysis of Capecitabine Resistant Barcoded HCT-116 cells

Monitoring the barcoded cell under the capecitabine treatment provides to observe clonal evolution under treatment and determine the possible causes of the drug

resistance. The cellular alterations that cause drug resistance can already be found in the cell; thus, pre-existed alterations can be crucial for the development of resistance (Acar et al., 2020) (Levy et al., 2015). These cellular alterations can be gain or loss during the treatment; in the presence of treatment, cellular altered cells can rapidly increase distribution (N McGranahan, 2017) (Levy et al., 2015). Barcodes were determined according to unique barcode sequences with NGS results. The barcodes observed in the DMSO population and two or three resistant cell populations, called resistant barcodes, indicated pre-existed cellular alterations in the population. The barcodes determined in DMSO and only one resistant cell population, called de novo, indicated the gain or loss of genetic alterations during the treatment. Resistant and de novo barcodes have a positive growth rate. Some lineages have no fitness advantage, and these barcodes have a negative growth rate called sensitive. The barcodes were determined in only the resistant population, not in DMSO or the initial population called not determined.

All groups were sequenced at the same run in NGS to eliminate the batch effect of sequencing. For capecitabine-resistant barcoded HCT-116 cells, there were 10827 unique barcodes determined in barcoded HCT-116 (initial) cells, 11327 unique barcodes determined in barcoded HCT-116 DMSO cells (Figure 3.7A), 67 unique barcodes determined in capecitabine-resistant barcoded HCT-116 group A, 2017 unique barcode observed in capecitabine-resistant HCT-116 group B, and 209 unique barcodes observed in capecitabine resistant barcoded HCT-116 group C cells (Figure 3.7B). This decrease in the unique barcode number indicated a strong selective pressure. The number of identified barcodes in the initial population was a small subsample of the total number of barcodes because of limitations of sequencing. The sequencing was performed in 200,000-400,000x depth, and DNA isolation was performed in 2,000,000 cells; thus, only some thousands of unique barcodes were determined. The assumptions of this experiment were the sequenced cell represent all the population so it contains every unique barcode in population.

The barcodes positively selected under treatment have a positive growth rate with respect to DMSO. Functional subclones were used to determine the growth

dynamics. Four functional subclones were identified in capecitabine-resistant HCT-116 cells. The first and second groups were the largest and represented not determined (grey) and sensitive clones (beige). Sensitive clones died under the drug, and not determined clones could not be observed in DMSO. There was no determination of the resistant barcode (Figure 3.7B). Two barcodes were found in only A replicate, which indicated de novo barcodes (blue), one barcode found in only B replicate, and two barcodes found only in C replicate (Figure 3.7C). These barcodes respond to de novo lineages. The barcode frequencies between treated groups were highly similar, showing that these treatment conditions could represent the drug-resistance evolution. Thus, the barcode analysis shows stochastic clonal behavior in the presence of de novo alterations in polyclonal drug resistance for capecitabine resistance in HCT-116 cells.

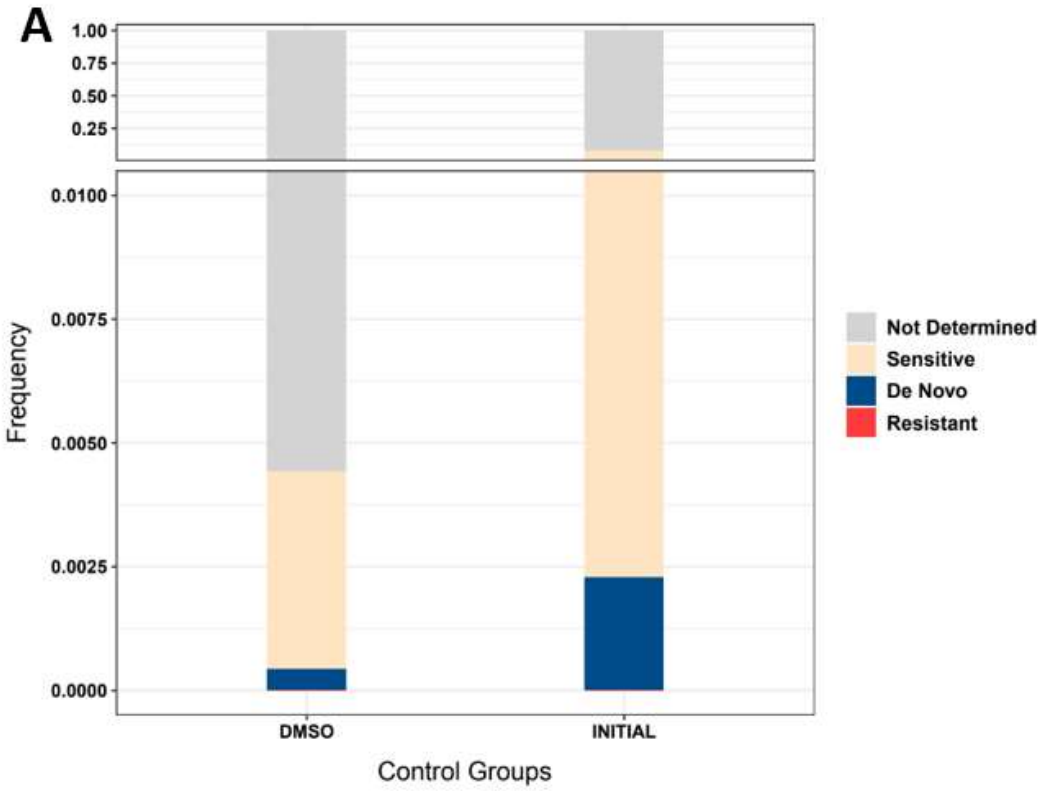
A
1.00
0.75
0.50
0.25
0.0100
0.0075
0.0050
0.0025
0.0000
Frequency
DMSO
INITIAL
Control Groups
Not Determined
Sensitive
De Novo
Resistant

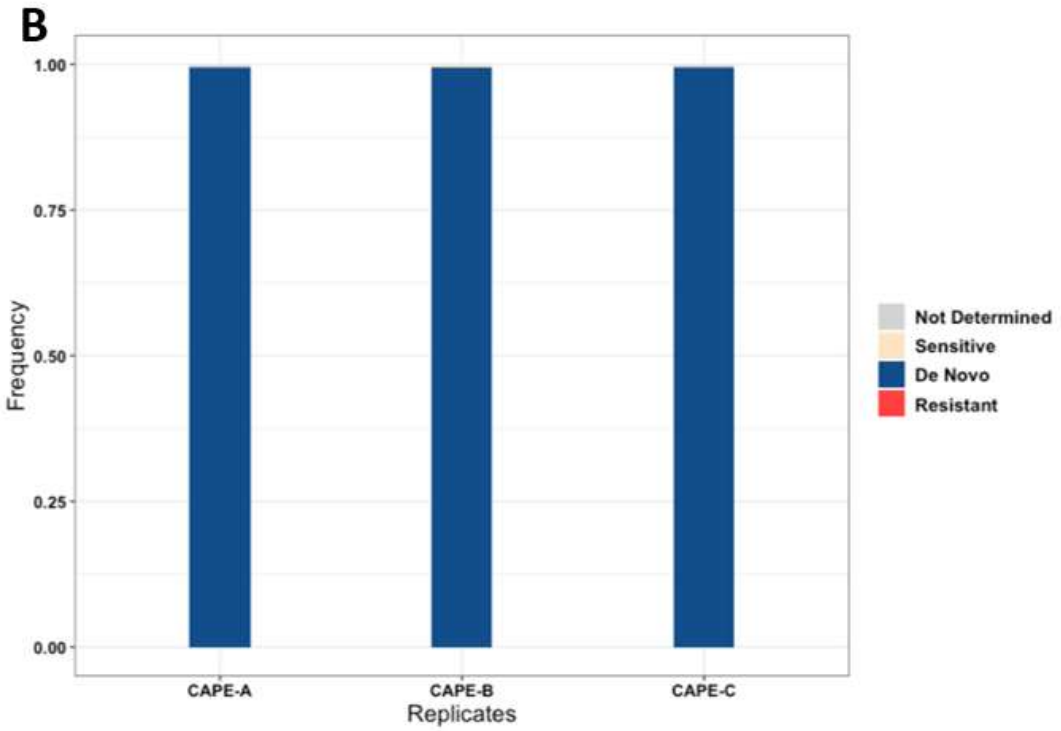
B
1.00
0.75
0.50
0.25
0.00
Frequency
CAPE-A
CAPE-B
CAPE-C
Replicates
Not Determined
Sensitive
De Novo
Resistant

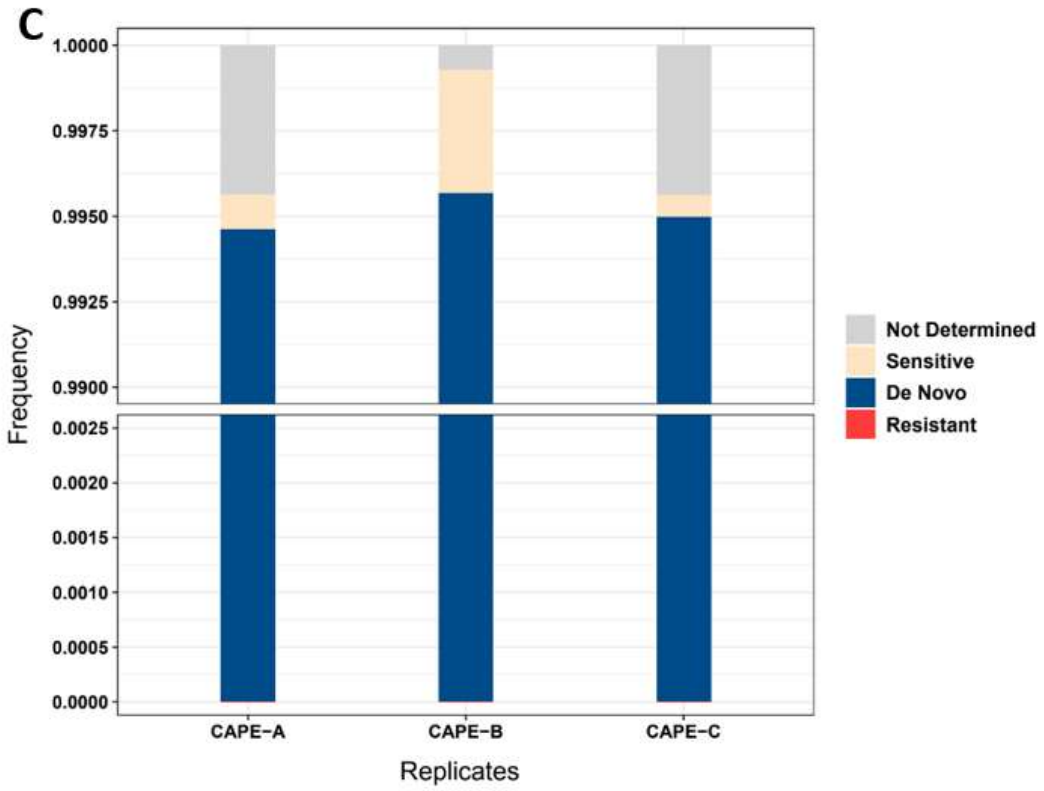
C
1.0000
0.9975
0.9950
0.9925
0.9900
0.0025
0.0020
0.0015
0.0010
0.0005
0.0000
Frequency
CAPE-A
CAPE-B
CAPE-C
Replicates
Not Determined
Sensitive
De Novo
Resistant

Figure 3. 7 Barcoding sequence results of capecitabine-resistant barcoded HCT-116 cells

Barcode frequency distributions of barcoded HCT-116, barcoded HCT-116 DMSO control, and capecitabine-treated barcoded HCT-116 cells were examined. Barcode colors and order are identical between replicates. Barcode phenotypes were determined by the growth rate and conserved distribution between replicates. Here, the red color represents resistant barcodes that have positive growth rate and were determined in two or more replicates; the blue color represents de novo barcodes that have positive growth rate and were determined in only one replicate; the beige color represents sensitive barcodes that have negative growth rate, and grey color represents not determined barcodes that not determined in DMSO or initial populations. (A) Evolutionary dynamics of barcoded HCT-116 (initial) and barcoded HCT-116 DMSO cells. (B) Evolutionary dynamics of capecitabine treated barcoded HCT-116 cells. (C) Evolutionary dynamics of capecitabine treated barcoded HCT-116 cells in focused frequency between 0,99 and 1,00.

In this experiment, one re-plating cells under the drug treatment can cause a stochastic effect and sampling bias. There was medium change twice a week. HCT-116 is an adherent cell line; the detachment of the surface indicates cell death. Collection of dead cells from floating media was done; however, there was no time-course barcode analysis since no resistant barcode was determined.

3.5 Developing dabrafenib resistance in barcoded HT-29 cells

Barcoded HT-29 cells thawed. They seeded into four different T-175 flasks (2x106 cells/ flask); when they reached confluency and cell pellets were taken, and the remaining cells were frozen. The cells reached confluency, and the dabrafenib treatment with a 2xIC50 dosage started in three flasks, and one flask was the solvent (DMSO) control. DMSO control flask reached confluency earlier than the treated groups. When the solvent control plate reached the confluency, the cells were frozen, and cell pellets were taken. The cells were treated with a 2xIC50 dosage of

dabrafenib for three months. The treated cells were passaged every month, and they were frozen, and cell pellets were taken. After the treatment, an MTT cell viability assay was performed for whether cells developed drug resistance (Figure 3.8) The resistance fold change was calculated according to the ratio of IC50 values of drug-treated and DMSO groups. The resistance changes were shown (Table 3.8).

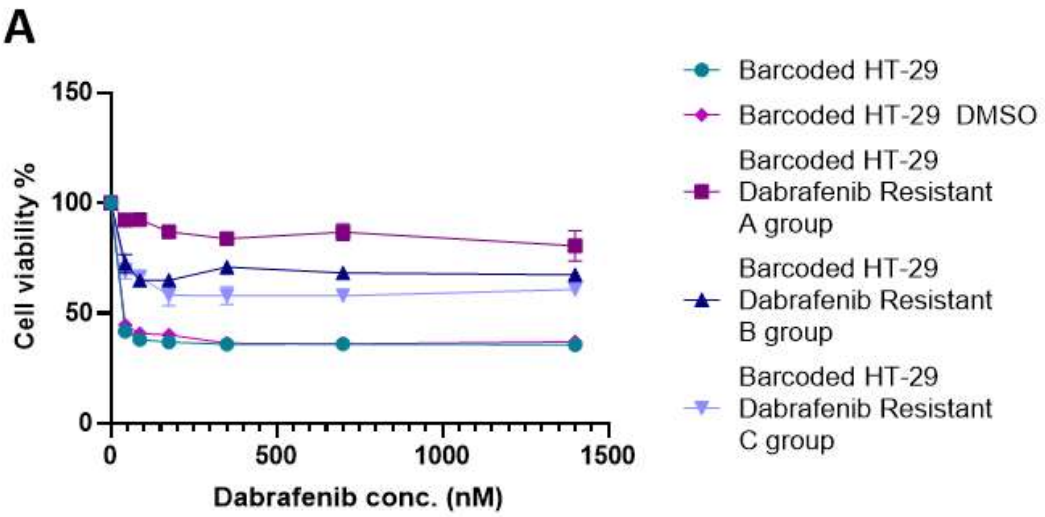

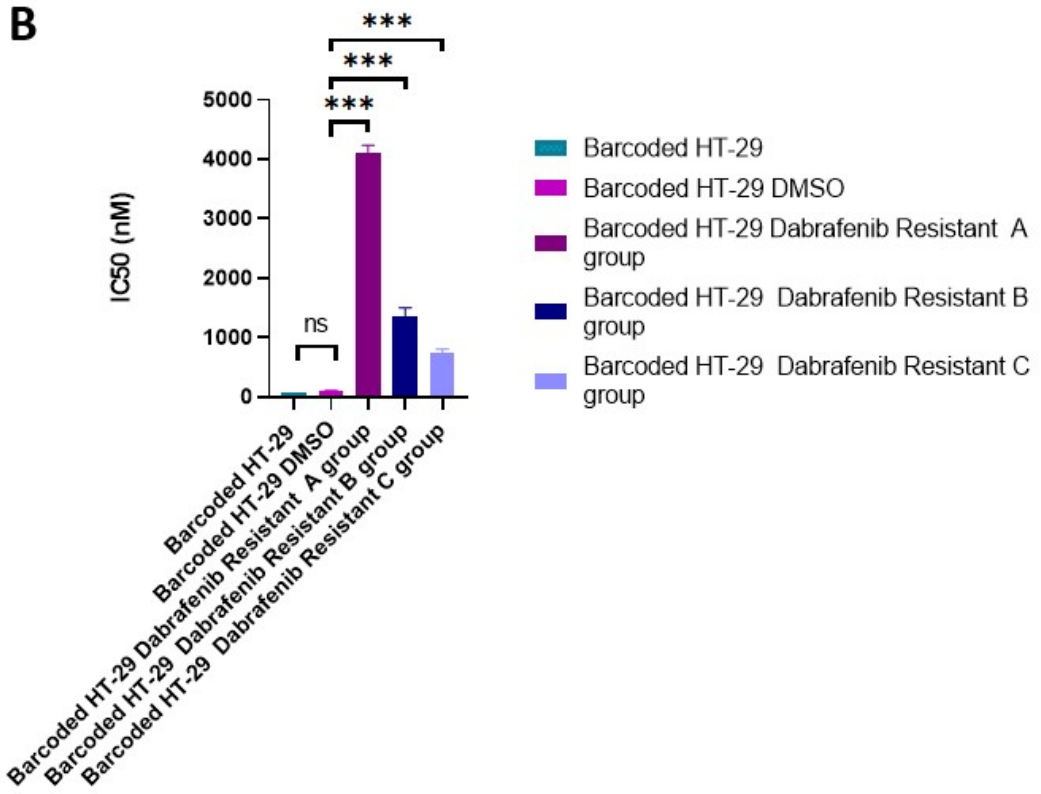

Figure 3. 8 Dose-response curve and comparison of IC values of dabrafenib in barcoded HT-29 cells

Barcoded HT-29, barcoded HT-29 DMSO, and three independent replicates of drug-treated barcoded HT-29 cells were plated at a density of 10,000 cells per well in a 96-well plate. After 24 hours of seeding, cells were incubated with the serial diluted dabrafenib treatment for 72 hours. MTT cell viability assay was performed according to standard procedure. Two independent biological replicated and three technical replicated for each group are shown. (A) dose-response curve of dabrafenib. (B) bar graph of the IC50 values of barcoded HT-29, barcoded HT-29 DMSO, and dabrafenib-treated barcoded HT-29 cells. Significant change in IC50 values of dabrafenib was found. ($p<0.05$, one-way ANOVA test).

Table 3. 2 The table of comparison for IC50 and drug resistance fold of dabrafenib

Cell line	IC_{50} Control group	IC_{50} Drug resistant	Resistance fold
Ht-29 Dabra A	82,98 ± 53,17 nM	4235 ± 1,986 nM	51,04
Ht-29 Dabra B	82,98 ± 53,17 nM	1229 ± 902 nM	14,8
Ht-29 Dabra C	82,98 ± 53,17 nM	677,0 ± 451,5 nM	8,16

Dabrafenib-treated HT-29 cells versus DMSO. Data are presented as means SD (n=2).

Three dabrafenib treated groups showed significant resistance fold change (figure 3.7B). The most significant change in resistance fold was observed in group A dabrafenib-resistant barcoded HT-29 (Table 3.2); thus, group A was chosen for further investigations.

3.6 Barcode analysis of Dabrafenib resistant HT-29 cells

Understanding the clonal evolution under the dabrafenib treatment, the barcoded cells were monitored, and the possible causes behind it were investigated. Several cellular alterations were essential to develop drug resistance (D'Angelo et al., 2020). These alterations can pre-exist in the cell or can be gain or loss during the treatment (N McGranahan, 2017)(Levy et al., 2015). Under selective pressure, the cells that have beneficial alterations can rapidly increase distribution (Levy et al., 2015). Unique barcodes were determined according to NGS results and divided into four subpopulations. The first group, resistant barcodes, were determined in two or three resistant populations and showed the pre-existed cellular alterations (Acar et al., 2020). De novo barcodes were determined in only one replicate and showed the gain or loss of genetic alterations during the treatment. Resistant and de novo barcode

lineages have fitness advantages, and there were some barcodes that have no fitness advantages called sensitive. The final group was determined only in resistant populations, not in DMSO or the initial population called not determined.

Barcodes were identified by NGS that allows all samples to be analyzed in a single run to eliminate the batch effect. For dabrafenib-resistant HT-29 cells, 12515 unique barcodes were determined in the barcoded HT-29 (initial) cell population, 3525 unique barcodes were determined in the barcoded HT-29 DMSO cells population (Figure 3.9A); for dabrafenib-treated groups, 942 unique barcodes determined in A group, 4054 unique barcodes determined in B group, 4596 unique barcodes determined in C group (Figure 3.9B). A decrease in identified unique barcode numbers indicated a strong selective pressure. There was a limitation in barcode analysis since the challenge of increasing the throughput of this method, the depth of sequencing, and the number of cells that extract DNA. The depth of sequencing was 200,000-400,000x and extraction of DNA from 2,000,000 cells; therefore, some thousand unique barcodes were determined. These experiments assumption was the sequenced population represents all the population.

The barcodes/clones can either be positively selected or negatively selected under treatment with respect to the DMSO control plate. The positively selected clones had a positive growth rate, and the negatively selected clones had a negative growth rate during the dabrafenib-treatment in the ratio with DMSO. Functional subclones were identified for determining the growth dynamics. Four functional subclones were used in dabrafenib-resistant HT-29 cells. The first two groups were the largest and represented not determined (grey) and sensitive clones (beige). Not-determined clones could not be observed in DMSO, and sensitive clones had a negative growth rate. The resistant barcodes were determined according to founding at least two replicates. There was one resistant barcode resolved in the A group, six resistant barcodes resolved in the B group, and five resistant barcodes resolved in the C group for dabrafenib-treated barcoded HT-29 cells (Figure 3.9C). These clones had very low frequency. The frequency between replicate B and C were highly similar, and clonal dominance increased the fitness in replicate A, which can be caused by the re-

planting since A group had one more passage than other replicates. Therefore, this may have caused an additional bottleneck to the population in the replicate A and a change in heterogeneity. This may well recapitulate the tumor surgery in clinic whereby a clone can be selected even further following surgery considered as a bottleneck. Moreover, the cell viability results of initial populations in figure 3.5 gives a clue about resistance can be caused by pre-existing cellular alterations since the cells show no increase in cell death with increase in drug dose. The de novo barcodes (blue) were determined; accordingly, 1 in group A, 9 in group B, and 1 in group C. It indicates de novo lineages. This dramatic clone reduction and development of dabrafenib resistance in HT-29 cell lines can be considered stochastic. The intrinsic properties of the clones can lead to these conditions.

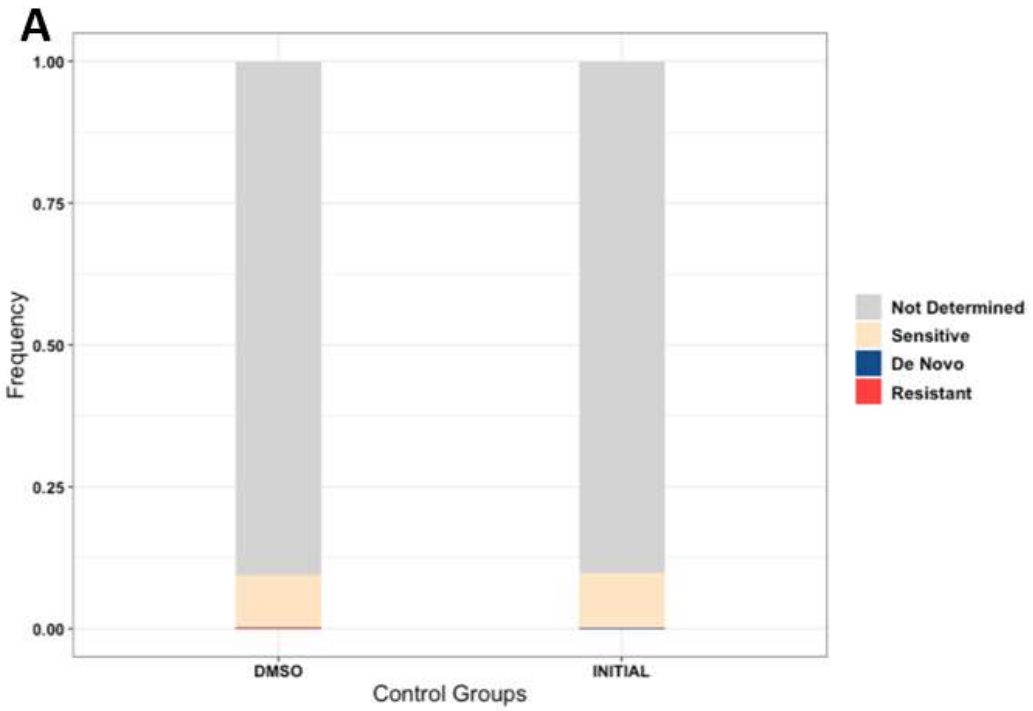

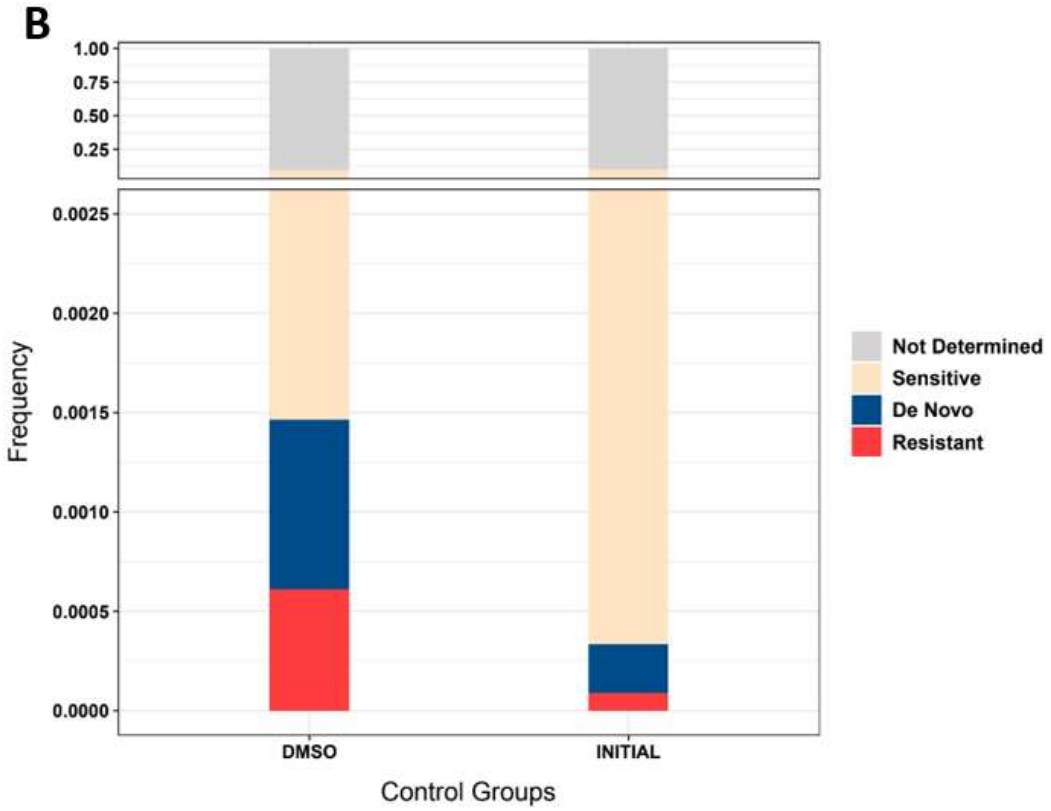
B
1.00
0.75
0.50
0.25
0.0025
0.0020
0.0015
0.0010
0.0005
0.0000
Frequency
DMSO
INITIAL
Control Groups
Not Determined
Sensitive
De Novo
Resistant

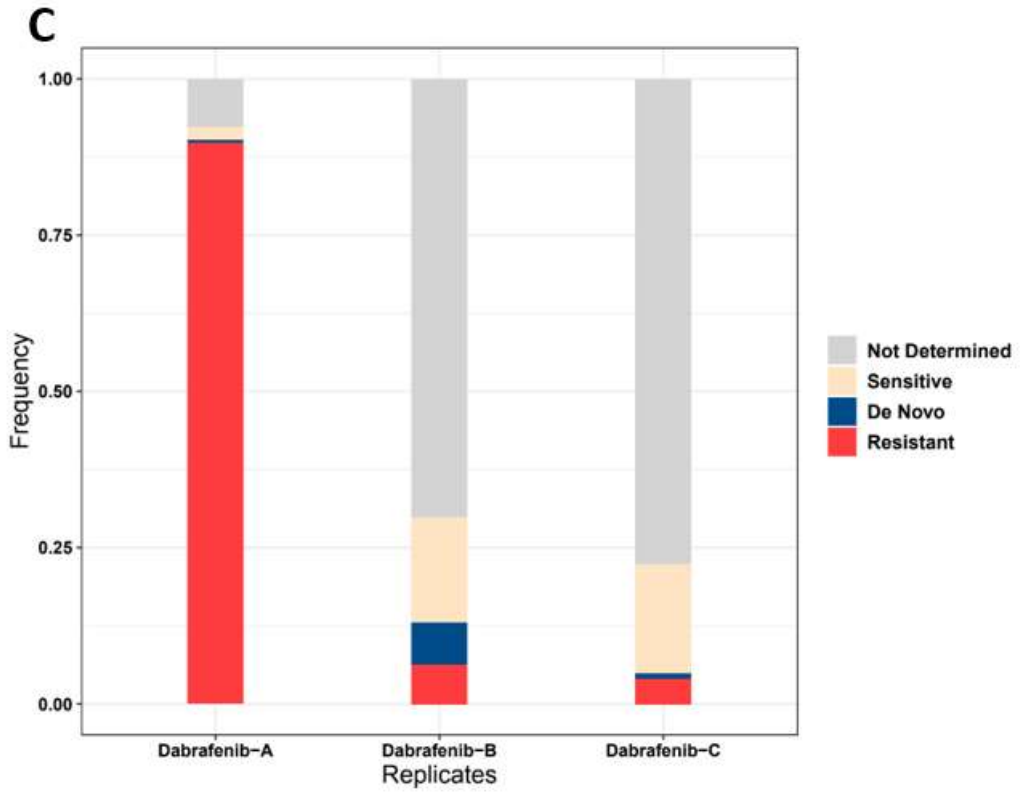

Figure 3. 9 Barcoding sequence results of dabrafenib-resistant barcoded HT-29 cells.

Barcode frequency distributions of barcoded HT-29, barcoded HT-29 DMSO control, and dabrafenib-treated barcoded HT-29 cells were determined. Barcode colors and order are identical between replicates. Barcode phenotypes were resolved by the growth rate and conserved distribution between replicates. Here, the red color represents resistant barcodes that have positive growth rate and were determined in two or more replicates; the blue color represents *de novo barcodes that have positive growth rate and were determined in only one replicate; the beige color represents sensitive barcodes that have negative growth rate, and grey color represents not determined barcodes that not determined in DMSO or initial populations. (A) Evolutionary dynamics of barcoded HT-29 (initial) and barcoded HT-29 DMSO cells. (B) Evolutionary dynamics of barcoded HT-29 (initial) and barcoded HT-29 DMSO cells focused in frequency between 0,0-0,0025. (C) Evolutionary dynamics of dabrafenib treated barcoded HT-29 cells.*

In this experiment, the dabrafenib-treated cells were passaged every month in a 1:10 ratio, and it can cause a sampling bias. The medium was changed twice a week. HT-29 is an adherent cell line. The detachment of cells from the surface shows cell death. The dead cells were collected from floating media; however, the time-course barcode analysis did not perform because of determining one unique resistant barcode.

3.7 Developing SN-38 resistance in barcoded HT-29 cells

Barcoded HT-29 cells thawed and seeded. When they reached confluency, they were divided into four flasks with $2x10^6$ cells seeding per flask. The remaining cells were frozen, and cell pellets were taken for further analysis. The SN-38 treatment started in three flakes. The solvent control (DMSO) flask reached confluency, the cells were frozen, and cell pellets were taken. The SN-38 treated flasks were treated with IC50 dosage of SN-38 until the cells reached confluency under treatment. The duration of treatment was four months. There was a drug holiday every 20 days for ten days, and SN-38 treated groups passaged three times. When they reached confluency, the treated cells were frozen, cell pellets were taken, and cells were seeded for the MTT cell viability assay (Figure 3.10). The resistance fold changes in each drug-treated group were shown (Table 3.3).

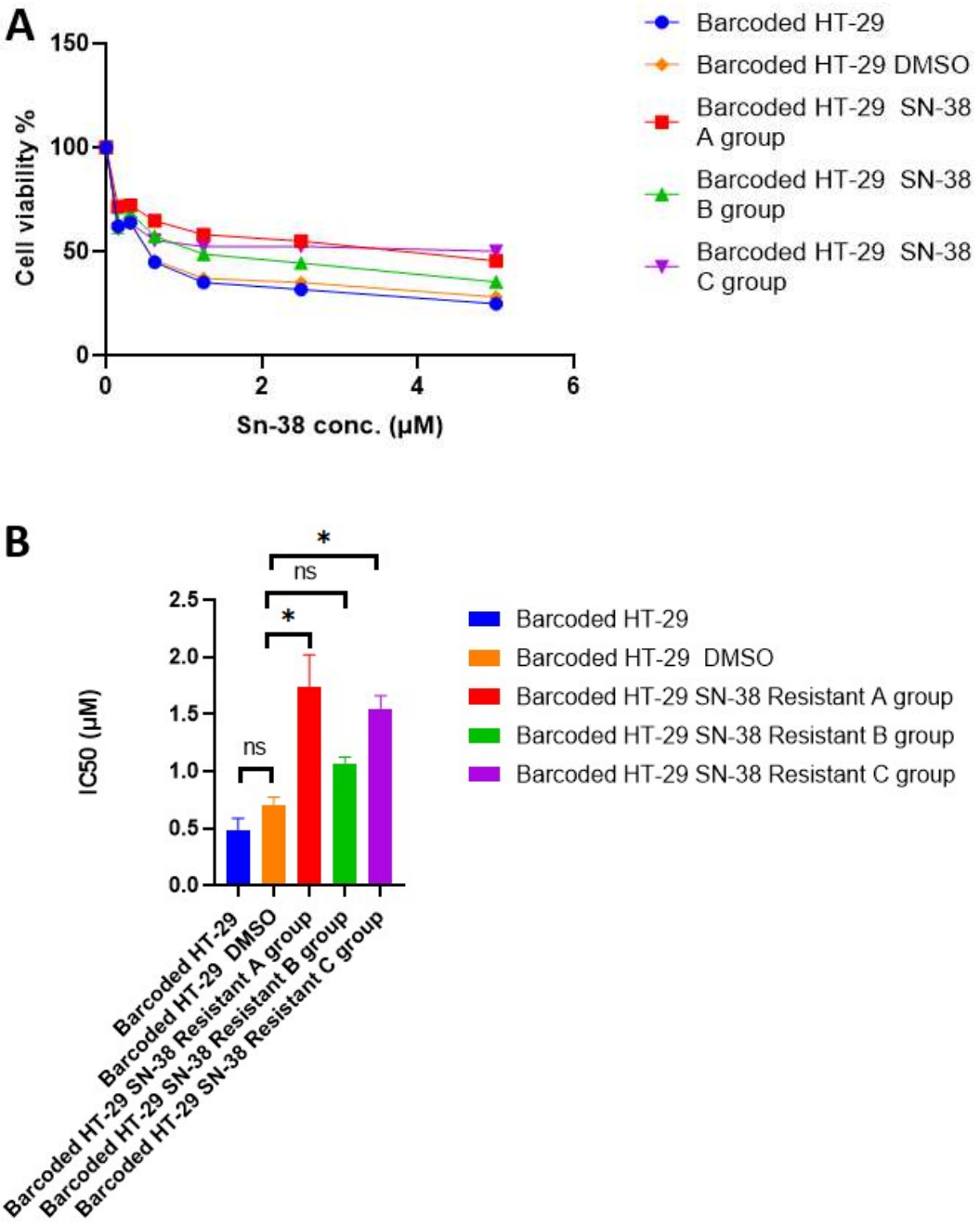

Figure 3. 10 Dose-response curve and comparison of IC values of SN-38 in barcoded HT-29 cells

Barcoded HT-29, barcoded HT-29 DMSO, and three independent replicates of drug-treated barcoded HT-29 cells were seeded (10,000 cells per well) in a 96-well plate. The cells were incubated for 24 hours to allow attachment. The cells were incubated

with the serial diluted SN-38 treatment for 72 hours. MTT cell viability assay was performed according to standard procedure. Two independent biological replicated and three technical replicated for each group are shown. (A) Dose-response curve of SN-38. (B) Bar graph of the IC50 values of barcoded HT-29, barcoded HT-29 DMSO, and SN-38-treated barcoded HT-29 cells. Significant change in IC50 values of SN-38 was found. ($p<0.05$, one-way ANOVA test).

Table 3. 3 The table of comparison for IC50 and drug resistance fold of SN-38

Cell line	IC_{50} Control group	IC_{50} Drug resistant	Resistance fold
Ht-29 Sn-38 A	0,3825 ± 0,0854 uM	1,447 ± 0,387 uM	3,783
Ht-29 Sn-38 B	0,3825 ± 0,0854 uM	1,013 ± 0,2611 uM	2,648
Ht-29 Sn-38 C	0,3825 ± 0,0854 uM	1,063 ± 0,58 uM	2,779

SN-38-treated HT-29 cells versus DMSO. Data are presented as means SD (n=2).

Two SN-38 treated groups showed significant resistance fold change (figure 3. 9B). Group A had the most significant change in the resistance fold (table 3.3); thus, this group was chosen for further analysis.

3.8 Barcode analysis of SN-38 resistant HT-29 cells

Investigating the possible reasons for clonal evolution in the presence of SN-38 treatment, the barcoded HT-29 cells were monitored. These possible reasons were cellular alterations, which can be pre-existing in the population or gain or loss under treatment (D'Angelo et al., 2020). The cells having beneficial alterations can rapidly increase fitness under selective pressure (Levy et al., 2015). NGS analysis allows us

to identify unique barcodes, and there were four subpopulations found. One of them was resistant barcodes determined in two or three replicates and indicated the pre-existed cellular alterations (Acar et al., 2020). De novo barcodes were determined in one replicate and indicated the gain or loss of genomic alterations under the drug exposure. Resistant and de novo barcodes have beneficial mutations and can increase the distribution of the population (Levy et al., 2015). Sensitive barcodes have no fitness advantage, and the final group was not determined and identified only in the resistant population, not in DMSO.

Determination of barcodes were performed by the NGS analysis. All samples were analyzed in a single run to eliminate the batch effect. For SN-38 treated barcoded HT-29 cells, 7555 unique barcodes resolved in the barcoded HT-29 initial cell population, and 7421 unique barcodes resolved in the barcoded HT-29 DMSO cell population (Figure 3.11A). The determined unique barcode numbers of SN-38 treated groups were 3199 for group A, 1465 for group B, and 777 for group C (Figure 3.11B). There was a strong selective pressure shown by diminishing the identified unique barcodes. The barcode analysis had a limitation in the depth of sequencing and the number of cells that isolated DNA. The depth of sequencing was 200,000-400,000x, and isolation of DNA was performed from 2,000,000 cells. Some thousand unique barcodes were determined because of these limitations. The barcodes can be positively selected, which has a positive growth rate, or negatively selected, which has a negative growth rate during the SN-38 exposure with respect to DMSO. According to the growth dynamics of barcodes, four functional subclones were identified. The first group was not determined (grey), and the second group was sensitive clones (beige). These groups had the largest frequencies. Not determined clones could not be observed in DMSO, and sensitive clones had a negative growth rate under SN-38 treatment. The barcodes identified in at least two replicates were called resistant barcodes. Five resistant barcodes were determined in group A, three resistant barcodes were determined in group B, and six resistant barcodes were determined in group C of SN-38 treated barcoded HT-29 cells (Figure 3.11C). There were seven unique resistant barcodes resolved (Figure 3.11C). The frequencies of

barcodes between replicates of drug-treated were highly similar (Figure 3.11C). Hence the clonal behavior is repeatedly observed in SN-38 treated cells. This indicates non-stochastic clonal evolution and intrinsic properties such as biological factors of the clones. Thus, these dynamics were deterministic and indicate that development of drug resistance for a chemotherapeutic can be caused by pre-existing cellular alterations which is unpredictable.

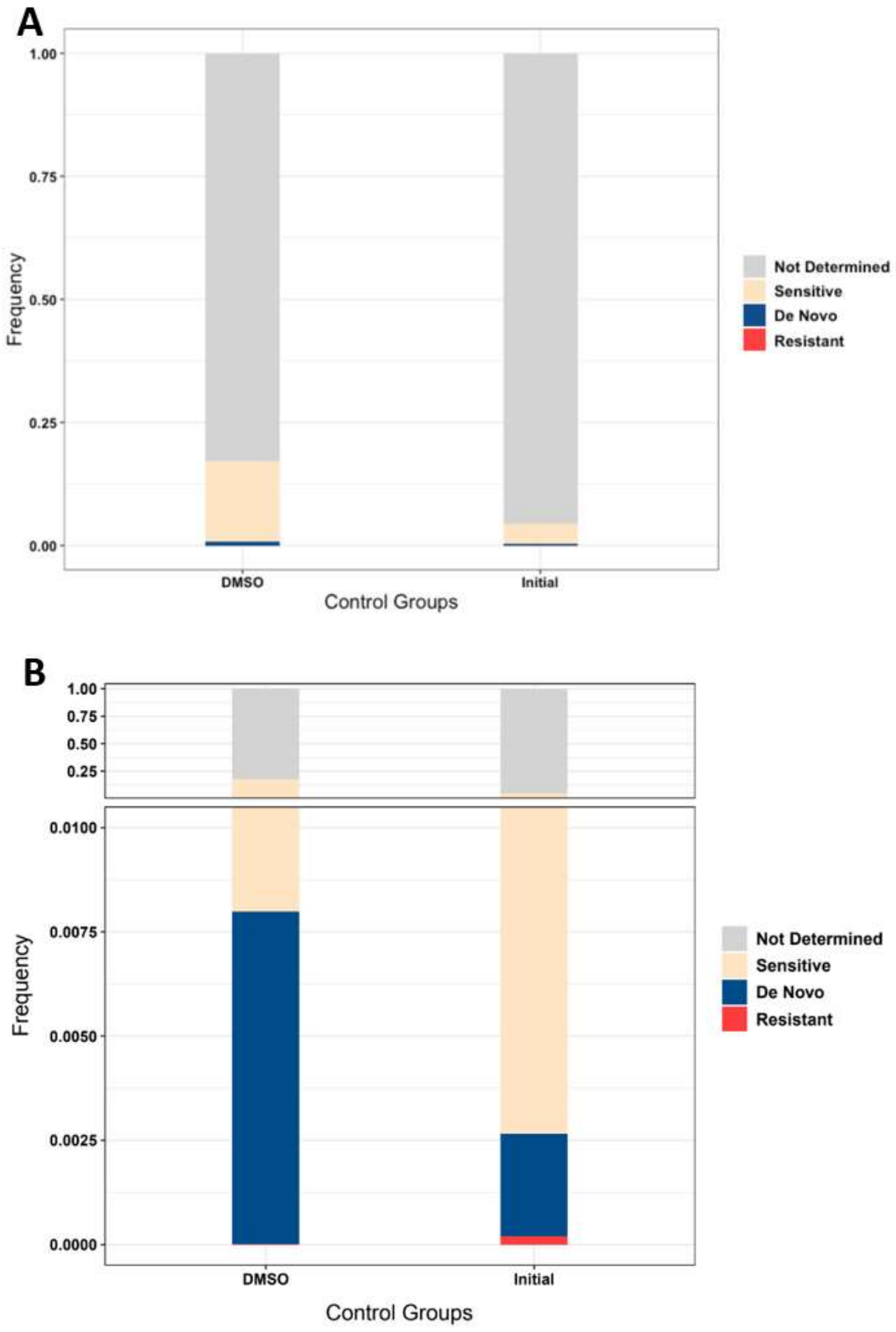
A
1.00
0.75
0.50
0.25
0.00
Frequency
DMSO
Initial
Control Groups
Not Determined
Sensitive
De Novo
Resistant
B
1.00
0.75
0.50
0.25
0.0100
0.0075
0.0050
0.0025
0.0000
Frequency
DMSO
Initial
Control Groups
Not Determined
Sensitive
De Novo
Resistant

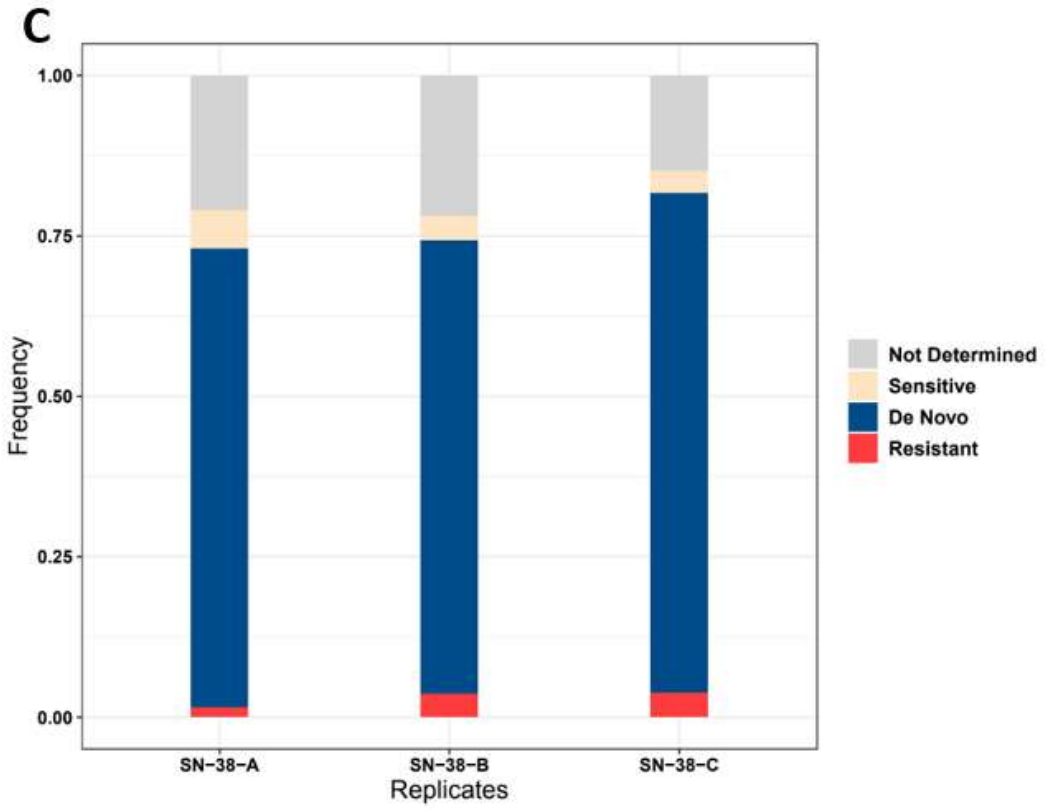

Figure 3. 11 Barcoding sequence results of SN-38-resistant barcoded HT-29 cells

Barcoded HT-29, barcoded HT-29 DMSO control, and SN-38-treated barcoded HT-29 cells' barcode frequency distributions were shown. Barcode colors and order are identical between replicates. The barcode growth rate and conserved distribution determine barcode phenotypes. Here, barcodes that had a positive growth rate and were determined in two or more replicates were resistant and shown in red color. Barcodes that had a positive growth rate and determined only one replicate were de novo barcodes and shown in blue color. The barcodes had a negative growth rate, sensitive barcodes, and shown in the beige color. The barcodes were determined only in resistant replicates not determined in DMSO, or initial populations were not determined barcodes and shown in grey color. (A) Evolutionary dynamics of barcoded HT-29 (initial) and barcoded HT-29 DMSO cells. (B) Evolutionary dynamics of barcoded HT-29 (initial) and barcoded HT-29 DMSO cells focused on 0,00 and 0,01. (C) Evolutionary dynamics of SN-38 treated barcoded HT-29 cells.

In this experiment, the SN-38-treated cells were passaged three times, and it can cause a sampling bias. The medium was changed twice a week. HT-29 is an adherent cell line; the detachment of the surface indicates cell death. The floating cells collected from media at every medium change.

3.9 Tracking the SN-38 resistance dynamics in barcoded HT-29 cells

Inherited genomic properties of the cell are crucial for developing drug resistance (Coffey et al., 2013). In cancer therapy, tumor heterogeneity is a challenge, and the clones can develop resistance to therapy (N McGranahan, 2017). The clones carried inherited genomic properties for drug resistance, could be low frequencies in a population before the therapy and could be enriched after the therapy (Serrano et al., 2022). Thus, drug exposure can cause drastic clonal selection. Apart from genomic characteristics leading the clonal selection during treatment, the plasticity of clones could have an essential role in treatment resistance (Marine et al., 2020). If there is no decrease in the barcode numbers in the presence of treatment, it indicates this resistance mechanism is not caused by pre-determined genetic factors; however, resistance can be developed by the transient state of a few clones that can resist (Serrano et al., 2022).

In this experiment, there was a collection of dead cells from floating media twice a week in every medium change. HT-29 is an adherent cell line since cell float in media was identified as cell death. The barcodes from floating cells were isolated and sequenced every month. Resistant cells died because of a natural causes released their barcode DNA into the medium and this floating barcodes were used to determine longitudinal barcode selection through the course of experiment. Monitoring the time-course of barcodes provides the tracking of evolution under SN-38 treatment.

The tracking evolution under drug exposure barcodes was determined with time-course. This result shows there is a similarity between the final time point of

barcodes collected from floating cells and the barcodes identified in the final population (Figure3.12A). This indicated the evolutionary dynamics under drug exposure. In the initial population, many of the barcodes were extinct of the sensitivity for SN-38. The harvested media barcode sequence results indicate both sensitive and resistant barcodes. They determined in the initial stages; the cells found in the floating media and identified them as different barcodes of sensitive cells (Figure 3.12B). there is no enrichment in those clones. The resistant cells grow under the SN-38 treatment, becoming dominant over the population at the end of the experiment. This indicates the resistant cells dividing and turning over under drug exposure. At the third time point, the resistant cells have a drastic increase in frequency overpopulation, which can cause by drug holidays; since there is no selective pressure, the frequencies of both sensitive and resistant cells increase (Figure 3.12A). Final time point shows that after the drug holiday was lifted selected barcode clones exhibited increased frequency suggesting the presence of drug induced selection in the system monitored by barcode technology.

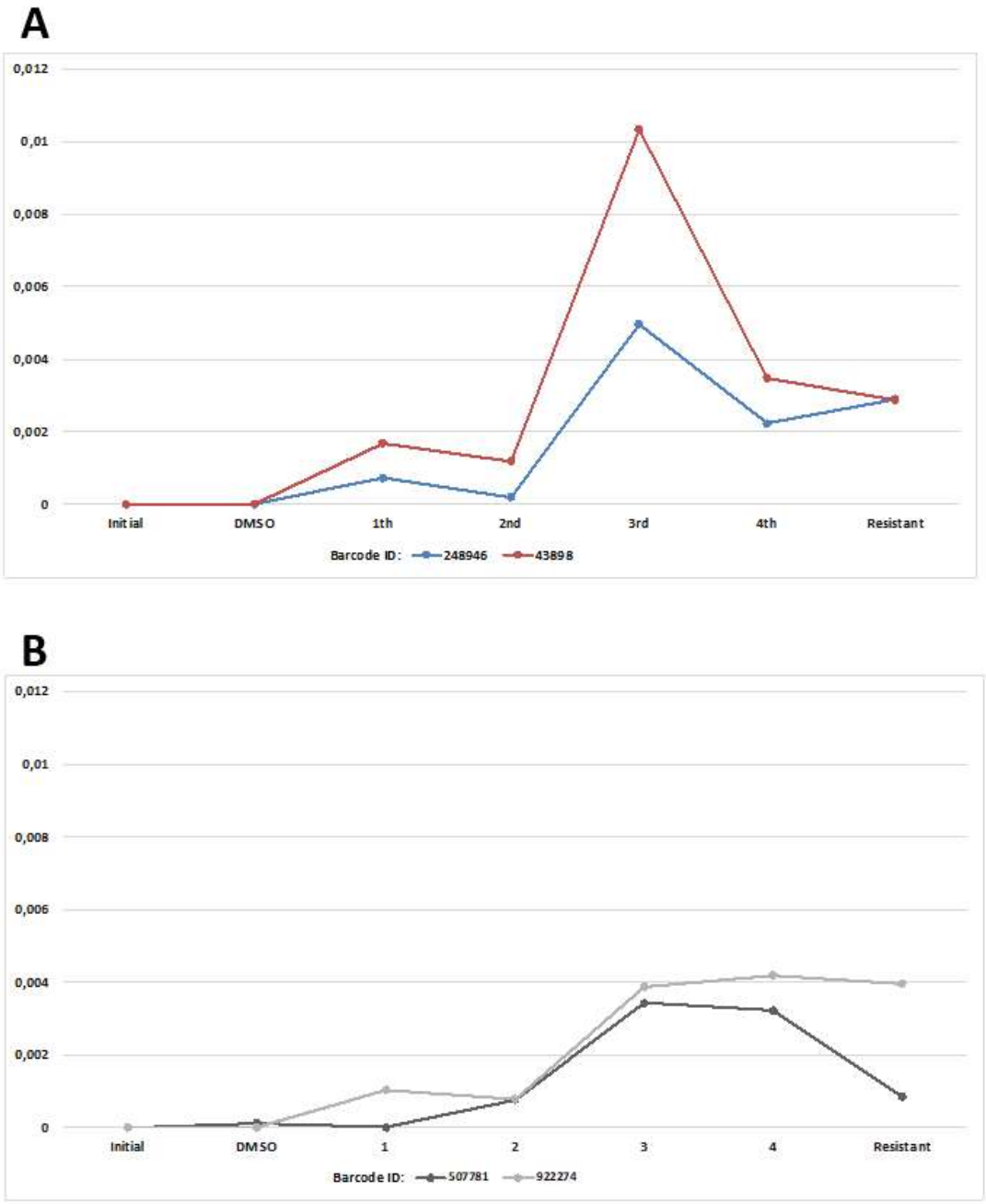

Figure 3. 12 Temporal frequencies for the floating barcodes in replicate A of SN-38 treated barcoded HT-29

Barcoded HT-29 (initial) and barcoded HT-29 DMSO measurements were harvested populations as is the final time point, and all others are floating barcode measurements. The harvested ones belong to live cells, and the floating ones belong to dead cells. The final sample's harvested population largely matched the last

floating barcode sample. After the second time, there was a drug holiday, and after the third one, drug exposure started again. (A) Temporal frequencies for resistant barcodes. (B) Temporal frequencies for sensitive barcodes.

3.10 Investigation of capecitabine resistance effect on the proliferation

Drug treatment impacts cellular processes such as proliferation (Gottesman et al., 2002). Thus, there can be a proliferation change in the drug adaptation stage since adaptive approaches use buffer therapy. The buffer therapy is developing resistance to a drug that can cause a diminish in proliferation (Acar et al., 2020).

The growth curve analysis and the proliferation experiments indicated a cost in terms of proliferation in drug resistance development (Figure 3.13). There is a reduction in terms of growth rate and proliferation when compared to the initial and DMSO population with drug-resistant cells (Figure 3.13B). It can be caused by buffer therapy since the drug-sensitive cell population can be more competitive, and the drug-resistant cell populations can be outcompeted in a drug-free environment.

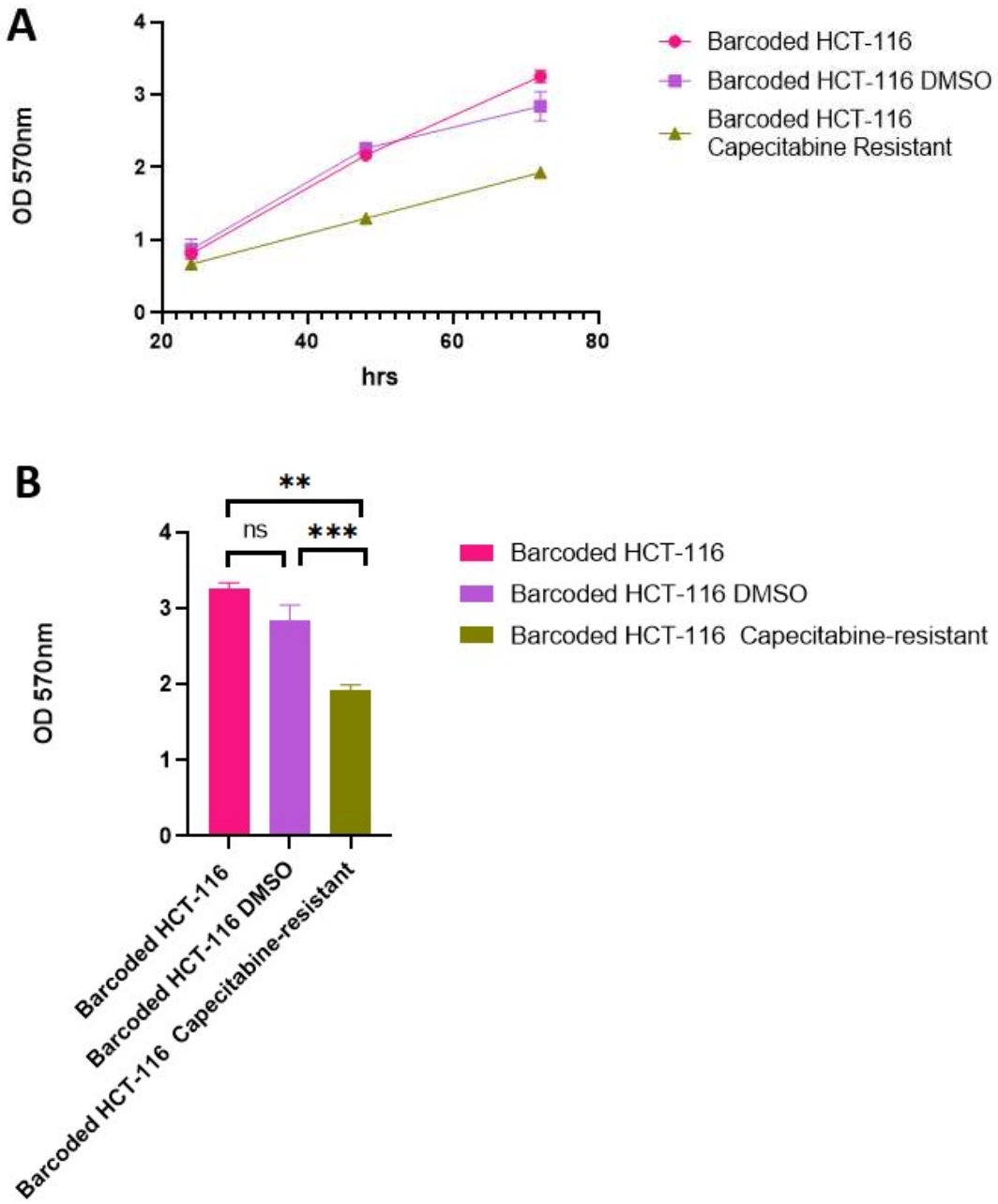

Figure 3. 13 The effects of capecitabine resistance in proliferation

The cells were plated in 10,000 cells per well into three 96-well plates, and cells were fixed with 2%formaldyde every 24 hours for 72 hours. Cells were stained with 0.1% crystal violet solution and 10% acetic acid solution used to dissolve crystal violet. The absorbance at 570 nm was measured using a microplate reader. (A)

growth curve of initial, DMSO, and capecitabine resistant HCT-116 cell lines. (B) the proliferation assay for 72 hours on barcoded HCT-116, barcoded HCT-116 DMSO, and barcoded HCT-116 capecitabine-resistant cells. Two independent biological replicates were carried out. Significant changes in cellular proliferation were observed.(p-value < 0.05, ANOVA).

3.11 Investigation of dabrafenib and SN-38 resistance effect on the proliferation

Cellular proliferation can be affected by the alterations during drug exposure (Gottesman et al., 2002). The buffer therapy can cause proliferation change that could occur in drug resistance development. It is used to check the resistant subpopulations by the sensitive subpopulation through competition (Acar et al., 2020).

The growth curve analysis and the proliferation experiments indicated there was no cost in terms of proliferation in drug resistance development (Figure 3.14A&B). Thus, dabrafenib and SN-38 resistance did not cause any change in proliferative pathways (Figure 3.14B).

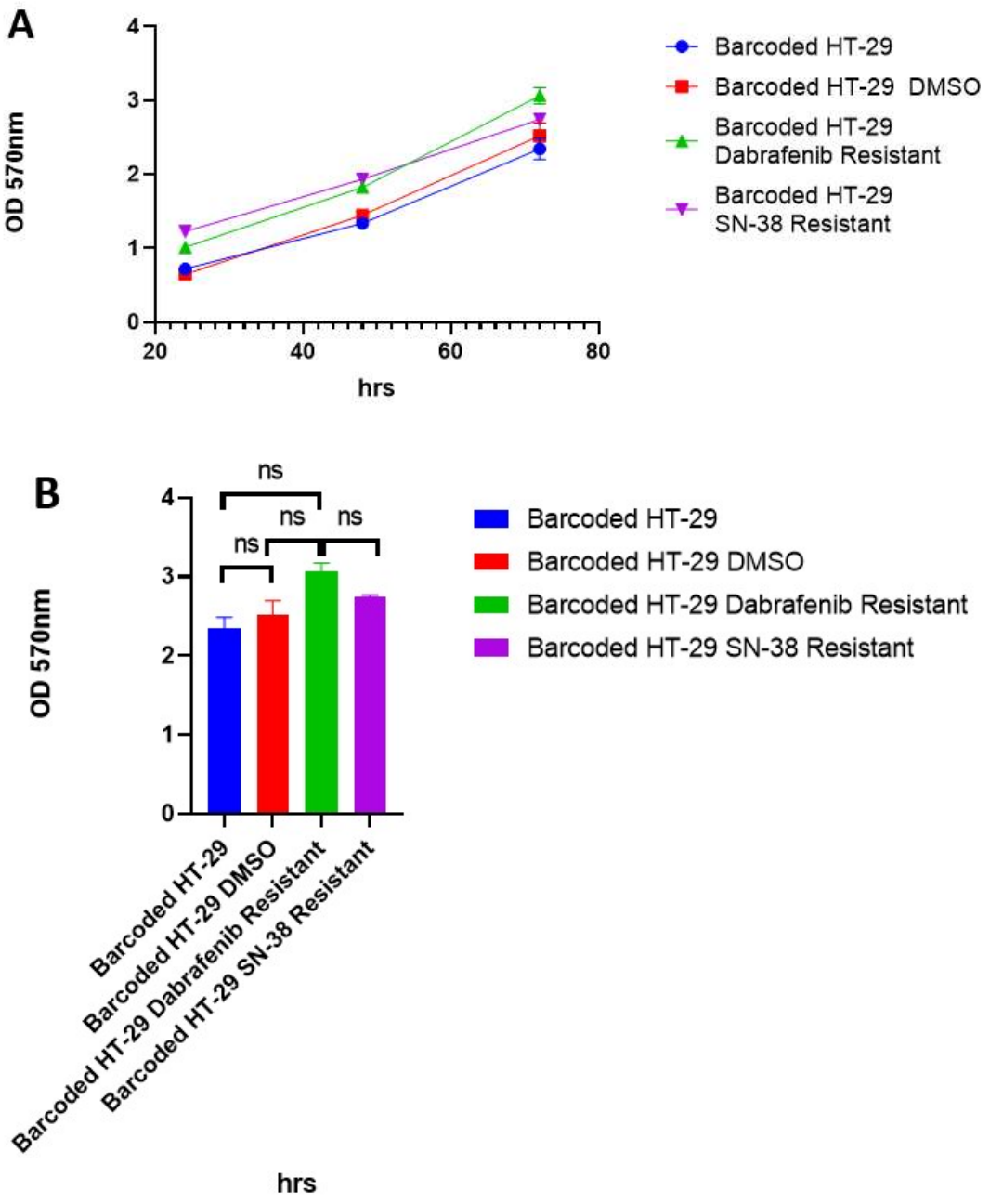

Figure 3. 14 The effects of dabrafenib and SN-38 resistance in proliferation

The cells were seeded in 10,000 cells per well into three 96-well plates. Cells were fixed with 2%formaldyde every 24 hours for 72 hours and stained with 0.1% crystal violet solution. To dissolve the crystal violet, 10% acetic acid solution was used, and the absorbance at 570 nm was measured using a microplate reader. (A) growth curve

of initial, DMSO, and dabrafenib-resistant and SN-38-resistant HT-29 cell lines. (B) the proliferation assay for 72 hours on barcoded HT-29, barcoded HT-29 DMSO, barcoded HT-29 dabrafenib-resistant, and barcoded HT-29 SN-38 resistant cells. Two independent biological replicates were carried out. No significant changes in cellular proliferation were observed.(p-value > 0.05, ANOVA).

3.12 Effect of capecitabine resistance on drug sensitivity

Collateral sensitivity and therapeutic resistance evolution to one drug can create sensitivity to another drug (Pluchino et al., 2012). Under selection pressure, the drug-exposed cells can have two different fitness. The fitness landscape can have a positive correlation against the second drug, which indicates collateral resistance (Scarborough et al., 2020). It is caused by genomic alterations that occur in the development of first drug resistance, which can allow fitness increase in the second drug exposure. The fitness landscape can have a negative correlation that indicates collateral sensitivity. It shows that the genotypic alterations in the presence of developing drug resistance lead to a fitness decrease in second drug exposure (Scarborough et al., 2020).

In this experiment, the investigation of three different chemotherapeutics, irinotecan (3.15A), oxaliplatin (figure 3.15B), and SN-38 (figure 3.15C) on capecitabine-resistant HCT-116 cells. The cell viability results were analyzed by comparing barcoded HCT-116 DMSO cells to capecitabine-resistant barcoded HCT-116 cells (Figure 3.15).

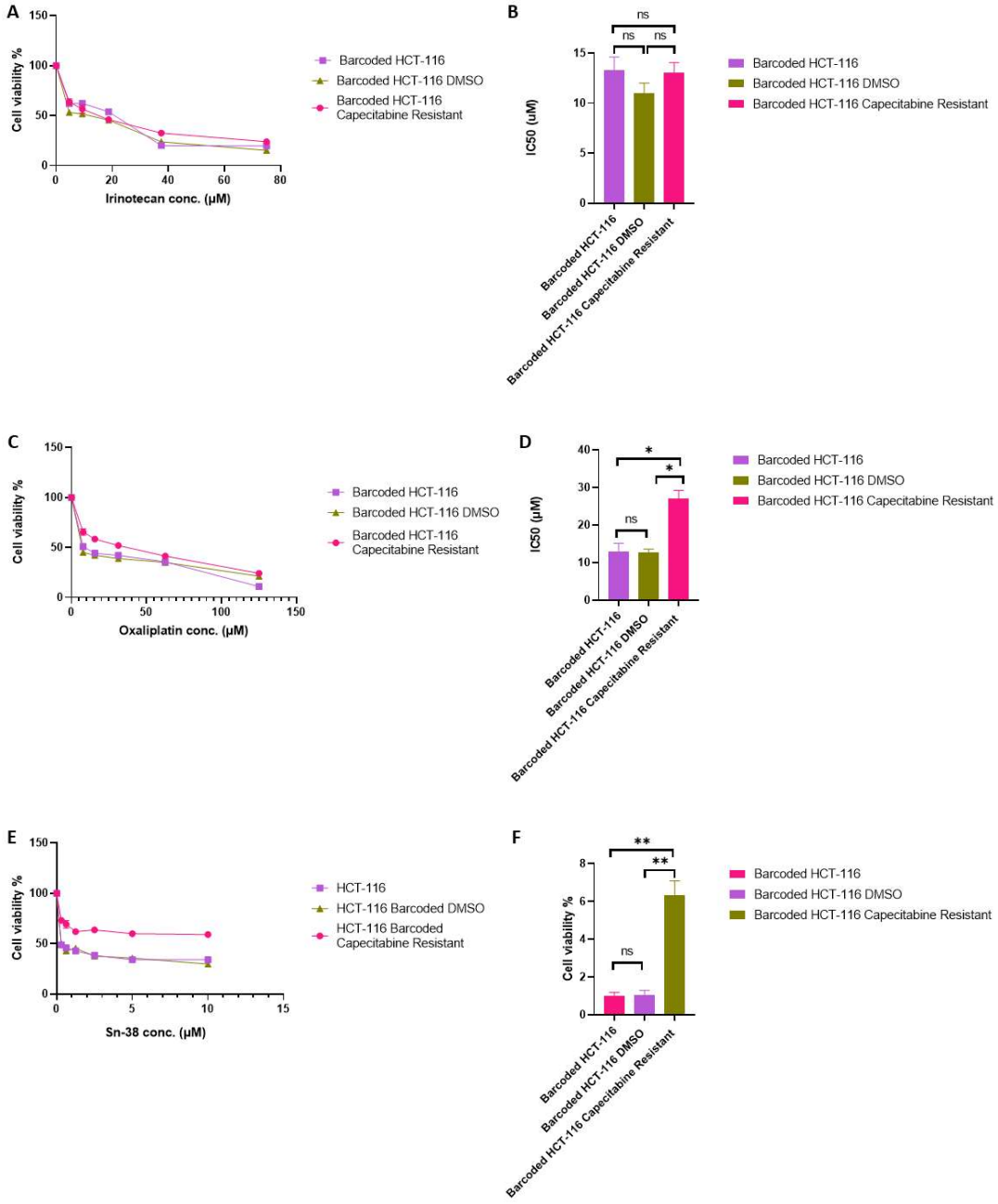

Figure 3. 15 The effect of capecitabine resistance in HCT-116 cells in the exposure of irinotecan, oxaliplatin, and SN-38 drugs

Barcoded HCT-116, Barcoded HCT-116 DMSO, and capecitabine-resistant barcoded HCT-116 cell plated in 96 well with 10,000 cells per well. The cells were allowed to attach for 24 hours. The medium was replaced, serial dilutions of drugs prepared and added, not drug included wells used as interval control. Cells were

incubated for 72 hours. MTT cell viability assay was performed. Two independent biological replicates and three technical replicates from each group are shown. (A) MTT cell viability graph of irinotecan. (B) Bar graph of IC 50 comparison with barcoded HCT-116 DMSO and capecitabine resistant HCT-116 cells with irinotecan treatment. No significant change was found in comparison with the initial cell population, DMSO cell population, and capecitabine-resistant cell population ($p > 0,05$, one-way ANOVA). (C) MTT cell viability graph of oxaliplatin. (D) Bar graph of IC50 comparison of oxaliplatin in barcoded HCT-116, barcoded HCT-116 DMSO, capecitabine-resistant barcoded HCT-116 cells. No significant change was found in comparison with the initial cell population, DMSO cell population ($p > 0,05$, one-way ANOVA); however, significant change was found in comparison with the DMSO population and capecitabine resistant population ($p < 0,05$, one-way ANOVA). (E) MTT cell viability graph of SN-38. (F) Bar graph of IC50 comparison of SN-38 in barcoded HCT-116, barcoded HCT-116 DMSO, capecitabine-resistant barcoded HCT-116 cells. No significant change was found in comparison with the initial cell population, the DMSO cell population ($p > 0,05$, one-way ANOVA). Significant change was found compared with the DMSO and capecitabine-resistant population ($p < 0,05$, one-way ANOVA).

There can be variable changes in feedback to the treatment of the second drug in the presence of capecitabine resistance. Figure 3.15 indicates the collateral sensitivity or resistance by fold change of IC50 to irinotecan, oxaliplatin, and SN-38. There is no significant change compared to the initial DMSO or capecitabine-resistant HCT-116 populations in irinotecan treatment (Figure3.15A). However, oxaliplatin and SN-38 treatment show a significant increase in IC50 in the presence of capecitabine resistance in HCT-116 cells (Figure 3.15B&C). The resistance ratio can calculate the collateral resistance. It is the ratio of IC50 values of the resistant cells to the parental cells (Hall et al., 2009). A higher than two ratio indicates the collateral cross-resistance (Hall et al., 2009).

The IC50 values of oxaliplatin in capecitabine-resistant cells were 25 µM, and the DMSO population was 12 µM; a 2,1-resistance ratio was calculated, indicating the

cross-resistance. The capecitabine resistant cells' IC50 value of SN-38 was 7 μM, and the DMSO control group IC50 value was 0,2 μM. The resistance ratio was 35-fold, indicating the cross-resistance in capecitabine-resistant HCT-116 cells. Thus, there was no collateral sensitivity observed in capecitabine-resistant HCT-116 cells. However, collateral cross-resistance was found in capecitabine HT-116 cells in oxaliplatin and SN-38 treatment.

3.13 Effect of dabrafenib resistance in HT-29 cells on drug sensitivity

Therapeutic resistance to one drug can cause sensitivity to another drug in cancer cells, called collateral sensitivity (Pluchino et al., 2012). In the presence of selection pressure, cancer cells alter genomic features to survive. Two different fitness can be observed in that case. First, the cells can have a positive correlation in terms of the fitness landscape against the second drug, and it was identified as collateral resistance (Scarborough et al., 2020). The genomic alterations that occur during the development of first drug resistance can cause it, and the cells' fitness increases in the second drug treatment. Last, the cells can have a negative correlation in the fitness landscape in the presence of second drug exposure, which is collateral sensitivity (Pluchino et al., 2012). The alteration of genomic features under the first drug therapy can cause a decrease in fitness during the second drug treatment (Acar et al., 2020).

In this experiment, the cell viability assays were performed against four different chemotherapeutics SN-38 (Figure 3.16A), oxaliplatin (Figure 3.16B), capecitabine (Figure 3.16C), irinotecan (Figure 3.16D) on dabrafenib-resistant HT-29 cells. The cell viability results compared barcoded HT-29 DMSO cells to dabrafenib-resistant barcoded HT-29 cells (Figure 3.16).

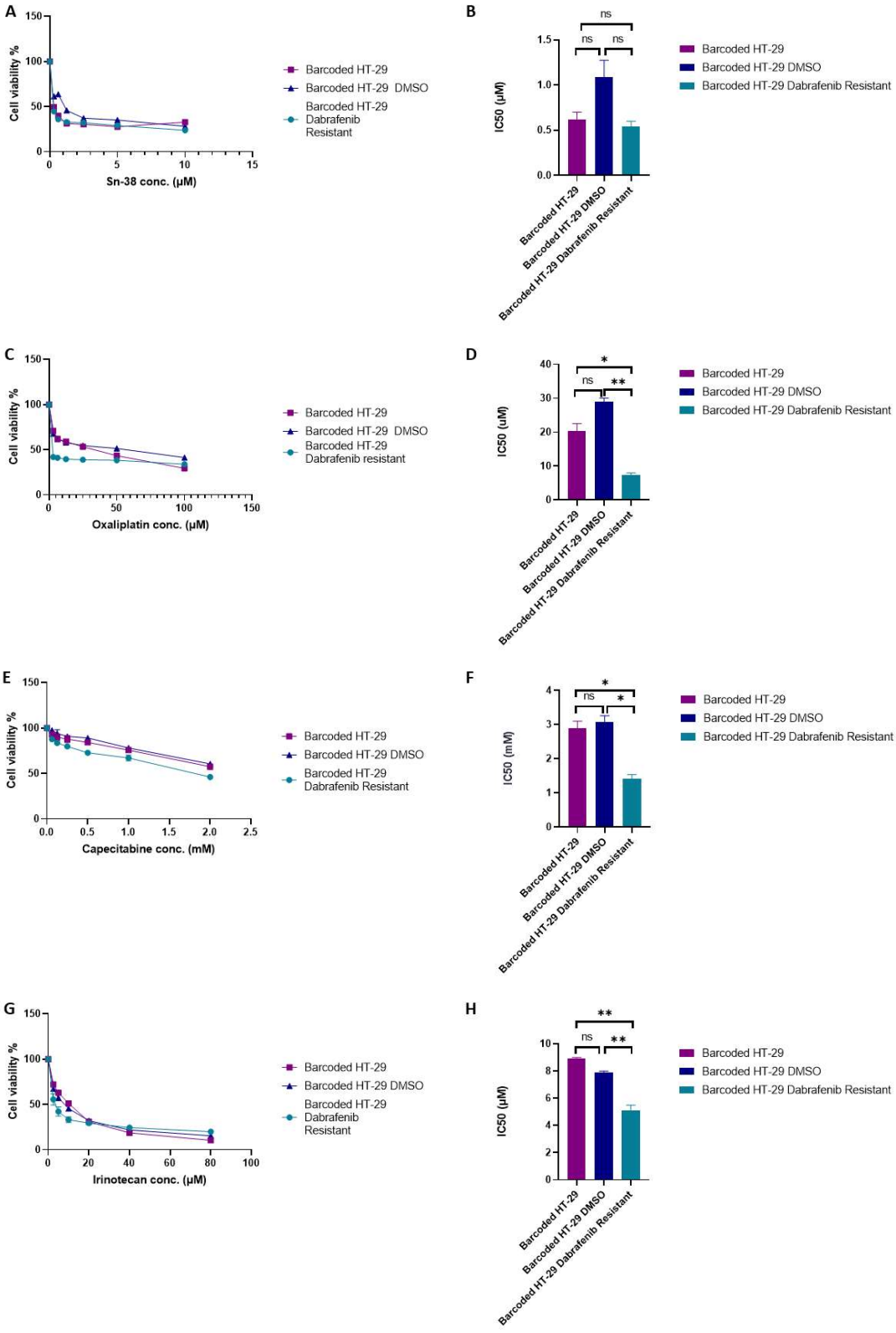
A
Cell viability %
Sn-38 conc. (μM)
Barcoded HT-29
Barcoded HT-29 DMSO
Barcoded HT-29 Dabrafenib Resistant
B
IC50 (μM)
ns
Barcoded HT-29
Barcoded HT-29 DMSO
Barcoded HT-29 Dabrafenib Resistant
C
Cell viability %
Oxaliplatin conc. (μM)
Barcoded HT-29
Barcoded HT-29 DMSO
Barcoded HT-29 Dabrafenib resistant
D
IC50 (uM)
*
ns
**
Barcoded HT-29
Barcoded HT-29 DMSO
Barcoded HT-29 Dabrafenib Resistant
E
Cell viability %
Capecitabine conc. (mM)
Barcoded HT-29
Barcoded HT-29 DMSO
Barcoded HT-29 Dabrafenib Resistant
F
IC50 (mM)
*
ns
*
Barcoded HT-29
Barcoded HT-29 DMSO
Barcoded HT-29 Dabrafenib Resistant
G
Cell viability %
Irinotecan conc. (μM)
Barcoded HT-29
Barcoded HT-29 DMSO
Barcoded HT-29 Dabrafenib Resistant
H
IC50 (μM)
**
ns
**
Barcoded HT-29
Barcoded HT-29 DMSO
Barcoded HT-29 Dabrafenib Resistant

Figure 3. 16 The effect of dabrafenib resistance in HT-29 cells in the exposure of SN-38, oxaliplatin, capecitabine, and irinotecan drugs

Barcoded HT-29, Barcoded HT29 DMSO, and dabrafenib-resistant barcoded HT-29 cell seeded in 96 well plates (10,000 cells per well). The cells were allowed to attach for 24 hours. The medium was replaced with serial dilutions of drugs included medium and not drug included medium added wells used as the internal control. Cells were incubated for 72 hours. MTT cell viability assay was performed according to standard procedure. Two independent biological replicates and three technical replicates from each group are carried out. (A) MTT cell viability graph of SN-38. (B) Bar graph of IC 50 comparison with barcoded HT-29 DMSO and dabrafenib resistant HT-29 cells with SN-38 treatment. No significant change was found in comparison with the initial cell population, DMSO cell population, and dabrafenib-resistant cell population ($p > 0,05$, one-way ANOVA). (C) MTT cell viability graph of oxaliplatin. (D) Bar graph of IC50 comparison of oxaliplatin in barcoded HT-29, barcoded HT-29 DMSO, dabrafenib-resistant barcoded HT-29 cells. No significant change was found in comparison with the initial cell population, DMSO cell population ($p > 0,05$, one-way ANOVA); however, a significant change was found in comparison with the DMSO population and dabrafenib resistant population ($p < 0,05$, one-way ANOVA). (E) MTT cell viability graph of capecitabine. (F) Bar graph of IC50 comparison of capecitabine in barcoded HT-29, barcoded HT-29 DMSO, dabrafenib-resistant barcoded HT-29 cells. No significant change was found in comparison with the initial cell population, the DMSO cell population ($p > 0,05$, one-way ANOVA). Significant change was found compared with the DMSO and dabrafenib-resistant population ($p < 0,05$, one-way ANOVA). (G) MTT cell viability graph of irinotecan. (H) Bar graph of IC50 comparison of irinotecan in barcoded HT-29, barcoded HT-29 DMSO, dabrafenib-resistant barcoded HT-29 cells. No significant change was found in comparison with the initial cell population, the DMSO cell population ($p > 0,05$, one-way ANOVA). Significant change was found compared with the DMSO and dabrafenib-resistant population ($p < 0,05$, one-way ANOVA).

Variable changes can be observed in response to second drug exposure when the dabrafenib resistance evolved.Figure 3.16 shows the collateral sensitivity with cell viability assay analysis and comparison of IC50 values for SN-38, oxaliplatin, capecitabine, and irinotecan. No significant change was found in the SN-38 treatment in initial DMSO and dabrafenib-resistant HT-29 cell populations.

The collateral sensitivity determined by the resistance ratio that is the ratio of resistant cells IC50 value to parental cells IC50 value (Hall et al., 2009). Whether the ratio less than 0.5 it shows the collateral sensitivity (Hall et al., 2009). Whether the ratio higher than 2 it can indicate the cross resistance (Hall et al., 2009).

The IC50 values of oxaliplatin in dabrafenib-resistant HT-29 cell was 7 μM and in barcoded HT-29 DMSO cell was 27.9 μM; thus the resistance ratio was 0,25 which indicates the collateral sensitivity. The capecitabine IC50 value was 1,3 mM in dabrafenib resistant HT-29 cells and 3,26 mM in barcoded HT-29 DMSO cells; hence the resistance ratio would be 0,39 that indicates collateral sensitivity. The IC50 value of irinotecan in dabrafenib-resistant cell was 4,8 μM and in DMSO control was 8 μM; thus the resistance ratio was 0,6. There was no collateral sensitivity found in dabrafenib-resistant HT-29 cells to irinotecan treatment. There is the identification of collateral sensitivity for oxaliplatin, and capecitabine in dabrafenib-resistant HT-29 cell line by a significant decrease in IC50 values against these drugs in comparison of dabrafenib-resistant HT-29 cells to DMSO population of HT-29 cells.

3.14 Effect of SN-38 resistance in HT-29 cells on drug sensitivity

The evolution of drug resistance to one drug can lead to sensitivity to another drug, and it is called collateral sensitivity (Pluchino et al., 2012). Different genomic alterations occur under drug exposure, which is crucial for surviving the clones. The clones can have a positive or negative correlation with fitness dynamics. The positive correlation indicates collateral resistance, that is, the fitness landscape increase in the presence of a second drug treatment (Scarborough et al., 2020). The negative

correlation identified as collateral sensitivity is the fitness landscape decrease in the exposure to second drug treatment (Pluchino et al., 2012). Thus, the genomic alterations that occur in the evolution of drug resistance can cause diminish in fitness under the second drug therapy (Acar et al., 2020).

There were the cell viability assays against four different chemotherapeutics irinotecan (Figure 3.17A), capecitabine (Figure 3.17B), oxaliplatin (Figure 3.17C), dabrafenib (Figure 3.17D) on initial, DMSO and SN-38 resistant HT-29 cell lines. The comparison of IC50 values indicates the correlation between barcoded HT-29 DMSO and dabrafenib-resistant barcoded HT-29 cells (figure3.17).

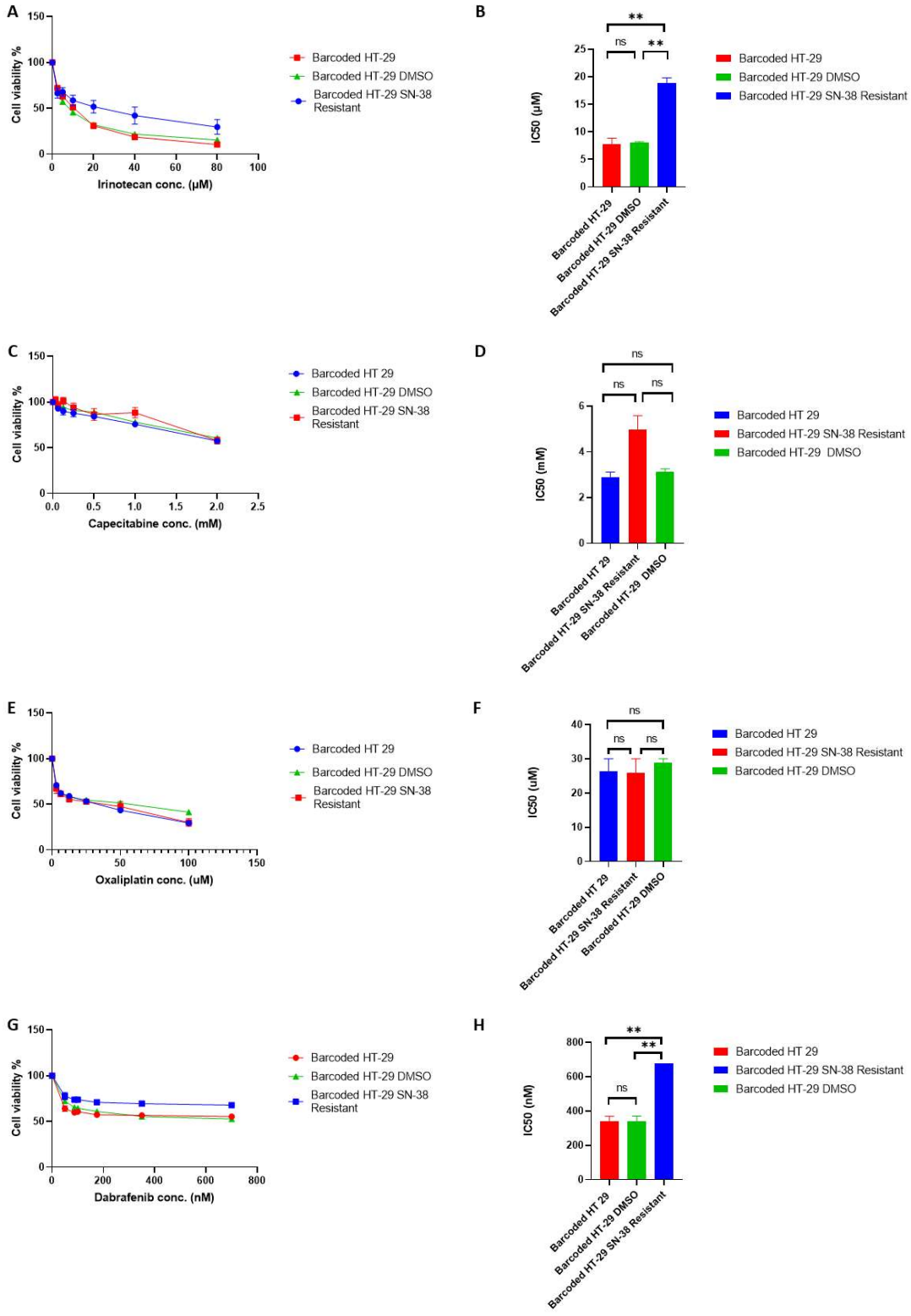

Figure 3. 17 The effect of dabrafenib resistance in HT-29 cells in treating irinotecan, capecitabine, oxaliplatin, and dabrafenib drugs

Barcoded HT-29, Barcoded HT29 DMSO, and SN-38-resistant barcoded HT-29 cells were plated in 96 well plates at 10,000 cells per well. After the cells were allowed to attach for 24 hours, the cells were either untreated or treated with DMSO as vehicle control or indicated doses of irinotecan, capecitabine, oxaliplatin, or dabrafenib. Cells were incubated for 72 hours, and an MTT cell viability assay was performed according to standard procedure. Two independent biological replicates and three technical replicates from each group are carried out. (A) Cell viability 72h after treatment of irinotecan. (B) The bar graph of IC 50 compares with barcoded HT-29 DMSO and SN-38 resistant HT-29 cells in treating irinotecan. No significant change was found in comparison with the initial cell population, the DMSO cell population ($p > 0,05$, one-way ANOVA). Significant change in IC50 dose was found in comparing DMSO cell populations and SN-38-resistant cell populations ($p<0,05$, one-way ANOVA). (C) Cell viability 72h after treatment of capecitabine. (D) The bar graph of IC 50 compares with barcoded HT-29 DMSO and SN-38 resistant HT-29 cells in capecitabine treatment. No significant change was found compared with the initial cell population, the DMSO cell population, and the SN-38-resistant cell population ($p > 0,05$, one-way ANOVA). (E) Cell viability 72h after treatment of oxaliplatin. (F) Bar graph of IC 50 comparison with barcoded HT-29 DMSO and SN-38 resistant HT-29 cells in the treatment of oxaliplatin. No significant change was found compared with the initial cell population, the DMSO cell population, and the SN-38-resistant cell population ($p > 0,05$, one-way ANOVA). (G) Cell viability 72h after treatment of dabrafenib. (H) Bar graph of IC50 comparison of dabrafenib in barcoded HT-29, barcoded HT-29 DMSO, dabrafenib-resistant barcoded HT-29 cells. No significant change was found in comparison with the initial cell population, the DMSO cell population ($p > 0,05$, one-way ANOVA). Significant change was found compared with the DMSO and SN-38-resistant population ($p < 0,05$, one-way ANOVA).

The resistant cell can respond to second therapy with various changes, including collateral resistance, collateral sensitivity, or no change. Figure 3.17 indicates no significant change in fold change of IC50 values in oxaliplatin and capecitabine

treatment on SN-38 resistant HT-29. There was a significant increase in IC50 values in SN-38 resistant HT-29 when compared to the initial and DMSO population in the presence of irinotecan and dabrafenib treatment. This can be caused by collateral resistance. Collateral resistance can be calculated by the ratio of the IC50 value of resistant cells to parental cells, and the ratio higher than two indicates multidrug resistance (Hall et al., 2009).

The IC50 values of irinotecan in SN-38 resistant cells were 17,8 μM, and the DMSO population was 7,9 μM. Thus, the resistance ratio was 2,3, which indicates cross-resistance. The dabrafenib IC50 value was 680 nM in SN-38 resistant HT-29 cells and 371 nM in barcoded HT-29 DMSO cells; thus, the resistance ratio was calculated as 1,8, which indicates insensitivity.

3.15 The investigation of changes in the MAPK pathway in relation to capecitabine resistance in HCT-116 cells

MAPK signaling plays a crucial role in many cellular processes (Yaeger & Corcoran, 2019). Change in cellular proliferation, dedifferentiation, and survival can be caused by dysregulation of MAPK signaling. Thus, MAPK pathway alterations are important for cancer cells (Bellio et al., 2021).

The RAS protein activation triggers the MAPK pathway by the external stimulus from EGFR ligand to activate guanine exchange factors such as son-of-sevenless (SOS), which catalyze small guanine triphosphatase (GTPase) (Bellio et al., 2021). This activation leads to a conformational change in RAS protein and facilitates interactions with downstream proteins (Yaeger & Corcoran, 2019). Activated RAS kinases cause the activation of RAF kinases which activates the MEK kinases (Yaeger & Corcoran, 2019). MEK kinase activation leads to phosphorylation of ERK kinases which has a crucial role in the regulation of cellular processes (Paillas et al., 2011).

The negative feedback mechanism is essential for the regulation of MAPK pathway signaling. The negative feedback loop from ERK signaling can inhibit the BRAF, RAS, and expression of multiple MAPK phosphatases (Dougherty et al., 2005). This mechanism directly affects the oncogenic alteration; thus, it has a crucial role in drug resistance and therapy response.

To examine MAPK pathway activity in the presence of capecitabine in barcoded HCT-116 cells, western blot analysis was performed (Figure 3.18).

Western blot analysis indicated the down-regulation of the MAPK pathway in the presence of capecitabine resistance in HCT-116 cells. Phosphorylation of EGFR, MEK, and ERK in capecitabine-resistant HCT-116 cells was diminished compared to the initial population and DMSO control. The result demonstrates that capecitabine resistance can cause a down-regulation in the MAPK signaling pathway.

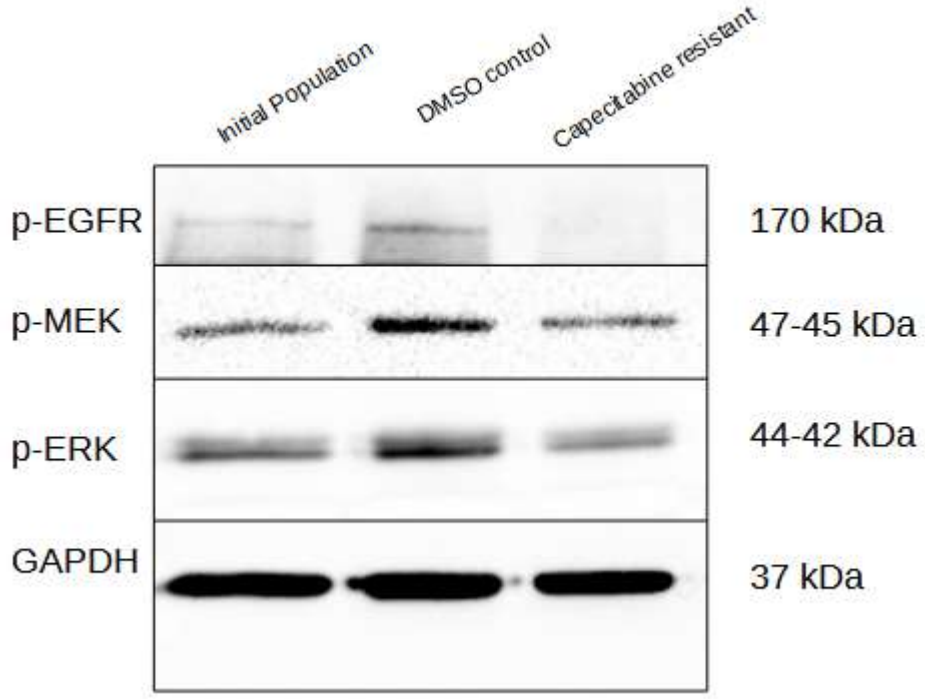

Figure 3. 18 Expression of p-ERK, p-MEK, and p-EGFR in barcoded HCT-116, barcoded HCT-116 DMSO, and capecitabine-resistant barcoded HCT-116 cell lines with western blot

Expression of p-ERK, p-MEK, and p-EGFR in barcoded HCT-116 DMSO and capecitabine-resistant barcoded HCT-116 cells determined with western blot. 50 µg total protein was loaded to 12% SDS-PAGE gel and wet transferred to nitrocellulose membrane. The membrane was processed to standard techniques. GAPDH was the loading control.

3.16 The investigation of changes in MAPK pathway in relation to dabrafenib and SN-38 resistance in HT-29 cells

The MAPK pathway was significant for cellular proliferation, differentiation, oncogenic transformation, and survival (Dougherty et al., 2005). The external stimulus targets the EGFR ligand and causes activation of guanine exchange factors such as son-of-sevenless (SOS). The activation of SOS catalyzes small guanine triphosphate, leading to RAS protein activation by conformational changes (Bellio et al., 2021). These changes cause interaction with downstream protein RAF and phosphorylation of it. Phosphorylated RAF kinases facilitate the phosphorylation of MEK kinases. Activation of MEK kinase leads to ERK kinase phosphorylation (Yaeger & Corcoran, 2019). ERK kinase has an essential role in cellular process regulations (Paillas et al., 2011).

There is a negative feedback mechanism found in MAPK pathway signaling. ERK kinase was essential for negative feedback. It can inhibit RAS, BRAF, and multiple MAPK phosphatase expression (Dougherty et al., 2005). This mechanism impacts the oncogenic alterations; thus, drug resistance and therapy response were affected by it.

To demonstrate the effect of dabrafenib and SN-38 resistance on activation of MAPK, the western blot with p-ERK, p-MEK, and p-EGFR was performed in HT-29 cell lines (Figure3.19).

Figure 3.19 indicates the up-regulation of the MAPK signaling pathway in the presence of dabrafenib and SN-38 resistance in HT-29 cells. There was an increase

in phosphorylation of EGFR and ERK in dabrafenib and SN-38 resistant HT-28 cells compared to initial and DMSO cell populations. There was no change in the phosphorylation of MEK, which might be due to the ERK feedback mechanism. This result suggests that dabrafenib and SN-38 resistance can cause up-regulation in the MAPK signaling pathway, including EGFR and ERK, and targeting these targetes can enhance the therapy efficiency.

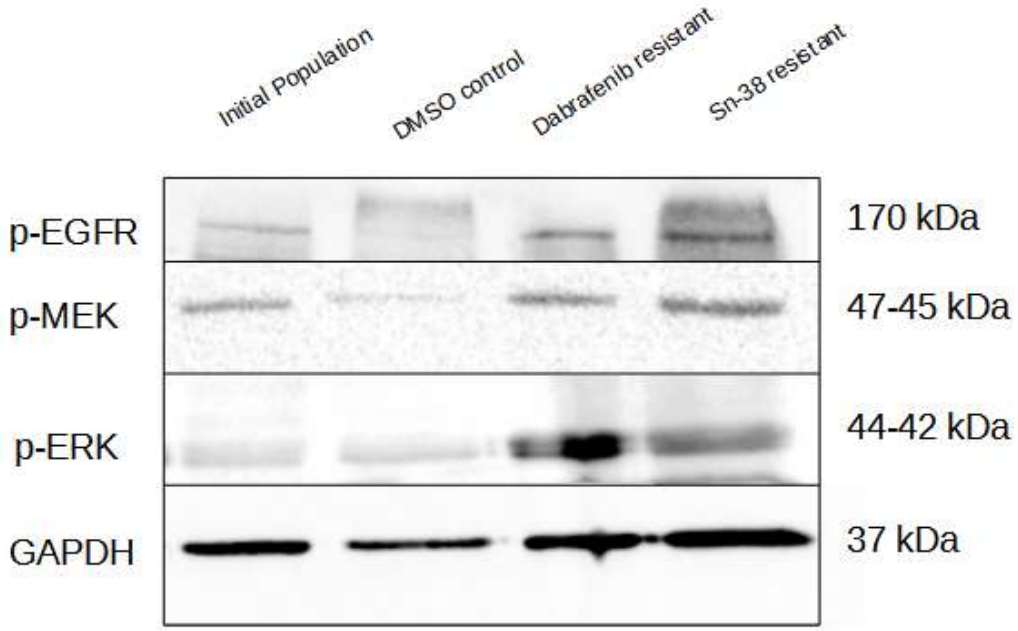

Figure 3. 19 The protein levels of p-ERK, p-MEK, and p-EGFR in barcoded HT-29, barcoded HT-29 DMSO, dabrafenib-resistant barcoded HT-29, and SN-38-resistant barcoded HT-29

50 µg total protein loaded, and GAPDH was used as a loading control for western blot. 12% SDS-PAGE gel was used and wet-transferred to nitrocellulose membrane. Protein levels of p-ERK, p-MEK, and p-EGFR were determined with western blot according to standard techniques.

3.17 Inhibition strategies for activation of p-ERK on dabrafenib-resistant HT-29 cell line

Drug combinations can be used in advanced cancers to enhance the therapeutic effect (Wu et al., 2018). Intolerable dose range can be found in chemotherapy, and therefore the drug combinations can be used in lower doses. Thus, drug combinations can be used to reduce the treatment side effects on CRC patients (Ianevski et al., 2020b). The degree of combination synergy or antagonism can be determined by comparing the observed drug response to the expected response.

According to open form (NCCN) guideline 2021, a combination of BRAF inhibitor and the ERK inhibitor could be used in BRAF V600E mutation-positive CRC (Lurie et al., 2021) . The investigation of the combined therapy effect of dabrafenib (BRAF V600E inhibitor) and SCH772984 (ERK inhibitor) also shows the efficiency of this therapy (Pratilas et al., 2009) .

The dabrafenib resistance could be dependent on the MAPK signaling pathway activity since the upregulation of pEGFR and pERK (figure 3.19); HT-29 has a RAS-independent BRAF mutation, using an ERK inhibitor could be beneficial for that case (L. Liang et al., 2018). SCH772984 is an ERK inhibitor and can show a favorable effect on dabrafenib-resistant HT-29 cells (L. Liang et al., 2018). Targeted MAPK pathway inhibitors can reduce the cell signaling response and tumor growth (Kirouac et al., 2017).

To inhibit the phosphorylation of ERK in dabrafenib resistant HT-29 cell line, the ERK inhibitor SCH77982 was used. In the presence of dabrafenib, the SCH77982 effect was investigated to determine whether a synergistic effect was found. To clarify the role of dabrafenib resistance in HT-29 cells, the synergy of dabrafeniba with SCH77982 was investigated (Figure 3.20). The synergictic effect investigated on initial (Figure 3.20A), DMSO (Figure 3.20B) and dabrafenib resistant HT-29 cells (Figure 3.20C).

No synergistic effect was found on the combination of dabrafenib and SCH77982 in both barcoded HT-29, barcoded HT-29 DMSO, and dabrafenib-resistant barcoded HT-29 cells.

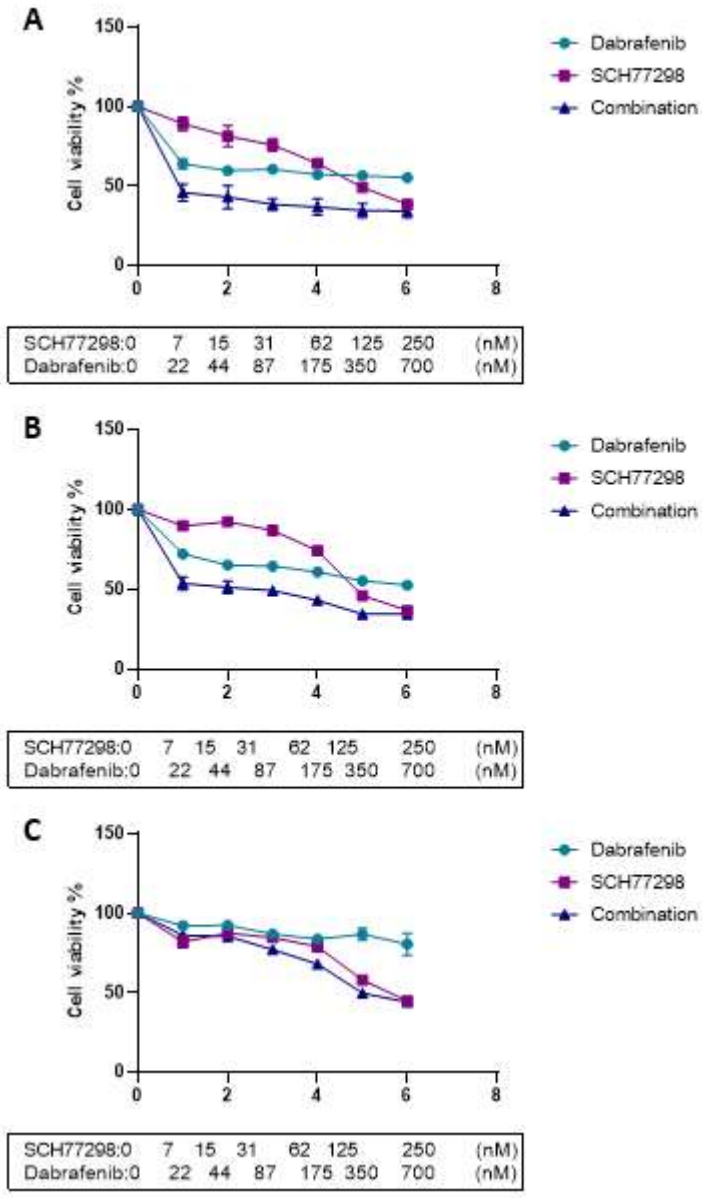

Figure 3. 20 The synergistic effect of SCH77982 and dabrafenib in barcoded HT-29, barcoded HT-29 DMSO, and dabrafenib-resistant barcoded HT-29 cells.

Cell lines were incubated at 37°C for 24 hours after plating at 10,000 cells per well at a 96-well plate. Cells were treated with stated concentrations of dabrafenib,

SCH77982, and dabrafenib and SCH7798. Cells were incubated for 72 hours, and cell viability was evaluated using the MTT cell viability assay. The results are the average of two independent biological replicates. Cell viability 72h after treatment of dabrafenib, SCH77982, and the combination of dabrafenib and SCH77982 in barcoded HT-29 cells(A), in barcoded HT-29 DMSO cells (B), and dabrafenib-resistant barcoded HT-29 cells (C).

3.18 Investigation of the synergistic effect of chemotherapeutics on dabrafenib-resistant HT-29 cells

The standard treatment of colorectal cancer could be limited to advanced cancer (Van Cutsem et al., 2005). In this case, drug combination strategies could be used. There is clinical evidence of the efficiency of some chemotherapeutic combinations in colon cancer treatment such as CAPEOX and dabrafenib plus oxaliplatin (Hattori et al., 2019).

The oxaliplatin combinations with capecitabine or dabrafenib can be used in the HT-29 cell line to reduce drug doses and enhance the treatment (Lurie et al., 2021).

According to NCCN guidelines 2021, CAPEOX (capecitabine plus oxaliplatin) and dabrafenib plus oxaliplatin could be used in second-line therapy in BRAF V600E mutated patients. Especially CAPEOX is a highly used second-line therapy because of the effect on the decrease in metastasis and to diminish the side effects of both oxaliplatin and capecitabine (Lurie et al., 2021).

There is a collateral sensitivity for oxaliplatin and capecitabine determined in dabrafenib exposed cells (Figure 3.16B&C). To enhance the chemotherapeutic effect of capecitabine and oxaliplatin (Figure 3.21), the combination of these drugs and the combination of dabrafenib and oxaliplatin was used in dabrafenib resistant HT-29 cells (Figure 3.22).

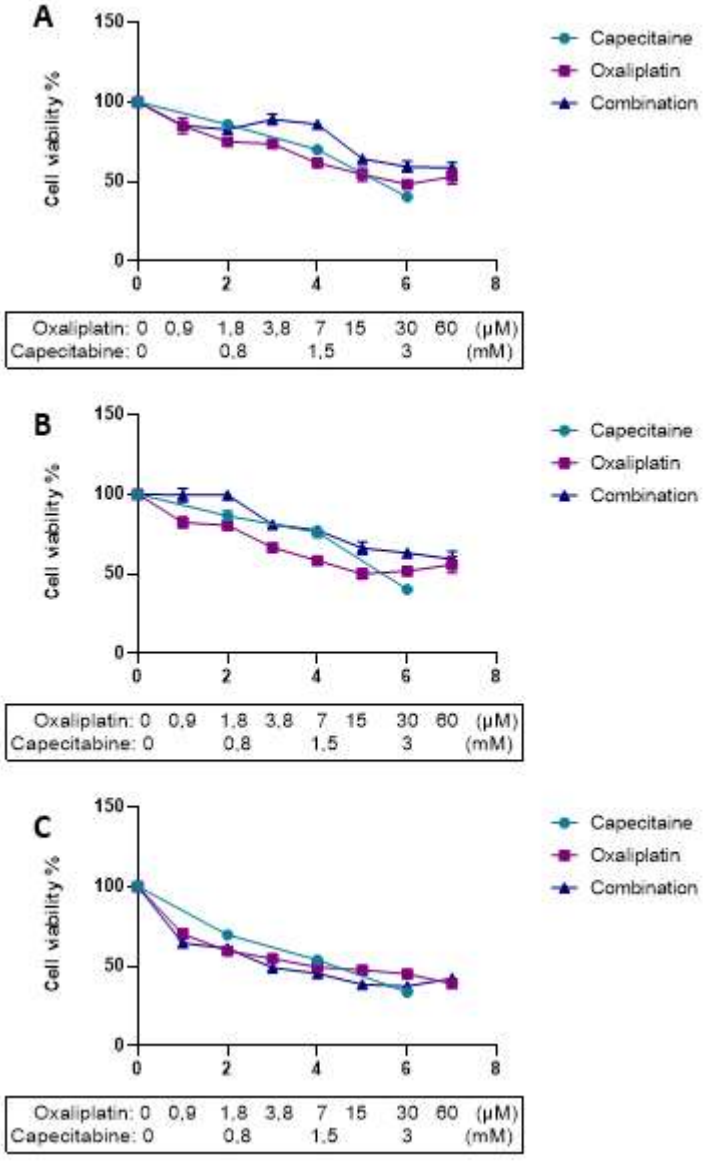

Figure 3. 21 The cell viability results from a combination of capecitabine and oxaliplatin

Cell lines were seeded into a 96-well plate at 10,000 cells per well density and incubated at 37°C for 24 hours after plating. Cells were treated with stated concentrations of oxaliplatin and capecitabine and the combinations of capecitabine and oxaliplatin. Cells were incubated for 72 hours, and cell viability was evaluated using the MTT cell viability assay. The results are the average of two independent biological replicates. Cell viability 72h after treatment of capecitabine, oxaliplatin,

and capecitabine plus oxaliplatin in barcoded HT-29 cells(A), in barcoded HT-29 DMSO cells (B), and dabrafenib-resistant barcoded HT-29 cells (C).

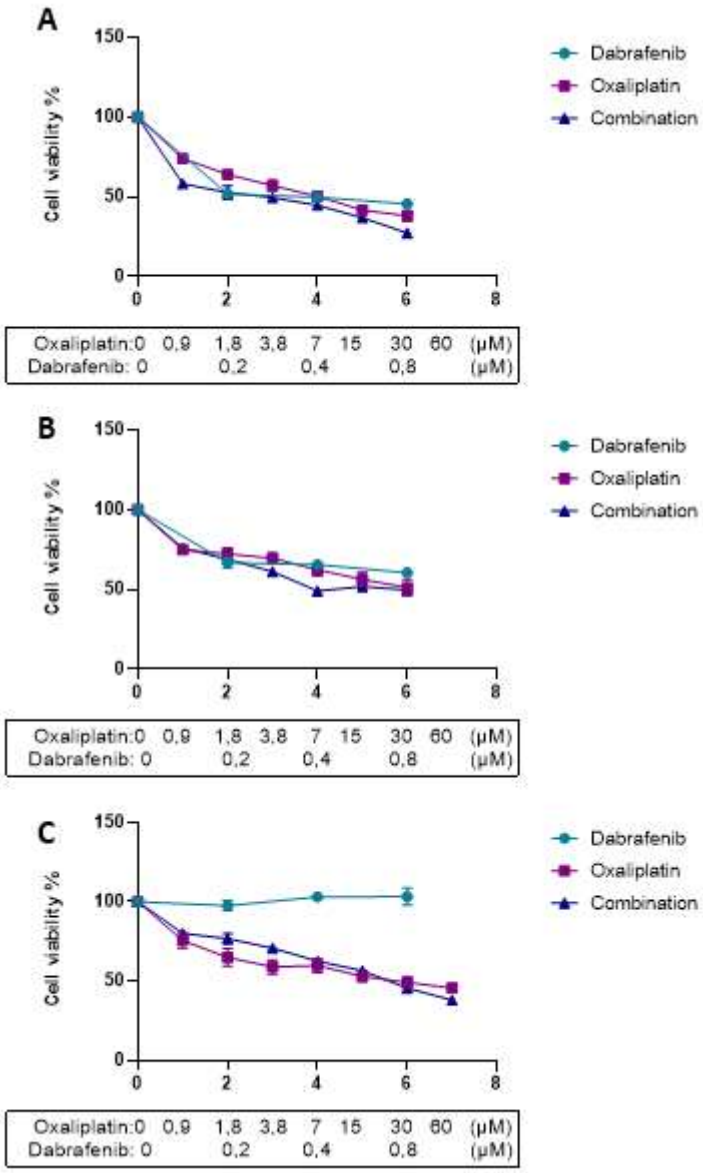

Figure 3. 22 The cell viability results from the combination of dabrafenib and oxaliplatin

Cell lines were plated into a 96-well plate with a density of 10,000 cells per well. Cells were treated with stated concentrations of oxaliplatin and dabrafenib and the combinations of dabrafenib and oxaliplatin. Cells were incubated for 72 hours, and

cell viability was performed using the MTT cell viability assay. The results are the average of two independent biological replicates. Cell viability 72h after treatment of capecitabine, oxaliplatin, and dabrafenib plus oxaliplatin in barcoded HT-29 cells(A), in barcoded HT-29 DMSO cells (B), and dabrafenib-resistant barcoded HT-29 cells (C).

For figure 3.21, the CAPEOX treatment shows an antagonistic effect in SynergyFinder. The initial (Figure 3.21A), DMSO (Figure 3.21B), and the dabrafenib resistant HT-29 cells (Figure 3.21C) show no significant difference. Thus, there was no significant change in the synergistic effect of CAPEOX in the presence of dabrafenib resistance.

For figure 3.22, the combination of dabrafenib and oxaliplatin treatment shows an antagonistic effect on initial and DMSO populations of HT-29 cells and the additive effect in dabrafenib resistant HT-29 cells in SynergyFinder. The additive effect in dabrafenib-resistant HT-29 cells indicated that dabrafenib resistance could create sensitivity to dabrafenib plus oxaliplatin combination treatment.

3.19 Inhibition strategies for activation of p-ERK on SN-38-resistant HT-29 cell line

To enhance the therapeutic effect, drug combinations can be used in advanced cancers (Wu et al., 2018). In some cases, the drug dose could be intolerable in chemotherapy for the patient, and using drug combinations could decrease the needed doses; since one drug dose could be used in high doses, however, using multidrug in therapy can be used in lower doses (Wu et al., 2018). Hence, drug combinations are important for reducing the side effects of treatment in CRC patients. Synergy and antagonism are the degrees of combination (Ianevski et al., 2020b). They can be calculated as the comparison of observed drug response to expected response (Ianevski et al., 2020b).

The SN-38 resistance can be dependent on the MAPK pathway because of the increased phosphorylation of EGFR and ERK (Figure 3.19). HT-29 has a RAS-independent BRAF mutation; thus, targeting the EGFR could not be beneficial. Targeting ERK using SCH772984 can decrease the cell viability of SN-38-resistant HT-29 cells.

To diminish the phosphorylation of ERK in SN-38-resistant barcoded HT-29 cells, the ERK inhibitor SCH77982 was combined with SN-38. To assess the possible synergistic effect of SCH77982 in the presence of SN-38 in barcoded HT-29 (Figure 3.23A), barcoded HT-29 DMSO (Figure 3.23B), SN-38 resistant barcoded HT-29 cells (Figure 3.23C).

The synergy scores were calculated on SynergyFinder. No significant synergistic effect was observed in the combination of SN-38 and SCH77982 in both barcoded HT-29, barcoded HT-29 DMSO, and SN-38-resistant barcoded HT-29 cells. This result indicates that SN-38 resistance does not impact the synergistic effect of ERK inhibitor SCH77982 and SN-38 combined treatment in HT-29 cells.

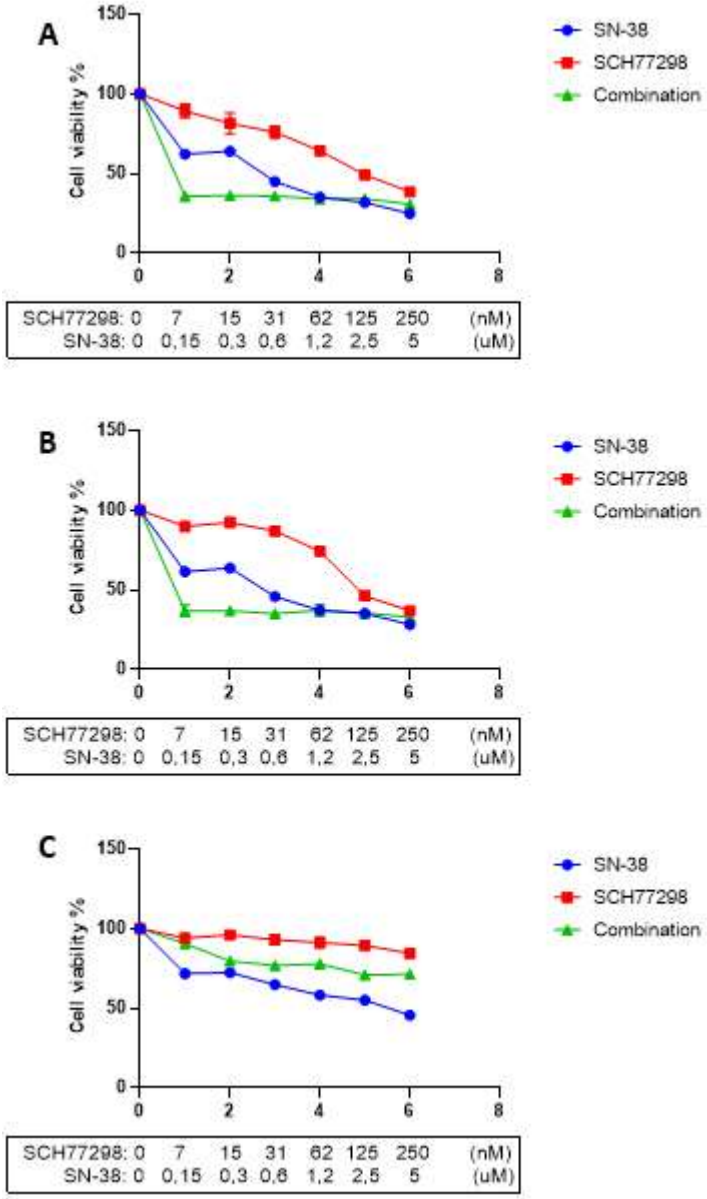

Figure 3. 23 The synergistic effect of SCH77982 and SN-38 in barcoded HT-29, barcoded HT-29 DMSO, and SN-38-resistant barcoded HT-29 cells

Cell lines were incubated at 37°C for 24 hours after plating at 10,000 cells per well at a 96-well plate to allow attachment. Cells were treated with stated concentrations of SN-38, SCH77982, and the combination of SN-38 and SCH7798. Cells were incubated for 72 hours. The cell viability was evaluated using the MTT cell viability assay. The results are the average of two independent biological replicates and three

technical replicates found on each. Cell viability 72h after treatment of SN-38, SCH77982, and the combination of SN-38 and SCH77982 in barcoded HT-29 cells(A), in barcoded HT-29 DMSO cells (B), and in SN-38-resistant barcoded HT-29 cells (C).

3.20 Effect of dabrafenib and SN-38 resistance on clonogenic capacity

Genetic evolution is an essential factor for therapeutic resistance; genetic alterations such as mutations, gene deletion, gene amplification, and chromosomal translocation provide cancer cells to escape from therapeutic pressure (Marine et al., 2020). Genetic clonal evolution plays an essential role in the development of resistance to therapy (Assenov et al., 2018).

Oncogenic mutations can inhibit the signaling pathways in the presence of therapeutic responses; this is caused by the addiction of cancer to activated pathways (Fernandes Neto et al., 2020). Secondary mutations can restore signaling in drug-inhibited pathways in advanced cancers. In acquired resistance, mutations have an impact on the drug target or upstream or downstream of the activated signaling molecule.

A colony formation assay was performed to investigate the effect of dabrafenib and SN-38 resistance in HT-29 cell survival and growth (Figure 3.24).

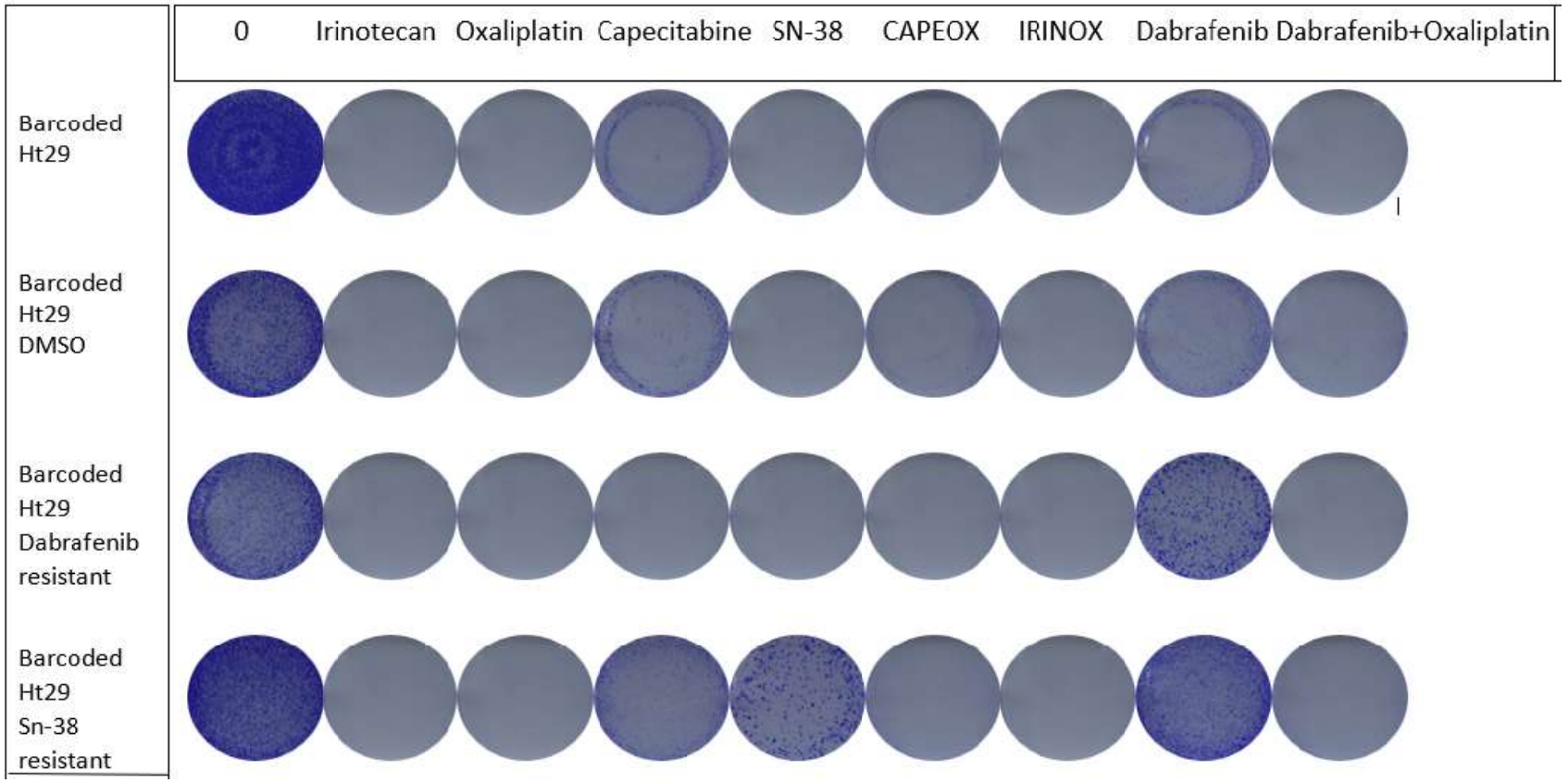
0
Irinotecan
Oxaliplatin
Capecitabine
SN-38
CAPEOX
IRINOX
Dabrafenib
Dabrafenib+Oxaliplatin
Barcoded Ht29
Barcoded Ht29 DMSO
Barcoded Ht29 Dabrafenib resistant
Barcoded Ht29 Sn-38 resistant

Figure 3. 24 The effects of dabrafenib and SN-38 resistance on clonogenic capacity in HT-29 cells

Barcoded HT-29, barcoded HT-29 DMSO, and dabrafenib-resistant barcoded HT-29 cells were plated at a density of 20,000 cells per well, and SN-38-resistant barcoded HT-29 cells were seeded at a density of 40,000 cells per well in a 6-well plate. Cells were incubated for three weeks in a humidified incubator with 5% CO_2 at 37° and treated with IC50 dosages of drugs. Colonies were fixed with 2% formaldehyde solution for two hours and stained with 0.1% crystal violet. Then plates were scanned. Three technical replicates from each group were shown. Two independent biological replicates were carried out.

There was a significant change in colony number between capecitabine, SN-38, a combination of capecitabine and oxaliplatin, and a combination of dabrafenib and oxaliplatin-treated groups. The surviving cells were able to proliferate and form colonies and could have an inherited resistance mechanism. The results indicated that drug-resistant HT-29 cells have a higher effect when treated with combination therapies, including capecitabine-oxaliplatin and dabrafenib-oxaliplatin combinations (Figure 3.24). In the presence of dabrafenib resistance on HT-29 cells, the capecitabine treatment demonstrated a favorable effect. No colony formation was observed on irinotecan, and a combination of irinotecan and oxaliplatin indicated that oxaliplatin, irinotecan, and its combinations could be used in BRAF mutated HT-29 cell lines (Figure 3.24). Thus, the treatment of the combination of capecitabine and oxaliplatin or combination of dabrafenib and oxaliplatin could be beneficial in dabrafenib, and SN-38 resistant HT-29 cells and capecitabine treatment could be used in dabrafenib-resistant HT-29 cells.

3.21 The investigation of motility capacities on Dabrafenib and SN-38 resistant HT-29 cells

The scratch wound healing assay shows the effects of major wound-healing growth factors, cytokines, and chemokines on cell migration (Q. Liang et al., 2021). A

scratch wound healing assay was performed to investigate the cellular motility in the presence of dabrafenib and SN-38 resistance on HT-29 cells. The scratch wound area was imaged every 4 hours for 60hours, and images were carried with 4x in a Nikon Eclipse ti2e Fluorescence Microscope and analyzed with ImageJ (Figure 3.25).

SN-38 resistant cells had no mobility in first 12 hours and dabrafenib resistant cells had lower motility than initial and DMSO populations of HT-29 cells. In 24, 36 and 48 hours, SN-38 and dabrafenib resistant HT-29 cells' gap closure was significantly lower than initial and DMSO populations of HT-29. However, the decrease in wound healing was significant in comparison of DMSO and Dabrafenib-resistant HT-29 cells at 60 hours.

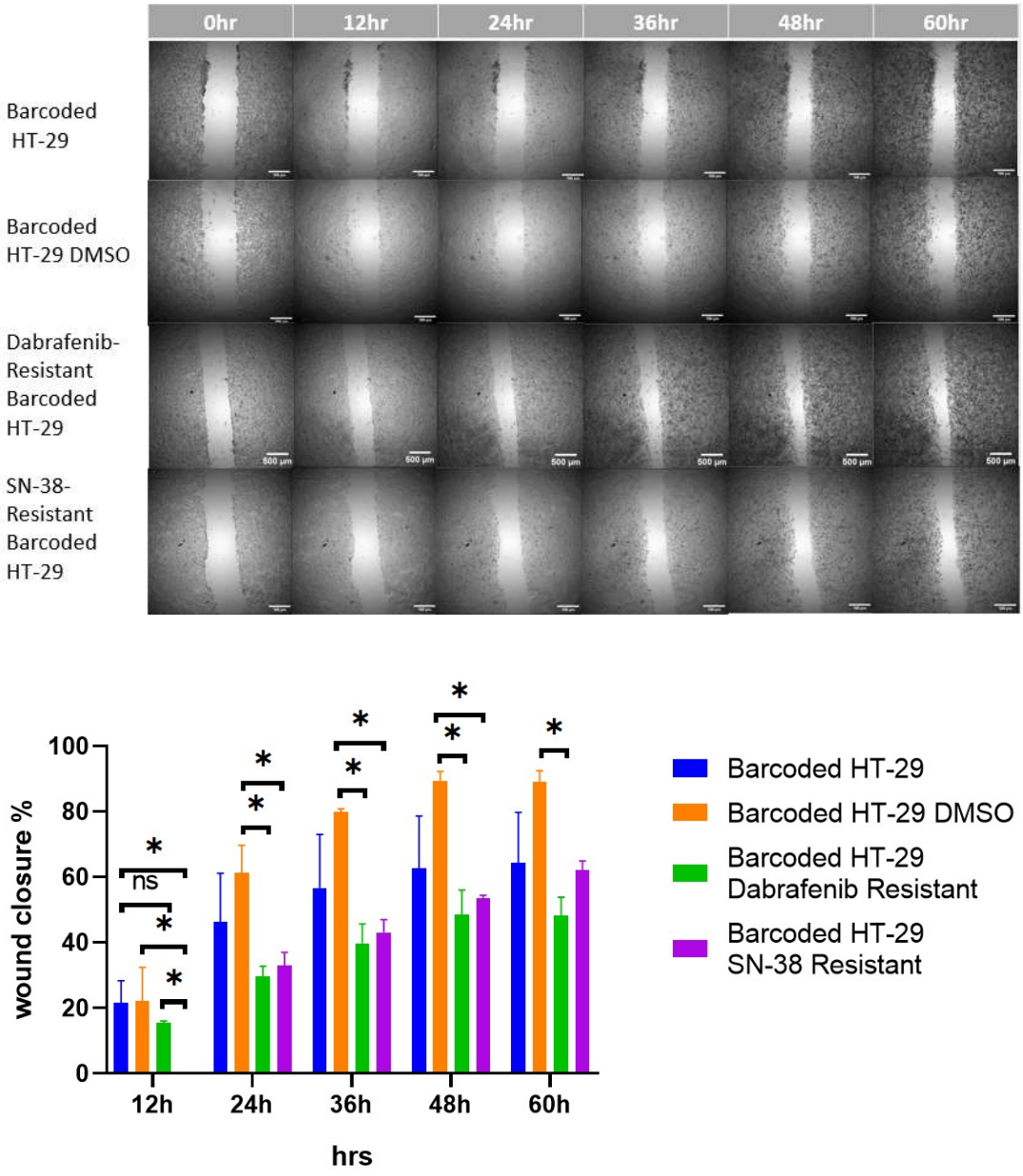

Figure 3. 25 Effect of dabrafenib and SN-38 resistance on the motility of HT-29 cells

Barcoded HT-29, barcoded HT-29 DMSO, dabrafenib-resistant barcoded HT-29, and SN-38-resistant barcoded HT-29 cells were plated in a 24-well plate at a density of 200,000 cells per well. After 24 hours, cells were incubated with 5 µg/ml mitomycin C for 2 hours, and scratch wounds were generated with 200 µl pipette tips. Cells were washed with PBS three times, and a complete medium was given.

Cells were incubated for 60 hours, and every 4 hours image was taken. Images analyzed with ImageJ. Two technical replications and two independent biological replicates were carried out.

Development of drug resistance impacts morphology, proliferation, living cell cycle and mobility of cells (Q. Liang et al., 2021). This result demonstrates that gaining drug resistance can have an impact in cellular motility; hence, there was a significant decrease in cellular motility in both Dabrafenib and SN-38 resistance in HT-29 cell line.

CHAPTER 4

CONCLUSION AND FUTURE DIRECTIONS

Development of drug resistance is one of the major problems in the survival of CRC patients (Smillie et al., 2019). Intra-tumor heterogeneity impacts clonal evolution and developing drug resistance (Acar et al., 2020). Understanding the clonal evolution dynamics can create a new perspective on that problem. The intra-tumor heterogeneity and clonal evolution monitoring pave the way to multidrug adaptive treatments. The cellular barcoding technology allows the monitoring of evolutionary dynamics in drug-exposed environments. The resistance mechanism can cause a proliferative cost. The drug-resistant cancer cells can be hypersensitive to other drugs, which is collateral sensitivity (Hall et al., 2009). Collateral sensitivity can improve response to chemotherapy. The molecular alterations occurred during drug exposure directly or indirectly affect cell growth, invasion, and metastasis (Morris et al., 2016). Thus, targeting these alterations can benefit treatment and lead to collateral sensitivity. In our experimental system, the proliferation rate of capecitabine-resistant HCT-116 cells significantly diminished which was presumably due to the impact of drug resistantance observed in our system.

Monitoring the capecitabine resistance in the HCT-116 cell line showed that de novo cellular alterations during treatment played a role in the development of capecitabine resistance. Performing cell viablity assays to assses second-line drug sensitivity did not show any collateral sensitivity which was presumably due to the acquired drug resistance gained in our model system was not strong enough or potential other drug combinations required to be tested as further.

Exploiting the Dabrafenib resistance and SN-38 resistance in the HT-29 cell line showed pre-existing cellular alterations play an essential role in dabrafenib and SN-38 resistance development. There was a sensitivity for oxaliplatin, capecitabine and

irinotecan in dabrafenib-resistant HT-29 cells; moreover, the drug combinations showed additive effects that can be an option for chemotherapy. There was no collateral sensitivity determined in SN-38-resistant HT-29 cells for irinotecan and capecitabine; however, if the same study was performed chemotherapeutics other than capeciatebine, irinotecan and oxaliplatin there may be potential collateral sensitivity observed.

The clonogenic capacity of drug-resistant cells is different from the initial population. Thus, it indicates the cell's survival and the ability of the cell to proliferate from a clone. Drug combinations have a clonogenic impact on drug-resistant cell lines. There is a dimisih in clonogenic capacity of dabrafenib resistant and SN-38 resistant HT-29 cell in the dabrafenib and oxaliplatin combination and CAPEOX combination therapies. This result indicates development of drug resistance impacts the cell survival in drug exposed environments.

The drug resistant cells' wound healing capacity was significanlty differrent from the DMSO population of HT-29 cells. Hence, this result demonstrated that the cellular motility can be efffected by drug resistance. Although the growth rate of dabrafenib and SN-38 resistant HT-29 cells had no significant differences from initial and DMSO populations, the cellular motility has decreased. In first 12 hours SN-38 resistant HT-29 cell had no wound healing ability. There was a diminish in wound healing ability in 12h, 24h, 36h, 48h in dabrafenib and SN-38 resistant HT-29 cells when compared to DMSO population. Therefore, the mobility of HT-29 cells can be directly effected by drug-resistance.

There are some limitations found in this study. First, the passage and re-plating in dabrafenib-resistant and SN-38-resistant HT-29 cell lines can cause sample bias. Second, the concentration of drugs may not be achievable in patients. Third, the genetic background of cell lines used in this study may not represent the patients. Fourth, future studies should include stromal cells to mimic the tumor tissue components of cancer patients. For example, the coculture studies of cancer-associated fibroblasts and immune cells with the cancer cell lines with the help of

cellular barcoding technology used in this study will further unravel true dynamics and underlying mechanisms of drug resistance.

Overall, this study provides an experimental evolution model system integrated with cutting-edge cellular barcoding technology to understand temporal dynamics of drug resistance and second-line drug options sensitizing initially drug resistant cell populations.

REFERENCES

Acar, A., Nichol, D., Fernandez-Mateos, J., Cresswell, G. D., Barozzi, I., Pil Hong, S., Trahearn, N., Spiteri, I., Stubbs, M., Burke, R., Stewart, A., Caravagna, G., Werner, B., Vlachogiannis, G., Maley, C. C., Magnani, L., Valeri, N., Banerji, U., & Sottoriva, A. (n.d.). *Exploiting evolutionary steering to induce collateral drug sensitivity in cancer*. https://doi.org/10.1038/s41467-020-15596-z

Assenov, Y., Brocks, D., & Gerhäuser, C. (2018). Intratumor heterogeneity in epigenetic patterns. *Seminars in Cancer Biology*, *51*, 12–21. https://doi.org/10.1016/j.semcancer.2018.01.010

Bellio, H., Fumet, J. D., & Ghiringhelli, F. (2021). *cancers Targeting BRAF and RAS in Colorectal Cancer*. https://doi.org/10.3390/cancers13092201

Blundell, J. R., & Levy, S. F. (2014). Beyond genome sequencing: Lineage tracking with barcodes to study the dynamics of evolution, infection, and cancer. *Genomics*, *104*, 417–430. https://doi.org/10.1016/J.YGENO.2014.09.005

Caputo, F., Santini, C., Bardasi, C., Cerma, K., Casadei-Gardini, A., Spallanzani, A., Andrikou, K., Cascinu, S., & Gelsomino, F. (n.d.). *Molecular Sciences BRAF-Mutated Colorectal Cancer: Clinical and Molecular Insights*. https://doi.org/10.3390/ijms20215369

Chan, X. Y., Singh, A., Osman, N., & Piva, T. J. (n.d.). *Molecular Sciences Role Played by Signalling Pathways in Overcoming BRAF Inhibitor Resistance in Melanoma*. https://doi.org/10.3390/ijms18071527

Chung, Y. R., Kim, H. J., Kim, Y. A., Chang, M. S., Hwang, K. T., & Park, S. Y. (2017). Diversity index as a novel prognostic factor in breast cancer. *Oncotarget*, *8*(57), 97114. https://doi.org/10.18632/ONCOTARGET.21371

Coffey, S. E., Giedt, R. J., & Weissleder, R. (2013). *Automated analysis of clonal cancer cells by intravital imaging*. https://doi.org/10.4161/intv.26138

Costa, A., Kieffer, Y., Scholer-Dahirel, A., Pelon, F., Bourachot, B., Cardon, M., Sirven, P., Magagna, I., Fuhrmann, L., Bernard, C., Bonneau, C., Kondratova, M., Kuperstein, I., Zinovyev, A., Givel, A. M., Parrini, M. C., Soumelis, V., Vincent-Salomon, A., & Mechta-Grigoriou, F. (2018). Fibroblast Heterogeneity and Immunosuppressive Environment in Human Breast Cancer. *Cancer Cell*, *33*(3), 463-479.e10. https://doi.org/10.1016/J.CCELL.2018.01.011/ATTACHMENT/E151F4B3-8B3D-4E68-8E65-E7998424EE30/MMC1

D'Angelo, E., Natarajan, D., Sensi, F., Ajayi, O., Fassan, M., Mammano, E., Pilati,

P., Pavan, P., Bresolin, S., Preziosi, M., Miquel, R., Zen, Y., Chokshi, S., Menon, K., Heaton, N., Spolverato, G., Piccoli, M., Williams, R., Urbani, L., & Agostini, M. (2020). Patient-Derived Scaffolds of Colorectal Cancer Metastases as an Organotypic 3D Model of the Liver Metastatic Microenvironment. *Cancers 2020, Vol. 12, Page 364*, *12*(2), 364. https://doi.org/10.3390/CANCERS12020364

De Falco, V., Napolitano, S., Roselló, S., Huerta, M., Cervantes, A., Ciardiello, F., & Troiani, T. (2020). How we treat metastatic colorectal cancer. *ESMO Open*, *4*, e000813. https://doi.org/10.1136/ESMOOPEN-2020-000813

Domenica, F., De Palma, E., D'argenio, V., Pol, J., Kroemer, G., Maiuri, M. C., & Salvatore, F. (2019). *cancers The Molecular Hallmarks of the Serrated Pathway in Colorectal Cancer*. https://doi.org/10.3390/cancers11071017

Dougherty, M. K., Müller, J., Ritt, D. A., Zhou, M., Zhou, X. Z., Copeland, T. D., Conrads, T. P., Veenstra, T. D., Lu, K. P., & Morrison, D. K. (2005). Regulation of Raf-1 by direct feedback phosphorylation. *Molecular Cell*, *17*(2), 215–224. https://doi.org/10.1016/J.MOLCEL.2004.11.055

Fernandes Neto, J. M., Nadal, E., Bosdriesz, E., Ooft, S. N., Farre, L., McLean, C., Klarenbeek, S., Jurgens, A., Hagen, H., Wang, L., Felip, E., Martinez-Marti, A., Vidal, A., Voest, E., Wessels, L. F. A., van Tellingen, O., Villanueva, A., & Bernards, R. (2020). Multiple low dose therapy as an effective strategy to treat EGFR inhibitor-resistant NSCLC tumours. *Nature Communications*, *11*(1). https://doi.org/10.1038/s41467-020-16952-9

Goldie, J. H. (1989). Mathematical models of drug resistance and chemotherapy effects. *Cancer Treatment and Research*, *48*, 13–26. https://doi.org/10.1007/978-1-4613-1601-5_2

Gottesman, M. M., Fojo, T., & Bates, S. E. (2002). Multidrug resistance in cancer: role of ATP–dependent transporters. *Nature Reviews Cancer 2002 2:1*, *2*(1), 48–58. https://doi.org/10.1038/nrc706

Greaves, M. (2015). Evolutionary determinants of cancer. *Cancer Discov.*, *5*, 806–820.

Greaves, Mel, & Maley, C. C. (2012). *Clonal evolution in cancer*. https://doi.org/10.1038/nature10762

Guglielmi, A. P., Sobrero, A. F., Guglielmi, A. P., & Sobrero, A. F. (n.d.). Second-Line Therapy for Advanced Colorectal Cancer. In *Gastrointest Cancer Res* (Vol. 1). www.myGCRonline.org

Hall, M. D., Handley, M. D., & Gottesman, M. M. (2009). Is resistance useless? Multidrug resistance and collateral sensitivity. *Trends in Pharmacological Sciences*, *30*(10), 546–556. https://doi.org/10.1016/J.TIPS.2009.07.003

Hanahan, D., & Weinberg, R. A. (2011). Hallmarks of cancer: the next generation.

Cell, *144*(5), 646–674. https://doi.org/10.1016/j.cell.2011.02.013

Hattori, N., Goro Nakayama, ·, Uehara, · Keisuke, Toshisada Aiba, ·, Kiyoshi Ishigure, ·, Sakamoto, E., Tojima, Y., Kanda, M., Kobayashi, D., Chie Tanaka, ·, Yamada, S., Koike, M., Fujiwara, M., Nagino, M., & Kodera, Y. (1234). Phase II study of capecitabine plus oxaliplatin (CapOX) as adjuvant chemotherapy for locally advanced rectal cancer (CORONA II). *International Journal of Clinical Oncology*, *25*, 118–125. https://doi.org/10.1007/s10147-019-01546-3

Heidorn, S. J., Milagre, C., Whittaker, S., Nourry, A., Niculescu-Duvas, I., Dhomen, N., Hussain, J., Reis-Filho, J. S., Springer, C. J., Pritchard, C., & Marais, R. (2010). Kinase-Dead BRAF and Oncogenic RAS Cooperate to Drive Tumor Progression through CRAF. *Cell*, *140*(2), 209–221. https://doi.org/10.1016/J.CELL.2009.12.040

Heydt, Q., Xintaropoulou, C., Clear, A., Austin, M., Pislariu, I., Miraki-Moud, F., Cutillas, P., Korfi, K., Calaminici, M., Cawthorn, W., Suchacki, K., Nagano, A., Gribben, J. G., Smith, M., Cavenagh, J. D., Oakervee, H., Castleton, A., Taussig, D., Peck, B., … Patel, B. (2021). Adipocytes disrupt the translational programme of acute lymphoblastic leukaemia to favour tumour survival and persistence. *Nature Communications 2021 12:1*, *12*(1), 1–18. https://doi.org/10.1038/s41467-021-25540-4

Hino, H., Shiomi, A., Kusuhara, M., Kagawa, H., Yamakawa, Y., Hatakeyama, K., Kawabata, T., Oishi, T., Urakami, K., Nagashima, T., Kinugasa, Y., & Yamaguchi, K. (2019). Clinicopathological and mutational analyses of colorectal cancer with mutations in the POLE gene. *Cancer Medicine*, *8*(10), 4587. https://doi.org/10.1002/CAM4.2344

Ianevski, A., Giri, A. K., & Aittokallio, T. (2020a). SynergyFinder 2.0: visual analytics of multi-drug combination synergies. *Nucleic Acids Research*, *48*. https://doi.org/10.1093/nar/gkaa216

Ianevski, A., Giri, A. K., & Aittokallio, T. (2020b). SynergyFinder 2.0: visual analytics of multi-drug combination synergies. *Nucleic Acids Research*, *48*. https://doi.org/10.1093/nar/gkaa216

Jensen, N. F., Agama, K., Roy, A., Smith, D. H., Pfister, T. D., Rømer, M. U., Zhang, H.-L., Doroshow, J. H., Knudsen, B. R., Stenvang, J., Brünner, N., & Pommier, Y. (2016). *Characterization of DNA topoisomerase I in three SN-38 resistant human colon cancer cell lines reveals a new pair of resistance-associated mutations*. https://doi.org/10.1186/s13046-016-0335-x

Kebschull, J. M., & Zador, A. M. (n.d.). *Cellular barcoding: lineage tracing, screening and beyond*. https://doi.org/10.1038/s41592-018-0185-x

Kirouac, D. C., Schaefer, G., Chan, J., Merchant, M., Orr, C., Huang, S.-M. A., Moffat, J., Liu, L., Gadkar, K., & Ramanujan, S. (2017). ARTICLE Clinical

responses to ERK inhibition in BRAF V600E-mutant colorectal cancer predicted using a computational model. *Npj Systems Biology and Applications*, *3*, 14. https://doi.org/10.1038/s41540-017-0016-1

Levy, S. F., Blundell, J. R., Venkataram, S., Petrov, D. A., Fisher, D. S., & Sherlock, G. (2015). *Quantitative evolutionary dynamics using high-resolution lineage tracking*. https://doi.org/10.1038/nature14279

Liang, L., Tian, J., Yu, Y., Wang, Z., Peng, K., Liu, R., Wang, Y., Xu, X., Li, H., Zhuang, R., Cui, Y., Zhu, C., Liu, T., Liang, L., & Tian, J. (2018). Cellular Physiology and Biochemistry Cellular Physiology and Biochemistry Original Paper An Analysis of Relationship Between RAS Mutations and Prognosis of Primary Tumour Resection for Metastatic Colorectal Cancer Patients. *Cell Physiol Biochem*, *50*, 768–782. https://doi.org/10.1159/000494242

Liang, Q., Wang, Y., Lu, Y., Zhu, Q., Xie, W., Tang, N., Huang, L., An, T., Zhang, D., Yan, A., Liu, S., Ye, L., & Zhu, C. (2021). RANK promotes colorectal cancer migration and invasion by activating the Ca2+-calcineurin/NFATC1-ACP5 axis. *Cell Death and Disease*, *12*(4). https://doi.org/10.1038/S41419-021-03642-7

Lin, L., & Lin, D.-C. (n.d.). *cancers Biological Significance of Tumor Heterogeneity in Esophageal Squamous Cell Carcinoma*. https://doi.org/10.3390/cancers11081156

Liu, P., Wang, Y., & Li, X. (2019). Targeting the untargetable KRAS in cancer therapy. *Acta Pharmaceutica Sinica B*, *9*(5), 871–879. https://doi.org/10.1016/J.APSB.2019.03.002

Lurie, R. H., & Cancer, C. (2021). *Colon Cancer*.

M Gerlinger, C. S. (2010). How Darwinian models inform therapeutic failure initiated by clonal heterogeneity in cancer medicine. *Br. J. Cancer*, *103*, 1139–1143.

Marine, J. C., Dawson, S. J., & Dawson, M. A. (2020). Non-genetic mechanisms of therapeutic resistance in cancer. *Nature Reviews Cancer*, *20*(12), 743–756. https://doi.org/10.1038/s41568-020-00302-4

Mcgavin, J. K., Goa, K. L., & Kahlert, S. (n.d.). *Capecitabine A Review of its Use in the Treatment of Advanced or Metastatic Colorectal Cancer*.

McGranahan, N., & Swanton, C. (2017). Clonal Heterogeneity and Tumor Evolution: Past, Present, and the Future. *Cell*, *168*(4), 613–628. https://doi.org/10.1016/J.CELL.2017.01.018

Mo, Y. Y., & Moschos, S. J. (2005). Targeting Ubc9 for cancer therapy. *Expert Opinion on Therapeutic Targets*, *9*(6), 1203–1216. https://doi.org/10.1517/14728222.9.6.1203

N McGranahan, C. S. (2017). Clonal heterogeneity and tumor evolution: past, present, and the future. *Cell*, *168*, 613–628.

Östman, A., & Augsten, M. (2009). Cancer-associated fibroblasts and tumor growth – bystanders turning into key players. *Current Opinion in Genetics & Development*, *19*(1), 67–73. https://doi.org/10.1016/J.GDE.2009.01.003

Paillas, S., Boissière, F., Bibeau, F., Denouel, A., Mollevi, C., Causse, A., Denis, V., Vezzio-Vié, N., Marzi, L., Cortijo, C., Ait-Arsa, I., Askari, N., Pourquier, P., Martineau, P., Del Rio, M., & Gongora, C. (2011). Targeting the p38 MAPK pathway inhibits irinotecan resistance in colon adenocarcinoma. *Cancer Research*, *71*(3), 1041. https://doi.org/10.1158/0008-5472.CAN-10-2726

Pluchino, K. M., Hall, M. D., Goldsborough, A. S., Callaghan, R., & Gottesman, M. M. (2012). Collateral sensitivity as a strategy against cancer multidrug resistance. *Drug Resistance Updates*, *15*(1–2), 98–105. https://doi.org/10.1016/J.DRUP.2012.03.002

Pratilas, C. A., Taylor, B. S., Ye, Q., Viale, A., Sander, C., Solit, D. B., & Rosen, N. (n.d.-a). *BRAF is associated with disabled feedback inhibition of RAF-MEK signaling and elevated transcriptional output of the pathway*. Retrieved August 2, 2022, from www.pnas.orgcgidoi10.1073pnas.0900780106

Pratilas, C. A., Taylor, B. S., Ye, Q., Viale, A., Sander, C., Solit, D. B., & Rosen, N. (n.d.-b). *BRAF is associated with disabled feedback inhibition of RAF-MEK signaling and elevated transcriptional output of the pathway*. Retrieved August 1, 2022, from www.pnas.orgcgidoi10.1073pnas.0900780106

Roma, C., Rachiglio, A. M., Pasquale, R., Fenizia, F., Iannaccone, A., Tatangelo, F., Antinolfi, G., Parrella, P., Graziano, P., Sabatino, L., Colantuoni, V., Botti, G., Maiello, E., & Normanno, N. (2016). BRAF V600E mutation in metastatic colorectal cancer: Methods of detection and correlation with clinical and pathologic features) BRAF V600E mutation in metastatic colorectal cancer: Methods of detection and correlation with clinical and pathologic features BRAF V600E mutation in metastatic colorectal cancer: Methods of detection and correlation with clinical and pathologic features. *Cancer Biology & Therapy*, *17*(8), 840–848. https://doi.org/10.1080/15384047.2016.1195048

Saus, E., Iraola-Guzmán, S., Willis, J. R., Brunet-Vega, A., & Gabaldón, T. (2019). Microbiome and colorectal cancer: Roles in carcinogenesis and clinical potential. *Molecular Aspects of Medicine*, *69*, 93–106. https://doi.org/10.1016/J.MAM.2019.05.001

Scarborough, J. A., McClure, E., Anderson, P., Dhawan, A., Durmaz, A., Lessnick, S. L., Hitomi, M., & Scott, J. G. (2020). Identifying States of Collateral Sensitivity during the Evolution of Therapeutic Resistance in Ewing's Sarcoma. *IScience*, *23*(7). https://doi.org/10.1016/J.ISCI.2020.101293

Schaufler, D., Ast, D. F., Tumbrink, H. L., Abedpour, N., Maas, L., Schwäbe, A. E., Spille, I., Lennartz, S., Fassunke, J., Aldea, M., Besse, B., Planchard, D., Nogova, L., Michels, S., Kobe, C., Persigehl, T., Westphal, T., Koleczko, S., Fischer, R., … Sos, M. L. (2021). Clonal dynamics of BRAF-driven drug resistance in EGFR-mutant lung cancer. *Npj Precision Oncology*, *5*(1). https://doi.org/10.1038/S41698-021-00241-9

Serrano, A., Berthelet, J., Naik, S. H., & Merino, D. (n.d.). *Mastering the use of cellular barcoding to explore cancer heterogeneity*. https://doi.org/10.1038/s41568-022-00500-2

Shao, M., Jiang, C., Yu, C., Jia, H., Wang, Y., & Mao, X. (2022). Capecitabine inhibits epithelial-to-mesenchymal transition and proliferation of colorectal cancer cells by mediating the RANK/RANKL pathway. *Oncology Letters*, *23*(3), 1–11. https://doi.org/10.3892/OL.2022.13216/HTML

Sharma, P., Hu-Lieskovan, S., Wargo, J. A., & Ribas, A. (2017). Primary, Adaptive, and Acquired Resistance to Cancer Immunotherapy. *Cell*, *168*(4), 707–723. https://doi.org/10.1016/J.CELL.2017.01.017

Smillie, C. S., Biton, M., Ordovas-Montanes, J., Sullivan, K. M., Burgin, G., Graham, D. B., Herbst, R. H., Rogel, N., Slyper, M., Waldman, J., Sud, M., Andrews, E., Velonias, G., Haber, A. L., Jagadeesh, K., Vickovic, S., Yao, J., Stevens, C., Dionne, D., … Regev, A. (2019). Intra- and inter-cellular rewiring of the human colon during ulcerative colitis. *Cell*, *178*(3), 714-730.e722. https://doi.org/10.1016/j.cell.2019.06.029

Sugimoto, H., Mundel, T. M., Kieran, M. W., & Kalluri, R. (2006). Identification of fibroblast heterogeneity in the tumor microenvironment. *Cancer Biology and Therapy*, *5*(12), 1640–1646. https://doi.org/10.4161/cbt.5.12.3354

Sun, C., & Bernards, R. (2014). Feedback and redundancy in receptor tyrosine kinase signaling: Relevance to cancer therapies. *Trends in Biochemical Sciences*, *39*(10), 465–474. https://doi.org/10.1016/J.TIBS.2014.08.010

Van Cutsem, E., Verslype, C., & Tejpar, S. (2005). Oral capecitabine: Bridging the Atlantic divide in colon cancer treatment. *Seminars in Oncology*, *32*(1 SPEC. ISS.), 43–51. https://doi.org/10.1053/J.SEMINONCOL.2004.09.028

Vasan, N., Baselga, J., & Hyman, D. M. (2019). A view on drug resistance in cancer. In *Nature* (Vol. 575, Issue 7782, pp. 299–309). Nature Publishing Group. https://doi.org/10.1038/s41586-019-1730-1

Velho, S., Moutinho, C., Cirnes, L., Albuquerque, C., Hamelin, R., Schmitt, F., Carneiro, F., Oliveira, C., & Seruca, R. (2008). *BRAF, KRAS and PIK3CA mutations in colorectal serrated polyps and cancer: Primary or secondary genetic events in colorectal carcinogenesis?* https://doi.org/10.1186/1471-2407-8-255

Wang, C., Vegna, S., Jin, H., Benedict, B., Lieftink, C., Ramirez, C., de Oliveira, R. L., Morris, B., Gadiot, J., Wang, W., du Chatinier, A., Wang, L., Gao, D., Evers, B., Jin, G., Xue, Z., Schepers, A., Jochems, F., Sanchez, A. M., … Bernards, R. (2019). Inducing and exploiting vulnerabilities for the treatment of liver cancer. *Nature 2019 574:7777*, *574*(7777), 268–272. https://doi.org/10.1038/s41586-019-1607-3

Wang, H., Quan, H., & Lou, L. (2017). AKT is critically involved in the antagonism of BRAF inhibitor sorafenib against dabrafenib in colorectal cancer cells harboring both wild-type and mutant (V600E) BRAF genes. *Biochemical and Biophysical Research Communications*, *489*(1), 14–20. https://doi.org/10.1016/J.BBRC.2017.05.110

Wang, Q., Shen, X., Chen, G., & Du, J. (2022). *Drug Resistance in Colorectal Cancer: From Mechanism to Clinic*. https://doi.org/10.3390/cancers

Wang, X., Zhang, H., & Chen, X. (n.d.). *Review Open Access Cancer Drug Resistance Drug resistance and combating drug resistance in cancer*. https://doi.org/10.20517/cdr.2019.10

Waters, A. M., & Der, C. J. (2018). *KRAS: The Critical Driver and Therapeutic Target for Pancreatic Cancer*. https://doi.org/10.1101/cshperspect.a031435

Wu, Z., Huang, M., Gong, Y., Lin, C., & Guo, W. (2018). BRAF and EGFR inhibitors synergize to increase cytotoxic effects and decrease stem cell capacities in BRAF(V600E)-mutant colorectal cancer cells. *Acta Biochim Biophys Sin*, *50*(4), 355–361. https://doi.org/10.1093/abbs/gmy018

Yaeger, R., & Corcoran, R. B. (n.d.). *Targeting Alterations in the RAF-MEK Pathway*. https://doi.org/10.1158/2159-8290.CD-18-1321

Yaeger, R., & Saltz, L. (2012). BRAF Mutations in Colorectal Cancer: Clinical Relevance and Role in Targeted Therapy. In *The Last Word Journal of the National Comprehensive Cancer Network © JNCCN-Journal of the National Comprehensive Cancer Network* | (Vol. 10).

Yalcin, G. D., Danisik, N., Baygin, R. C., & Acar, A. (2020). *Systems Biology and Experimental Model Systems of Cancer*.

Zhu, G., Pei, L., Xia, H., Tang, Q., & Bi, F. (2021). Role of oncogenic KRAS in the prognosis, diagnosis and treatment of colorectal cancer. *Molecular Cancer*, *20*, 143. https://doi.org/10.1186/s12943-021-01441-4

Zugazagoitia, J., Guedes, C., Ponce, S., Ferrer, I., Molina-Pinelo, S., & Paz-Ares, L. (2016). Current Challenges in Cancer Treatment. *Clinical Therapeutics*, *38*(7), 1551–1566. https://doi.org/10.1016/j.clinthera.2016.03.026